The Role of Primary Producer Traits in Moderating Community Structure and Ecosystem Function

by

Marina Diane Lauck

A Dissertation Presented in Partial Fulfillment
of the Requirements for the Degree
Doctor of Philosophy

Approved April 2022 by the
Graduate Supervisory Committee:

Nancy B. Grimm, Chair
Alison Appling
Dan Childers
John Sabo

ARIZONA STATE UNIVERSITY

May 2022

ABSTRACT

Primary producers, from algae to trees, play a pivotal role in community structure and ecosystem function. Primary producers vary broadly in their functional traits (i.e., morphological, physiological, biochemical, and behavioral characteristics), which determine how they *respond* to stimuli and *affect* ecosystem properties. Functional traits provide a mechanistic link between environmental conditions, community structure, and ecosystem function. With climate change altering environmental conditions, understanding this mechanistic link is essential for predicting future community structure and ecosystem function. Competitive interactions and trait values in primary producers are often context dependent, whereby changes in environmental conditions and resources alter relationships between species and ecosystem processes. Well-established paradigms concerning how species in a community respond to each other and to environmental conditions may need to be re-evaluated in light of these environmental changes, particularly in highly variable systems. In this dissertation, I examine the role of primary producer functional traits on community structure and ecosystem function. Specifically, I test a conceptual framework that incorporates *response traits*, *effect traits*, and their interaction, in affecting primary producer communities and ecosystem function across different aquatic systems. First, I identified species-specific *responses* to intensifying hydrologic stressors important in controlling wetland plant community composition over time in an aridland stream. Second, I found that *effect traits* of submerged and emergent vegetation explained differences in ecosystem metabolism and carbon dynamics among permafrost mire thaw ponds. Next, I examined *response-effect* trait interactions by comparing two dominant wetland plant species over a water-stress gradient, finding that *responses* to changes in hydrology (i.e., altered tissue chemistry) in turn *affect* ecosystem processes (i.e., subsurface CO_2 concentration). Finally, I demonstrate how indirect effects of diatom functional traits on water chemistry and ecosystem metabolism help explain disconnects between resource availability and productivity in the Colorado River. By expanding my understanding of how metabolic processes and carbon cycling in aquatic ecosystems vary across gradients in hydrology, vegetation, and organic matter, I contributed to my understanding of how

communities influence ecosystem processes. A response-effect trait approach to understanding communities and ecosystems undergoing change may aid in predicting and mitigating the repercussions of future climate change.

DEDICATION

To my mother, father, and brother – Diane Jarboe, Robert Kevin and Robert James Lauck. You made me who I am. This is as much yours' as mine.

To my grandparents – James and Patricia Clinton, and Robert Hubert and Mary Lauck. Thank you for your love and wisdom. This is your legacy.

To my nieces, Allyson Belle and Katrina Ariel Denton, and Meara Major. Do what you love. Go little rockstars.

To my forever friends – Meghan Major, Brittany Denton, Alison Lee, and Kathleen Torrence. Thank you for putting up with me all these years and never letting go. I love you so.

To my husband, Gyan Harwood. Thank you for your love and support, and for keeping me grounded and fed.

And of course, Aoife.

ACKNOWLEDGMENTS

I would like to thank all my amazing mentors. Without your guidance throughout the years, this would not have been possible. Special thank you to my dissertation chair, Nancy Grimm, for her unwavering support, and for being my biggest advocate. You are an amazing role model for women in STEM, and your passion for continual learning and exploration is inspirational. Thanks to my committee, Alison Appling, Dan Childers, and John Sabo, for sharing your guidance and wisdom. And thank you to my past advisers throughout my undergraduate and master's programs who helped mold me into the person I am today: Thomas Miller, Brian Benscoter, Evelyn Frazier, and Dianne Owen.

Huge thanks to my academic siblings, Amalia Handler, Mendi Li, Stephen Elser, Jason Sauer, Katie Kemmitt, and Mandy Kuhn, and the Grimm lab managers, Lindsey Pollard, Sophia Bonjour, Leah Gaines-Sewell. Your support, both emotional and technical, was invaluable. This work would not have been possible without the support and encouragement of our amazing academic family.

This research would not have been possible without the massive amount of help in the field, lab, and office. Thank you, Sarah McGregor, Cathy Kochert, Stevan Earl, Quincy Stewart, Megan Gaitan, Miguel Carrillo Dominguez, and Robert Booher for your technical assistance. Thank you, Tearsa Saffell, Michael Convey, Kody Landals, Miranda Turner, Neesha Basnyat, and Brandi Harris for your assistance in the field.

Thank you, all the organization and programs, funding my research: ASU SOLS, RTI, Graduate Professional Student Association, CAP LTER, National Science Foundation INTERN program, Association for the Sciences of Limnology and Oceanography Limnology and Oceanography Research Exchange (LOREX) program, and the ASU Graduate College.

Many thanks to the numerous friends and family who supported me every step of the way. Special shout out to the friends of Grimm lab reading group (also known as the FoG).

It takes a village. Sincerely, from the bottom of my heart, thank you all.

TABLE OF CONTENTS

LIST OF TABLES

LIST OF FIGURES

Figure Page

CHAPTER 1

INTRODUCTION

Primary producers play a key role in the structure and function of ecosystems. These primary producers vary in their structural and functional characteristics, hereafter *traits*, affecting their response to stimuli and, in turn, their effects on ecosystem properties. In this dissertation, I examine the role of primary producer traits on community structure and ecosystem function. Specifically, I test components of a conceptual framework incorporating response traits, effect traits, and their interactions in influencing primary producer communities over time (Figure 1.1).

Functional traits moderate species' interactions with their environment and other organisms and vary among primary producer species (Violle et al. 2007). Functional traits can further be categorized as either *response traits* or *effect traits*. The influence of environmental conditions on a species is moderated by its tolerance for stressors and is imparted by *response traits*. For example, primary producers possess characteristics promoting tolerance to low resource availability (e.g., water, nutrients), physical perturbances (e.g., wind, flooding), and biological interactions (e.g., competition, predation). Traits often respond to environmental gradients, and ecological processes such as abiotic and biotic filtering, selection, and plasticity may influence observed patterns between traits and the environment (Garnier et al. 2016). Conversely, primary producers possess traits that influence ecosystem processes and properties. These consequences, and the traits that confer them, are *effect traits*. Plant traits can be both response and effect traits and are often related to resource acquisition and use, size, and regeneration (Wright et al. 2002; Garnier et al. 2016). For instance, leaf mass per unit area is a function of aridity (response) but also slows decomposition (effect) (Wright et al. 2002).

Quantifying the effects of individuals and communities on ecosystem function is complex due to the interrelated effects of context dependence, relative abundance, and diversity. First, the effect of an individual can vary as a function of their response to environmental conditions. Measures of an effect are specific to the conditions at the time. Second, observed effects in situ are the sum of multiple concurrent individual effects. According to the mass ratio hypothesis, the

total effect of a species on ecosystem processes can be calculated as proportional to its relative abundance in the community (Grime 1998). Additionally, the functional diversity of biological communities can moderate ecosystem function (Díaz et al. 2007). The biodiversity-function hypothesis shows that biodiversity loss can lead to reduced rates of key ecosystem processes, like productivity and decomposition (Hooper et al. 2012). This framework, individual species' effects on ecosystem processes are challenging to predict due to nonadditive effects of complementary resources and species interactions (Hooper et al. 2005; Dias et al. 2013). However, the positive linear relationship between species richness and ecosystem function assumes random species assemblages, often not observed in nature (Díaz and Cabido 2001). Rather, aggregations of plant species in niche space and nonrandom community assemblage are often the norm because of environmental filtering and the limitations of dispersal mechanisms. Species are limited by their requirements and tolerances to resources, like light, water, and nutrients, and hence, species with similar requirements and tolerances are likely to aggregate together. Support has been found for both mass-ratio and biodiversity-function perspectives. Discrepancies between these two perspectives may be resolved with a focus on the abundance and diversity of traits rather individuals.

Functional traits provide a mechanistic link between biotic communities and ecosystem function (Lavorel and Garnier 2002). Currently, climate change is altering ecosystem processes (Band et al. 1996; Grimm et al. 2013; Lipton et al. 2018), as well as the distribution and dynamics of biotic communities (Kelly and Goulden 2008; Staudinger et al. 2013). These changes challenge well-established paradigms, such as precipitation– productivity correlations, prompting ecologists to reevaluate these relationships, especially in highly variable systems (Knapp et al. 2017). A functional trait perspective incorporating context dependent responses and effects helps elucidate the mechanisms by which communities influence processes will aid in predicting future changes and mitigating adverse outcomes.

Ecosystem metabolism is a function that describes the total flow of energy in an ecosystem. Various processes and metrics express these energy flows. Net ecosystem production (NEP) quantifies energy flow as the difference between gross primary production

(GPP) and ecosystem respiration (ER), or simply production minus consumption. Net carbon balance (NECB) quantifies energy flow through the production and consumption of carbon, including GPP, ER, and other biotic and abiotic carbon cycle processes (Chapin et al. 2006). In aquatic systems, ecosystem metabolism is often measured using diel oxygen fluxes to estimate GPP through daytime oxygen production and ER through nighttime oxygen consumption (Odum 1956).

Ecosystem metabolism is a large-scale metric related to many ecosystem properties and processes, including ecosystem health, nutrient uptake, trophic structure, and carbon flux through food webs (Riley and Dodds 2013). Numerous factors influence aquatic ecosystem metabolism, including watershed size, nutrient availability, land use, and canopy cover (Hoellein et al. 2013a; Bernhardt et al. 2018). Recent work compiling ecosystem metabolism data across spatial and temporal scales (Appling et al. 2018) suggests that river and stream ecosystem metabolism is primarily regulated by light and flow regimes (Bernhardt et al. 2022). Similarly, light regulates aquatic metabolism in wetland systems (Kominoski et al. 2021). However, discussions around ecosystem metabolism do not generally consider the composition of the primary producer community nor their functional differences.

Freshwater ecosystems, including streams, lakes, and wetlands, are vital for biodiversity. They are “hot spots” for biogeochemical reactions (Mcclain et al. 2003; Abnizova et al. 2012; Cheng and Basu 2017), they enhance biodiversity (Sabo et al. 2005a), and they are responsible for material transport and transformation (Meyer and Likens 1979). Freshwater systems are also experiencing dramatic shifts as a result of climate change. Examples include effects on streamflow (DeWalle et al. 2000; Mulholland et al. 2005), shorter hydroperiods (Montrone et al. 2019), increased intermittency (Reynolds et al. 2015), and increased temperatures (Grimm et al. 2013). All these factors have substantial effects on the structure and function of ecosystems.

The relationship between aquatic plant traits and community production varies across species and over environmental gradients, emphasizing the need to resolve the influence of these variable interactions and the environmental factors that drive them (Gustafsson and Norkko 2018). Environmental factors under change, like temperature and hydrology, drive trait responses

that significantly affect ecosystem processes. For example, temperature and hydrology impact adaptive wetland traits like root porosity (Pan et al. 2020). Root porosity, in turn, can promote the oxidization of sediments in reduced environments (Clarke 2002; Dodds et al. 2017) or alleviate organic matter limitation in the hyporheic zone of desert streams (Schade et al. 2001; Heffernan et al. 2007). The ultimate effect is dependent on the environmental context, which is an ever-shifting baseline.

There is a growing consensus that community functional composition regulates ecosystem functioning (Lavorel and Garnier 2002; Petchey and Gaston 2006; Díaz et al. 2007) and governs community assembly of primary producers (Hillerislambers et al. 2012; Pérez-Ramos et al. 2019; Ács et al. 2019). Diversity increases function, with different species having various effects on function (Gustafsson and Norkko 2018). Still, the identification of effect traits and the linkage between response and effect traits is less understood. Given changing climatic norms, understanding the interaction between primary producer responses and their effects is pivotal to understanding effect traits and projecting future change.

This research explores the role of primary producer functional traits in controlling community structure and ecosystem function in highly variable ecosystems. Specifically, I test components of a conceptual framework proposed by Lavorel and Gardiner (2002) that incorporates the influence of functional response traits on community composition, the impact of functional effect traits on ecosystem function, and the interaction between primary producer responses and effects (Figure 1.1).

Chapter 2 explores differences in species-specific responses to hydrologic stressors in an aridland stream and the effects on community composition over time. Using 10 years of data from a long-term study of Sycamore Creek in central Arizona, I examined the *responses* of dominant wetland plant species to hydrological variation and the resulting change in community composition over time. Sycamore Creek is a spatially intermittent and highly variable desert stream that experiences regular drying and scouring floods associated with summer monsoon and winter storms. This study elucidates the hydrologic disturbance factors that influence biomass production of riparian wetland plant species in an aridland riparian-stream ecosystem

that is vulnerable to ongoing climate change. My results demonstrate that interannual interactions between wetland plant biomass produced in previous years, disturbances in the current year, and species-specific tolerances to flood and drought stressors (i.e., *response traits*) moderate patterns of riparian wetland productivity in aridland ecosystems (Lauck et al. in preparation-a).

Chapter 3 explores the influence of *effect traits* on ecosystem metabolism and carbon dynamics on permafrost mire thaw ponds in Abisko, Sweden. Warming in recent years has resulted in degrading permafrost in subarctic mires, decreasing the extent of permafrost (Kohler et al. 2006; Åkerman and Johansson 2008) and resulting in changes in plant composition and carbon balance of the mire ecosystem (Malmer et al. 2005). I investigate how species-specific functional effect traits of macrophyte functional groups (mosses and sedges) influence ecosystem metabolism and carbon dynamics using published morphological trait data, diel changes in oxygen concentration, gas emission, and biomass sampling. I found primary producers have diverse impacts on carbon dynamics and ecosystem metabolism attributable to functional group-specific traits. Broadly, sedges increase carbon evasion via aerenchyma, increase CO_2 concentration in pore-water via methane oxidation and decomposition, promote greater ecosystem respiration, and positively influence carbon gas evasion. Moss ponds had higher GPP but exhibited NEP rates similar to non-vegetated, less metabolically active ponds; however, they may trap gases and effectively prevent evasion (Lauck et al. in preparation-b).

Chapter 4 explores the interaction between the *response* and *effect traits* of dominant wetland plant species across a gradient of hydrologic conditions in Sycamore Creek. I collected trait data and quantified carbon and oxygen dynamics in species-specific patches of dominant primary producers as the streamed dried over the summer season (May – July). I found species-specific responses in tissue chemistry in response to water and nutrient availability, and which, in turn, influenced system properties, including dissolved gases (oxygen and carbon dioxide) in the root zone. This link between plants' response to environmental conditions and their effect serves as an example of response-effect traits interaction (Lauck and Grimm in preparation-c).

Chapter 5 examines the influence of diatom functional traits on water chemistry and ecosystem metabolism in the Colorado River. The Colorado River is a vital water resource serving the southwestern US and Mexico. I developed a model to explore relationships between ecosystem metabolism, phosphorus availability, quantified as soluble available phosphorus (SRP), and primary producer community traits using long-term time series of metabolism, diatom surveys, and water chemistry data collected by the USGS. My results demonstrate the complexity and importance of phytoplankton traits in mediating primary productivity. Interactions in trait responses to soluble reactive phosphorus, biovolume, and GPP appeared to dampen or buffer the biovolume mediation on the SRP–GPP relationship (Lauck et al. in preparation-d).

In Chapter 6, I synthesize the findings from this dissertation and discuss their implications for other ecosystems and the field of ecology. I compare findings across the diverse systems studied in this dissertation, including small, highly variable desert streams, an arctic mire undergoing permafrost thaw, and a large, highly managed river. This comparison across systems contributes to my general understanding of the role of primary producers and their functional traits in ecosystem processes as environmental changes continue to change around the world.

This research contributes to contemporary theory in two ways. First, I apply the functional response-effect trait framework to highly variable ecosystems experiencing the impact of climate change. The variability observed in these systems allows for investigating interactions between response and effect traits by providing multiple conditions to compare over a relatively brief period of time. Functional effect traits have been used to explain the relationship between biodiversity and ecosystem function (Lavorel et al. 1997; Lavorel and Garnier 2002), whereas functional response traits have been used to explain species loss and distribution (Steffan 1996; Elmqvist et al. 2003). However, response and effect traits may or may not be correlated with one another (Chapin et al. 1996a; Lavorel and Garnier 2002). Understanding links between functional response and effect traits remains a significant challenge but is critical to understanding the dynamics of ecosystem functioning in a changing world (Hooper et al. 2012).

Second, my research explicitly tests species-specific effects. While the relationship between biodiversity and ecosystem function is still an area of interest, there is a consensus among ecologists that species functional traits can strongly influence ecosystem properties beyond what is explained by biodiversity metrics alone (Tilman and Downing 1994; Tilman et al. 1997b; a; Hooper et al. 2012). Such an understanding is useful in the development of community-level ecological theory (Mcgill et al. 2006). Likewise, this research considers species-specific effects on ecosystem metabolism, which are not often incorporated in metabolism models. Expanding my understanding of how metabolic processes and carbon cycling in aquatic ecosystems vary across gradients in hydrology, vegetation, and organic matter could enhance my understanding and protection of conditions that maximize carbon storage.

Tables and figures

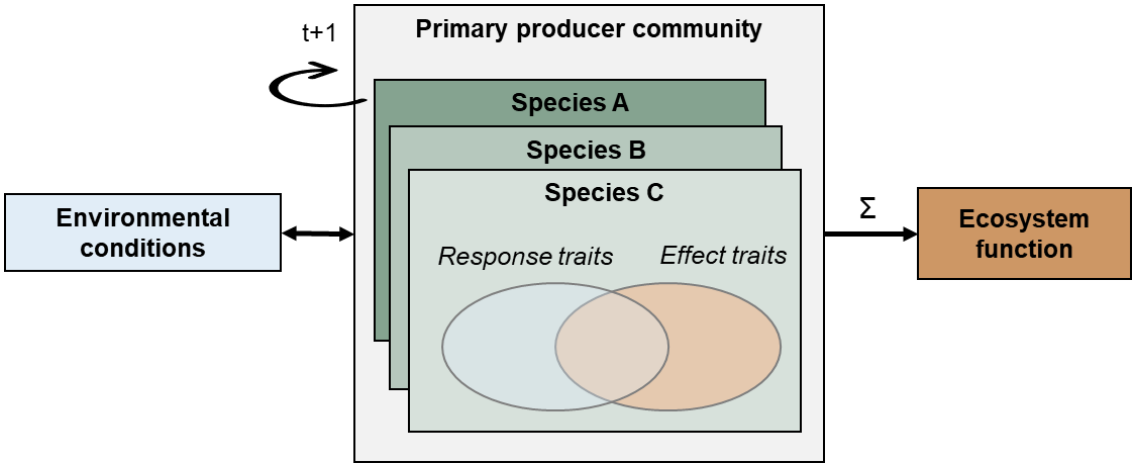

Figure 1.1 A conceptual framework describing the interactions between environmental stimuli, primary producer communities, and ecosystem metabolism adapted from Lavorel and Garnier. Environmental factors influence individual species as a function of their response traits, which influences the composition of the community over time. The sum of species effect traits in the community affects ecosystem functions, like aquatic metabolism.

CHAPTER 2

WETLAND PLANT RESPONSES TO A GRADIENT OF HYDROLOGIC DISTRUBANCES IN AN ARID RIPARIAN SYSTEM

Introduction

Riparian ecosystems, whether ephemeral or perennial, are vital for supporting biodiversity (Sabo et al. 2005a) and ecosystem functioning at the ecotone between upland terrestrial and aquatic ecosystems. This is especially so in arid and semi-arid regions (Serrat-Capdevila et al. 2011), where riparian areas regulate ecohydrological processes (Tabacchi et al. 2000; Dent et al. 2007), sediment retention and movement (Naiman and Decamps 1997), nutrient dynamics (Fisher et al. 1998; Schade et al. 2001, 2002, 2005a), species distributions (Williams et al. 2006), and carbon flux (Harms and Grimm 2008), among others. Riparian ecosystems are vulnerable to ongoing climate change (Perry et al. 2012), largely because they are typically modified or controlled for anthropogenic uses including hydroelectric dams, water diversion for agricultural and urban use, and flood control (LeRoy Poff et al. 1997; Nilsson and Berggren 2000; Jones et al. 2010). These direct impacts influence plant species distributions and productivity (Patten 1998; Beauchamp and Stromberg 2008) but also have consequences for related systems that, although not directly impacted by human-caused disturbances, have been and will continue to be altered by climate changes including drought (Perry et al. 2012).

Water availability in arid and semi-arid riparian systems shapes plant community composition, richness, and species abundance (Sabo et al. 2005a; Dong et al. 2016), which in turn can influence ecosystem-level carbon and water flux (Scott et al. 2014). This is an important consideration in regions like the U.S. Southwest, where recent water shortages in the Colorado River typify the overall decline in water supplies the region has experienced (Milly et al. 2005) as well as continued declines projected under future climate scenarios (Udall and Overpeck 2017). The latest report from the Intergovernmental Panel on Climate Change projects average annual temperature to rise as much as 4.7^{o} C by 2100 in the U.S. Southwest (Masson-Delmotte et al. 2021), which is likely to increase water loss through evapotranspiration and thereby reduce

streamflow (Serrat-Capdevila et al. 2011). Subsequent declines in native plant species presence and production are expected (Gremer et al. 2015; Winkler et al. 2019), increasing the vulnerability of these systems to invasion (Richardson et al. 2007; Stromberg et al. 2010) and wildfires (Littel et al. 2009). These trends are not specific to arid regions of the U.S. but are documented or forecast in arid and semi-arid regions across the globe (Pettit and Naiman 2007; Linstadter and Zielhofer 2010; Schlesinger and Westerhuis 2021).

Though nutrient-limited (Adair and Binkley 2002), productivity in arid and semi-arid riparian ecosystems exhibits high interannual variability due to the hydrological regime, including short-term flood impacts and intermittent water flow owing to highly seasonal precipitation (Dong et al. 2020). These events can result in mechanical damage to plants (Stromberg et al. 2007) but are also important for seed and propagule dispersal (Nilsson et al. 1991; Greet et al. 2011), nutrient inputs (Martí et al. 2000), and structuring the wetland to upland species continuum present in most arid riparian areas (Stromberg et al. 1996). Thus, the timing and frequency of intermittence in arid-land riparian ecosystems is important since more than half of streams and rivers globally are already experiencing at least one zero flow day (ZFD), when discharge is at or near zero, per year (Messager et al. 2021). Increasing temperature will increase intermittence, both in the number of ZFDs, and the waterways experiencing zero flow. Flash floods are already a fact of life in the US Southwest, where aridity and physiographic factors result in overland flow and intense flood peaks (Baker 1977). Combined with higher temperature and prolonged droughts, the more intense precipitation forecast for many arid regions like the U.S. Southwest may result in increasingly destructive flash floods (Lawrence et al. 2021).

A majority of past research has focused on woody riparian vegetation, including native and non-native trees, primarily because of the relative ease of measuring perennial trees using remote sensing approaches (Nagler et al. 2005; Webb and Leake 2006). As a result, relatively little is known about herbaceous riparian species like perennial graminoids, which can live for decades and provide critical ecosystem services to arid lands including soil stabilization, habitat to support biodiversity, and filtering of already limited water resources important for human populations (Woodward et al. 2009; Bateman et al. 2015; Dong et al. 2020). Herbaceous plants

lack the structural components that make woody vegetation more resilient to mechanical damage by flood and water loss, though variability in rooting structures and flood inundation tolerances (Moor et al. 2017) imply differential responses to stress. Thus, the persistence of herbaceous riparian plants in aridland systems may rely on species-specific traits that confer tolerance or resistance to stressors like flooding or prolonged drought.

My study sought to identify the primary abiotic and biotic factors influencing the productivity and persistence of riparian wetlands in a highly variable aridland ecosystem responding to climate change. I used long-term data from Sycamore Creek, Arizona, USA to examine wetland plant community composition and productivity change over 10 years that coincided with one of the most severe drought periods recorded. I modeled species-level and community-level productivity as a function of hydrologic conditions and disturbance, including stream discharge and flood frequency and magnitude at two spatiotemporal scales. I also investigated the relationship between prior-year biomass production and current-year productivity to explore the effect of interannual biomass accumulation on the resilience of species to flood perturbations.

Known species-specific differences in functional traits, including tolerance to hydrologic disturbance (inundation and drought) and root structure, were expected to moderate productivity and resistance to disturbances. The dominant species examined here represent a gradient of hydrologic tolerance and growth forms within wetland plants. For instance, *Paspalum distichum* is the least drought tolerant of my focal species, requiring greater water permanence, while *Juncus torreyi* requires moist soils, but is intolerant of prolonged inundation. As such, I expected the productivity of these two species to be most responsive to fluctuations between flooding and drought. Alternatively, *Typha domingensis* is fairly tolerant of prolonged periods of inundation and drought, aided by its tall stature that prevents submergence and thick rhizomes and leaves which store water. All focal species are rhizomatous but vary in root-mat density and rhizoid thickness, traits that were anticipated to differentially influence the resilience of species to flood disturbance and represent between-year amplifying feedbacks on species biomass as described by Heffernan (2008).

Methods

My study system was located along Sycamore Creek (33.7423 N, -111.5132 W) northeast of Phoenix, Arizona, United States. Sycamore Creek is a mid-sized desert stream that drains an ca. 500-km2 watershed with elevation ranging from ca. 700-2000+ m a.s.l.. Annual precipitation in the region averages about 250 mm. This stream-riparian corridor has been the subject of continuous investigation since the 1970's; the most recent period, from 2010-2020 (hereafter referred to as ' LTREB-2') is the focus of my present study. During this period, the stream has been subject to increasing levels of drying, channel narrowing owing to the encroachment of woody riparian vegetation, and an ecosystem state transition from one dominated by algae to one currently dominated by wetland plant species (Heffernan 2008; Dong et al. 2016). Variation in valley-floor width controls depth to bedrock, which subsequently influences the duration of water permanence. The streambed is a matrix dominated by sand, cobble, and boulders, with varying degrees of fine, organic sediment associated with vegetated reaches. There is strong seasonality in annual temperature, averaging > 40 C in the summer and 7 C in the winter. Winter rains typically replenish the system, but sections of the stream dry over much of the hot summers. The system also experiences summer monsoonal rains, oftentimes resulting in flash floods that scour streambeds and vegetation patches. Most monsoonal rain is quickly lost to evapotranspiration.

Five wetland plant species dominate the riparian macrophyte community in Sycamore Creek: *Typha domingensis, Schoenoplectus americanus, Paspalum distichum, Equisetum laevigatum,* and *Juncus torreyi*. These species differ in functional traits, including tolerance to hydrologic disturbance (i.e., inundation and drought tolerance) and rooting structures and architecture (Figure 2.1). *T. domingensis* is a cosmopolitan graminoid commonly associated with sites that are regularly inundated and is flexible, fast-growing, and highly competitive (Lorenzen et al. 2001). Likewise, *S. americanus* is an amphiphyte, a wetland plant tolerant to submergence, that produces densely packed root structures that stabilize sediments (Ikegami et al. 2009). *P. distichum* is a low-lying rhizomatous knotgrass with a relatively low tolerance for dry conditions and a simultaneous low tolerance for submergence (Hsiao and Huang 1989). *E. laevigatum* is

one of the oldest plants in the world (over 300 million years old) with a distinct suite of adaptations to tolerate disturbance (Husby 2013). Lastly, *J. torreyi* is a hydric rush commonly occurring near and along the edges of perennial water bodies (Stromberg et al. 2005).

Vegetation surveys

I used long-term survey data from Sycamore Creek that records the distribution and abundance of dominant wetland plant species. Surveys were conducted at two spatiotemporal scales between 2010 and 2020: monthly transect sampling of 160-m long reaches (i.e., a segment of a stream with similar hydrologic and environmental conditions) over the spring-summer growing season, and a comprehensive, annual survey recording the size and distribution of wetland plant patches along the 12-km section in mid-June each year (Figure 2.2). Wetland plant cover, species-specific density, and height data were collected monthly between 2010 and 2020 from April to June, contingent upon stream conditions, in three 160-meter stream reaches divided into eight permanent transects (1-m width, ~20 m apart) across two sites along Sycamore Creek: Round Valley (RV) and Dos S Ranch (SS).

RV-W (Reach 1) is the most upstream site (33.7890, -111.5018), and is located in a canyon section that usually maintains flow year-round. This site was selected for the LTREB-2 study to represent a stream reach dominated by riparian wetland vegetation. The active stream channel was narrow (ca. 1-5 meters wide) during the 10-year study period, resulting in shading by a continuous riparian tree canopy and greater quantities of fine organic sediment within a cobble-boulder matrix, compared to wider gravel reaches. Dense patches of primarily *S. americanus* occur along and across the streambed, though *T. domingensis* and *E. laevigatum* are also commonly present.

SS is approximately 4 km downstream of RV and is divided into two 160-m reaches: wetland (SS-W, Reach 2) and gravel (SS-G, Reach 3). Sycamore Creek widens at SS-G (33.7494, -111.5070), where the gravel-rich streambed stretches ca. 30 m wide and is dominated by non-vascular in-stream primary producers (e.g., filamentous algae, cyanobacteria, and diatoms), with patches of *T. domingensis* along the edge of the active channel. The SS wetland

reach (SS-W) is approximately 200 m downstream (33.7483, -111.5081) from SS-G. Like the RV site, a dense riparian tree canopy shades the relatively narrow (ca. 1-9 m) streambed containing comparatively more fine, organic substrate within a matrix of cobble-boulder. Smaller patches of *T. domingensis* in the stream, and thin, wispy patches of E. laevigatum at the riparian edge, are common along the SS-W reach.

A 12-km section of Sycamore Creek (Figure 2.2) encompassing the aforementioned monthly transect reaches was extensively surveyed annually for vegetation and water cover over two to five days in mid-June (June 15 $\pm$ 4 d) when biomass was near its annual peak but before the start of the summer monsoon—known hereafter as the 12K survey. The location (GPS coordinates), size (length and width, averaged across three measurements per patch), stem density (counts in 0.25, 0.50, or 1-m^2 quadrats, depending on patch size), and height (cm; calculated as an average of five randomly selected stems) of every wetland plant patch encountered along the 12-km section were recorded, between 57 (2018) and 144 (2013) patches each year, along with water presence and depth .

Biomass calculations

Plants were harvested each year between late June to mid-July for the length of the study to create species-specific height-biomass relationships. Biomass harvests were conducted across study sites but immediately outside my study reaches and occurred over 2-4 days. Between five and ten stems of each species representing a range of sizes were collected in the field each year, dried at 60°C for 48 h, and weighed in the lab. Data for each individual species were aggregated and fitted to second-order polynomial regressions of stem biomass as a function of stem height (Table 2.1). Biomass estimates per patch were calculated by multiplying individual stem biomass estimates by stem density and height from the survey data. For the monthly transect data, stem density and height were averaged across each reach for a given species, and biomass values were standardized to unit area by extrapolating the biomass per transect area to the total reach area. In the 12K data, individual patch density and average height in an individual patch were calculated, and the total biomass was summed across 100-m windows (N = 120)

along the entire 12-km reach. I did this to account for spatial variability in productivity and potential masking effects of a single window or patch in driving overall trends across the 12-km reach.

Hydrology

Daily average discharge data were acquired from a USGS gauge (station ID: 09510200) on Sycamore Creek, approximately 8 km downstream from the southern extent of my study site. This gage was used to approximate broad scale changes in water conditions over time but is not a perfect measure given its distance downstream and intersection with smaller tributaries (e.g., Mesquite Wash). The complete mean daily discharge dataset (from 1967-12-19 to 2020-09-30) was used to calculate hydrology metrics via the *discharge* package in R (Shah and Ruhi 2019, R Core Team 2020), including daily baseflow rates, one- and two-sigma flood events (i.e., floods exceeding one to two standard deviations from detrended baseflow), and net annual anomaly (NAA), or deviation from long-term trends. Cumulative discharge and the number of zero flow days (ZFDs; Q = 0) were calculated using daily mean discharge data. All calculations were by water year from October 1st to September 30th.

Model selection

I evaluated the influence of hydrologic variables on biomass production of riparian wetland plants over the 10-year study period using multi-model comparisons of multiple linear regression. Models were built using maximum annual biomass per species and aggregated data by reach (for monthly transects) or 100-m window (12K surveys). I selected twelve disturbance-related variables expected to influence wetland vegetation. Correlations between hypothesized explanatory variables were tested by calculating Pearson's correlation coefficients (r) for all pairs, and the candidate variables were retained if the correlation coefficients were under |0.70|. The six predictor variables remaining comprised the global first-order, multiple linear-regression model used in multi-model inference analyses (Table 2.2). I used the glmulti package in R (Calcagno and De Mazancourt 2010; Team 2015) to assess each candidate model using Akaike Information

Criterion (AIC) scores and model weights (Akaike weights; w_i), and to calculate the model-weighted relative importance (reported as a value from 0-1) of individual explanatory variables. Explanatory variables with a model-averaged importance value > 0.80 were considered significant, while model-averaged importance values between 0.5 and 0.80 were considered moderately important. Added-variable, or partial-regression, models were used to evaluate the relationship of each explanatory variable with the dependent variable (biomass or production rate) given the concurrent influence of all other modeled variables. Linear regression was used to evaluate the fit and significance of each individual variable in the added-variable analyses. All analyses were performed in R v. 4.1.3 (R Core Team 2020).

Results

Hydrology

Discharge and water availability varied over the study period (Figure 2.3). Water years 2010 and 2011 experienced almost no ZFDs. The number of ZFDs appeared to increase after 2013 and reached a maximum of >300 ZFDs in 2018, the driest year in my sample period. After the exceptionally dry 2018, Sycamore Creek experienced few to no ZFDs in 2019 and 2020. Cumulative discharge exhibited a pattern that was the inverse of ZFDs. Cumulative discharge was substantially higher in 2010 (approximately 4.0 x 10^6 m^3), followed by 2020, (3 x 10^6 m^3), 2019, 2017 and 2013 (ca. 2 x 10^6 m^3). 2014-2016 and 2018 annual cumulative discharge values were < 1 x 10^6 m^3.

There were 16 sigma flood events over the study period. The only two-sigma event, in which flood magnitudes were greater than two standard deviations from seasonal baseflow, occurred at the beginning of the study period, in January 2010, and had a peak discharge of 438.9 m^3/s. The other 15 were one sigma floods, in which flood magnitudes were greater than two standard deviations from seasonal baseflow. Only five events reached peak discharge rates over 100 m^3/s: January 2010, 2013, and 2017, August 2018 and September 2019. Those fall events occurred after the field season, and hence were not reflected in my analyses for that year

but were incorporated into prior-year anomalies (i.e., NAA $_{t-1}$). For example, the second-largest flood (238 m^3/s) in my dataset occurred in September 2019.

Pearson correlation of the model predictor variables (Table 2.2 and 2.3) indicated several highly correlated variables ($r > 0.70$), many describing single floods (e.g., peak discharge of the last sigma flood), which were removed in favor of more broadly descriptive variables (e.g., in this case, maximum flood peak per water year).

Wetland biomass

Over the study period (2010-2020), biomass production of wetland species in Sycamore Creek varied considerably across reaches and spatial scales (i.e., reach and 12K surveys), and years (Figure 2.4). *S. americanus* dominated the RV wetland reach except in 2018 when its productivity declined and *T. domingensis* produced slightly higher amounts of biomass (Figure 2.2A top panel). *T. domingensis* produced the highest amounts of aboveground biomass each year at the section scale (whole-stream scale) and in the SS-W reach, but its total biomass and amounts relative to other species varied through time (Figure 2.4C). *S. americanus* biomass production fluctuated in the 12K section surveys from the least to the second most productive. *E. laevigatum* biomass was relatively high in the 12K surveys though highly variable across years, and generally low in reaches. *P. distichum* and *J. torreyi* biomass declined over time, disappearing entirely from the reaches in the last few years of the study. *J. torreyi* disappeared from both the 12K and monthly reach surveys in 2018 and 2019 following a particularly extended period of ZFDs (Figure 2.4).

Species responses to disturbance

Multi-model analyses of reach data across reaches yielded 5-7 best-fit models per species (Table 2.4-2.6), and each included prior-year biomass and the maximum event peak discharge as independent variables, though these terms were not always significant in the best-fit models. The number of ZFDs prior to each annual survey was also prevalent in most of the best-fit models of *T. domingensis* and *S. americanus*. Prior biomass and maximum event peak were

also significantly important (model-averaged importance = 1) for all species based on the model-averaged importance of each environmental variable (Figure 2.5A). Results were similar for the 12K data, in that B_{t-1} and Q_{max} remained among the most important variables explaining species' biomass (model-averaged importance = 1, except Q_{max} for JUTO). Water cover within a patch, which was not available for the reaches, was also significantly important (model-averaged importance > 0.90). ZFDs were much less important in explaining species biomass at the 12-km scale (model-averaged importance < 0.50, Figure 2.5B).

Partial regression was performed to describe the relationship of each variable on species-specific biomass using residuals from each of the best-fit models (Figure 2.6, Table 2.7). For each species in the reach data, B_{t-1} had a significant positive relationship with species biomass each year ($P < 0.01$, $R^2 = 0.06$-0.34). *J. torreyi* and *S. americanus* biomass increased with increasing Q_{max}, whereas *E. laevigatum* biomass decreased ($P < 0.05$, $R^2 = 0.017$-0.13). Each of the modeled variables, except for prior biomass, had a significant negative correlation with *J. torreyi* biomass.

While B_{t-1} was also a significant predictor variable for all species in the 12K data, the direction of the relationship differed between the reach and 12K analyses (Figure 2.7, Table 2.7). *T. domingensis*, *S. americanus,* and *E. laevigatum* biomass exhibited a negative relationship with B_{t-1} at the 12-km section-scale ($P < 0.01$, $R^2 < 0.1$). Species biomass tended to be negatively related to Q_{max}, except for a small positive effect exhibited in *J. torreyi* biomass ($P < 0.001$, $R^2 = 0.04$). All species had a significant, positive relationship with water cover within the patch ($P << 0.001$, $R^2 = 0.11$-0.24). *E. laevigatum*, *J. torreyi*, *and P. distichum* each exhibited a significant, negative relationship with t_σ ($P << 0.001$, $R^2 = 0.5$-0.20) and ZFDs ($P << 0.001$, $R^2 = 0.5$-0.49).

Reach-specific models of species-specific biomass (using data only from the SS-W reach, the most data-rich reach) yielded models with significantly greater predictive power (best-fit models $R^2 > 0.90$ for each species). Again, B_{t-1} demonstrated a significant positive relationship with each species at the SS reach ($P << 0.001$, $R^2 = 0.94$). Interestingly, the reach-specific models showed divergent relationships between ZFD and *E. laevigatum* (positive) and *S.*

americanus (negative) biomass. Time since flood was significantly negatively correlated with both *T. domingensis* and *S. americanus* biomass ($P < 0.001$, $R^2 > 0.7$). E. laevigatum biomass was negatively correlated with flood frequency, and S americanus biomass decreased whereas E laevigatum biomass increased with maximum flood peak ($p < 0.01$, $R2 > 0.5$).

Discussion

This study elucidates the hydrologic disturbance factors that influence biomass production of riparian wetland plant species in an aridland riparian-stream ecosystem that is vulnerable to ongoing climate change. My results demonstrate that interannual interactions between wetland plant biomass produced in previous years, disturbances in the current year, and species-specific tolerances to flood and drought stressors moderate patterns of riparian wetland productivity in aridland ecosystems.

Patterns of change

Over the ten-year study, I observed significant variation in water availability, including a seven-year drought that peaked in 2018 with nearly 300 ZFD. Subsequently, the observed pattern indicates a shift from the drought-dominated hydrologic regime that prevailed for most of the study, to a wet regime that appeared in the first and last two years of the study. This pattern affirms previous work asserting that aridland rivers in the region experience approximately decadal hydrologic regime shifts (Sabo et al. 2019), and supports predictions of more frequent high-magnitude floods over the next decade. While the pattern of roughly decadal regime shifts may persist in the Southwest, the magnitude and frequency of extreme events, particularly drought and flash floods, are expected to increase with climate change (Prein et al. 2016).

Early work in desert streams describing post-flood algal community dynamics in a successional framework proposed that producer communities in aridland stream systems reset after unpredictable but seasonal flash floods (Fisher et al. 1982; Grimm and Fisher 1989). Later, wetland reaches were recognized as an alternative stable state aided by amplifying root-stabilization feedback that confers resistance to flood damage (Heffernan 2008), and moderated

by interactions between the geomorphic template and water permanence (Dong et al. 2016, 2017, 2020). The positive relationship between biomass $_{t}$ and biomass $_{t-1}$ in my study, as well as a significant relationship across all species with maximum annual flood peak and previous biomass, support the alternative stable state framework: biomass begets greater subsequent biomass but is dampened or restricted by high-magnitude disturbance. The geomorphic template may first determine where wetland plants initially occur (e.g., Dong et al., 2016), but once established, macrophytes can stabilize and accumulate sediments, providing substrate for further colonization, until a high enough threshold disturbance shifts the system. Disturbance includes intense, period events, like flash floods, as discussed by Heffernan (2008) and Dong et al (2016), but may also be prolonged, like extreme drought....

Increasing prevalence of drought conditions is likely to alter communities. For example, *J. torreyi,* whose abundance was relatively high at the beginning of the study when water availability was highest, maintained a small, but respectable presence at the beginning of the drought regime but disappeared following intense drought in 2018 and was not observed in either the 12K or reaches the following, relatively wet year (2019). This is indicative of drought conditions surpassing the threshold of drought resistance provided by underground root reserves for this particular species. Other species' biomass production in 2019 appeared stunted relative to water availability that year, potentially owing to reduction of between-year biomass reserves during drought but persisted in the system. As such, predicting change in this system in the future will require a species-specific perspective that incorporates differing tolerances. Accounting for species-specific tolerance will improve my understanding of how increased drought prevalence will affect wetland species persistence.

Species-specific responses

While the positive relationship with the previous year's biomass at the reach scale was ubiquitous, the relative importance and direction of the effect of other modeled variables varied among focal species. These differences may result partially from biotic factors not measured in this study, including plant age (Gattringer et al. 2017), herbivore pressure (Van Den Wyngaert

and Bobbink 2009), and light (Bernhardt et al. 2018), among others. Still, hydrologic variables displayed clear trends. For example, ZFD was a principal factor for both *T. domingensis* and *J. torreyi* at the reach scale. Given all other factors, *T. domingensis* biomass tended to increase with ZFD whereas *J. torreyi* biomass decreased sharply with ZFD and disappeared from both the reach and 12K surveys following the high ZFD year. *T. domingensis*' high tolerance of drying and inundation (Grace 1989; Newman et al. 1998; Chabbi et al. 2000) allows it to be fairly successful in this relatively extreme environment. On the other hand, *J. torreyi* occurs exclusively on the riparian edge, and its tolerances for both inundation and low water availability are lower, as demonstrated by the negative influence of floods (both magnitude and number of flood events) and prolonged periods without flow, both of which are expected to become more common and extreme with climate change. Likewise, the range of *P. distichum*'s tolerance to water availability is relatively narrow. Like J. *torreyi, P. distichum* biomass is reduced seemingly as a function of worsening drought conditions over the course of the study, disappearing from the 12K survey in 2018, the driest year. However, unlike *J. torreyi, P. distichum* resurfaced in 2019, a relatively wet year. This reappearance of P. distichum suggests root reserves may have persisted and sprouted in more favorable conditions. The resurgence of *P. distichum* and not *J. torreyi* may be a product of *J. torreyi'*s low tolerance to both inundation and drought conditions or may be potentially due to differences in their root structure providing not only structural support but resource storage.

All five focal species are rhizomatous; however, rhizome size and structure differ among species, which may partly explain the species' different tolerances to droughts and floods. *T. domingensis* possesses larger rhizome structures compared to the others, which provides it with greater resource storage and hence resistance to limited water and nutrient resources (da Cunha Cruz et al. 2020). *S. americanus* produce a combination of short and long rhizome ramets (Ikegami et al. 2009), which occur as dense mats that stabilize sediment and are likely more resistant to scouring by flash floods compared to others, like *E. laevigatum* and *J. torreyi*, which possess thinner, less dense rhizomes.

Spatial scale

Species-specific responses to predictor variables varied between the 160-m reach and 12-km section scales. The values of the predictor variables were slightly different despite being derived from the same USGS gauge data, as they were calculated relative to survey dates. The reach data monitored change in permanent transects through time, whereas the 12K survey analysis monitored broad-scale changes across a much larger section of the stream from year to year. I expected the variation in species-specific trends observed between the 160-m reach and 12-km section scales of analyses to capture different processes at the two scales. For instance, B_{t-1} was one of the most important predictor variables at both scales, and the relationship was positive for all species at the reach scale, but divergent (some positive, some negative) at the 12-km section scale. The unanimous positive relationship at the smaller reach scale may be capturing the kind of amplifying feedback described by Heffernan (2008) where species stabilize patches and provide root reserves to jumpstart production. Conversely, the divergent relationship observed in the 12-km section models may be indicative of competition for limited space and water resources on a larger scale.

Projecting future change

With impending climate change, the Southwest is expected to experience further drying and drought (Masson-Delmotte et al. 2021); even without a change in precipitation, increased temperature drives greater evapotranspiration and thus reduced inputs to streams and rivers. As a result, intermittent or ephemeral freshwater systems, which are most prevalent in the arid Southwest, are likely to experience more ZFDs and be less suitable to sustaining populations of wetland plants. Previous studies on freshwater systems in drylands have demonstrated that riparian species richness declines across gradients of flow permanence (Stromberg et al. 2005). The increased prevalence of stressors like drying, increased temperatures, and flash floods is likely to select for those species with functional traits that provide better resistance (i.e., thicker cuticles may reduce water loss) or resilience (i.e., root reserves may reduce recovery time) to such disturbances. I may already be witnessing this transition in light of the virtual disappearance of more specialized species (e.g., *J. torreyi*) within my study reaches.

Tables and figures

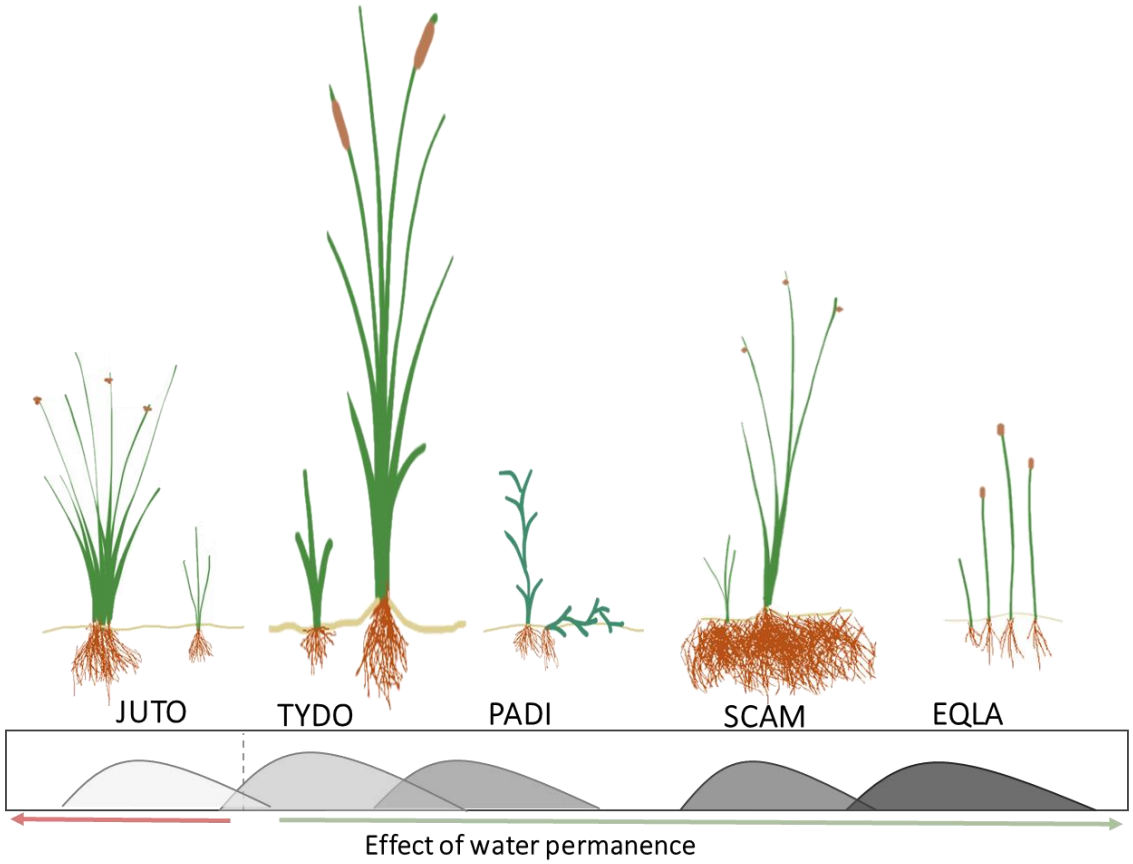

Juncus torreyi	***Typha domingensis***	***Paspalum distichum***	***Schoenoplectus americanus***	***Equisetum laevigatum***
Intolerant to inundation	Tolerant to wet and dry	Intolerant to drying	Intolerant to drying	Intolerant to inundation
Riparian edge	Cosmopolitan	Channel edge	Dense root mats	Riparian edge
Short rhizome	Thick roots & rhizome	“Runner” rhizome	Structural carbon	Thin roots & rhizome
Clumping rush	Tall, robust sedge	Clumping-forming grass	Stiff-stemmed sedge	Thin silicate shoots

Figure 2.1. Focal wetland plant species and related traits, including the effect of water permanence adapted from Dong et al 2016. Each species varies in water permanence requirements, inundation tolerance, where it occurs relative to the stream, as well as physical traits, such as root density, and growth form.

Figure 2.2. Sycamore Creek LTREB site map including the 12-km section (blue) surveyed once annually in July (15±3) and three reaches (1 - RV wetland [RW]; 2 - Dos S Ranch gravel [SG], 3 - - Dos S Ranch wetland [SW]) surveyed monthly from April to June.

Table 2.1. Species-specific height-to-biomass conversion formulas for individual plant stems derived from annual biomass harvests. Height (cm) was averaged, either per patch or reach, for each sampling event. Individual stem biomass was then multiplied by the density of stems in a given area and the surface area occupied by that species and then standardized by reach area (160-m multiplied by the average stream width).

Species	*n*	R^2	Biomass formula
Equisetum laevigatum	165	0.88	$0.02094 + 0.002892\ h + 0.00003573\ h^2$
Typha domingensis	135	0.83	$6.0419751 + (-0.151604\ h) + 0.0011391\ h^2$
Schoenoplectus americanus	211	0.93	$0.2260 + (-0.0008607\ h) + 0.00005471\ h^2$
Juncus torreyi	18	0.92	$0.1240 + (-0.01181\ h) + 0.0004028\ h^2$
Paspalum distichum	10	0.88	$0.06284 + 0.01891\ h + 0.00003675\ h^2$

Table 2.2. Pearson correlation results for candidate covariates to include in model selection. Correlation values (r) greater than 0.70 are bolded. Variables removed from model selection are highlighted in gray. Variables derived from manual list of flood events (e.g., $t_{\text{since flood}}$, $Q_{\text{peak last flood}}$, flood frequency) correlated with sigma flood-related variables. I retained the sigma flood event data in lieu of the manual flood data, as sigma flood events are expected to be more impactful.

	Q_{flood}	N_{σ}	Q_{max}	$Q_{t,rate}$	$Q_{t,day}$	Q_{Σ}	ZFD_t	ZFD_{Σ}	DOY_{wtryr}	NAA_{t-1}	B_t
t_{σ}	0.05	-0.57	0.3	-0.31	-0.31	-0.6	**0.97**	0.7	0.1	0.2	0.02
Q_{flood}	1	-0.69	-0.05	-0.26	-0.26	-0.46	0.06	0.19	0.03	-0.7	0.04
N_{σ}		1	-0.18	0.35	0.35	**0.88**	-0.62	-0.64	-0.06	0.36	-0.1
Q_{max}			1	-0.03	-0.03	-0.05	0.3	0.27	-0.21	-0.47	-0.06
$Q_{t,rate}$				1	1	0.23	-0.18	-0.15	-0.57	0.18	-0.09
$Q_{t,day}$					1	0.23	-0.18	-0.15	-0.57	0.18	-0.09
Q_{Σ}						1	-0.68	**-0.87**	0.01	-0.03	-0.13
ZFD_t							1	0.77	0	0.21	0.03
ZFD_{Σ}								1	0.01	0.17	0.11
DOY_{wtryr}									1	-0.01	0.17
NAA_{t-1}										1	0.02

Table 2.3. Explanatory variables included in model selection after removing correlated or redundant variables. Each variable is calculated with respect to the date of data collection or the survey date. Note: sigma events (N_σ) are those exceeding one standard deviation from the detrended baseflow. Traits in gray were not included in multi-model inference.

Variable	Description
t_σ	Time (in days) since the last sigma flood
N_σ	Number of sigma events per water year
Q_{max}	Flood peak discharge (m^3/s) of the highest magnitude flood event per water year
ZFD	The number of zero flow days per water year
NAA_{t-1}	Net annual anomaly the previous year
B_{t-1}	Peak species biomass in the previous year
$Q_{t\ day}$	Cumulative discharge up to the sampling date
ZFD_t	Consecutive zero flow days
DOY_{wtryr}	Day of water year

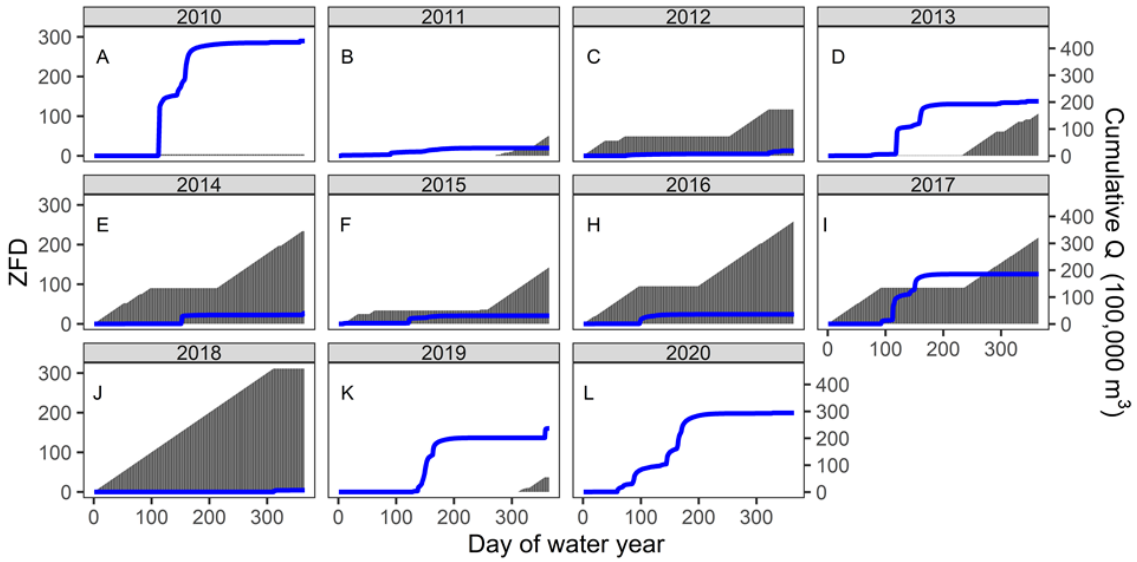

Figure 2.3. Cumulative zero flow days (ZFD; gray bars) and discharge (*Q;* blue line) per water year across the 2010-2020 study period.

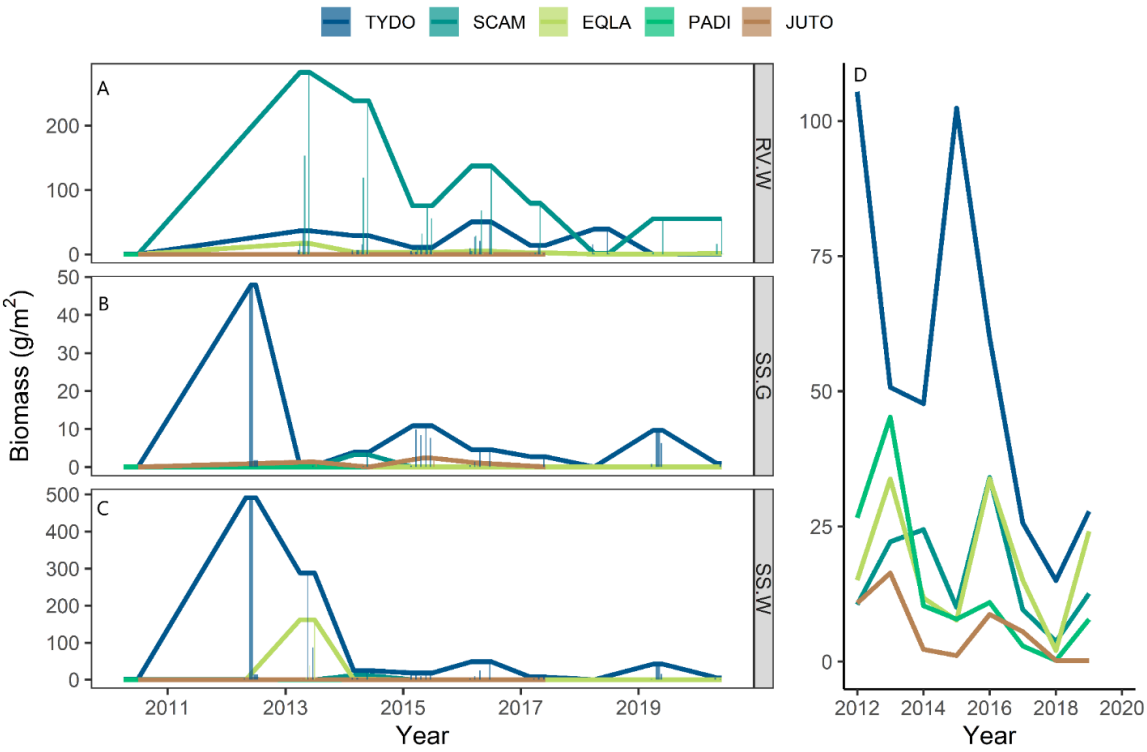

Figure 2.4. Annual biomass per species. Maximum annual biomass per species per reach (A - RV-W, B - SG, C - SW) observed in the monthly reach survey is denoted by the line, and monthly biomass values are shown in bars (A-C) and total biomass (g) across all patches by species by year in the 12K survey (D). Biomass values are standardized per unit area.

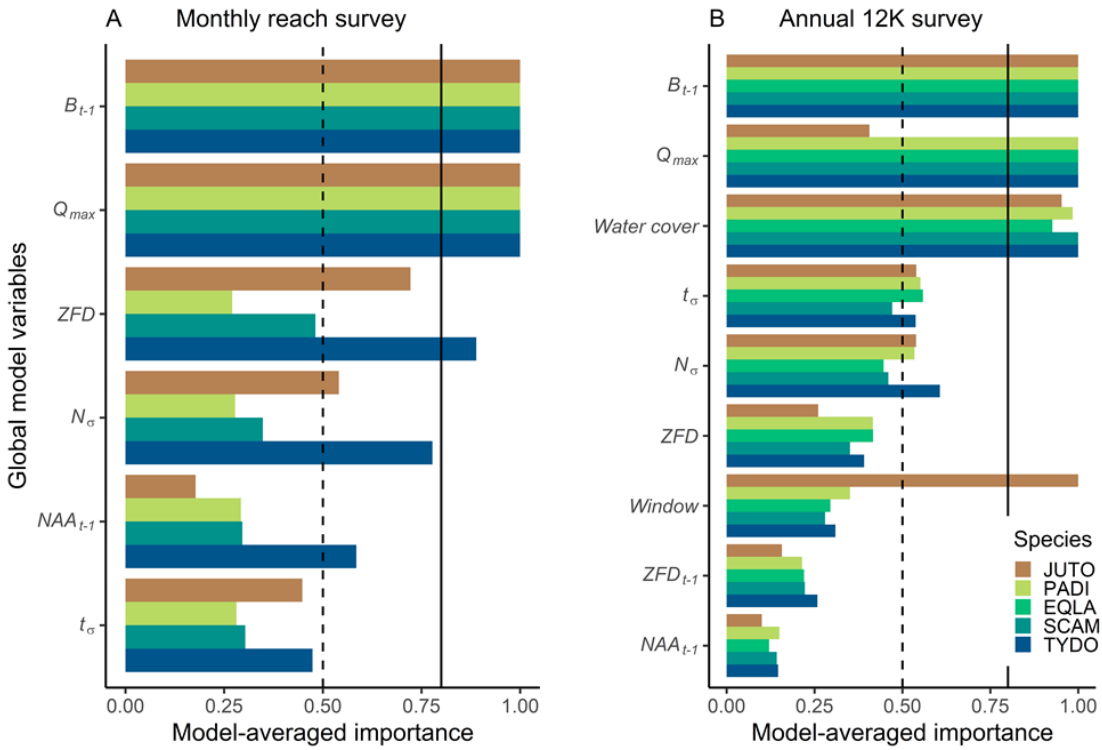

Figure 2.5. Model-averaged importance of terms used in model selection for maximum annual biomass in the reach surveys (A) and the 12K survey (B), for each species based on the AIC weight of each of models in which the variable occurs.

Table 2.4. Multi-model inference table using reach-scale data.

	Variable	Est	se	z value	p value	ci_{low}	ci_{high}	Import
EQLA	B_{t-1}	1.53E-05	2.03E-07	1.576	0.115	0.000	0.000	1.000
	Q_{max}	3.80E-02	5.00E-02	0.750	0.453	-0.061	0.136	1.000
	NAA_{t-1}	-1.00E-03	2.00E-03	-0.290	0.772	-0.004	0.003	0.286
	T_σ	1.00E-03	3.00E-03	0.223	0.824	-0.005	0.006	0.278
	N_σ	-1.50E-02	1.71E-01	-0.090	0.928	-0.351	0.320	0.274
	ZFD	0.00E+00	4.00E-03	0.028	0.977	-0.008	0.008	0.271
JUTO	B_{t-1}	3.68E-05	3.94E-04	1.576	0.115	0.000	0.000	1.000
	Q_{max}	3.80E-02	5.00E-02	0.750	0.453	-0.061	0.136	1.000
	NAA_{t-1}	-1.00E-03	2.00E-03	-0.290	0.772	-0.004	0.003	0.286
	T_σ	1.00E-03	3.00E-03	0.223	0.824	-0.005	0.006	0.278
	N_σ	-1.50E-02	1.71E-01	-0.090	0.928	-0.351	0.320	0.274
	ZFD	0.00E+00	4.00E-03	0.028	0.977	-0.008	0.008	0.271
PADI	B_{t-1}	-	-	1.576	0.115	0.000	0.000	1.000
	Q_{max}	3.80E-02	5.00E-02	0.750	0.453	-0.061	0.136	1.000
	NAA_{t-1}	-1.00E-03	2.00E-03	-0.290	0.772	-0.004	0.003	0.286
	T_σ	1.00E-03	3.00E-03	0.223	0.824	-0.005	0.006	0.278
	N_σ	-1.50E-02	1.71E-01	-0.090	0.928	-0.351	0.320	0.274
	ZFD	0.00E+00	4.00E-03	0.028	0.977	-0.008	0.008	0.271
SCAM	B_{t-1}	4.50E-05	2.75E-06	2.015	0.044	0.000	0.000	1.000
	Q_{max}	-8.30E-02	8.20E-02	-1.017	0.309	-0.244	0.077	1.000
	ZFD	5.10E-02	3.00E-02	1.735	0.083	-0.007	0.109	0.891
	N_σ	2.00E+00	1.64E+00	1.216	0.224	-1.223	5.215	0.779
	NAA_{t-1}	-7.00E-03	1.00E-02	-0.716	0.474	-0.026	0.012	0.578
	T_σ	-8.00E-03	1.30E-02	-0.633	0.527	-0.034	0.017	0.471
TYDO	B_{t-1}	8.52E-06	7.69E-07	2.015	0.044	0.000	0.000	1.000
	Q_{max}	-8.30E-02	8.20E-02	-1.017	0.309	-0.244	0.077	1.000
	ZFD	5.10E-02	3.00E-02	1.735	0.083	-0.007	0.109	0.891
	N_σ	2.00E+00	1.64E+00	1.216	0.224	-1.223	5.215	0.779
	NAA_{t-1}	-7.00E-03	1.00E-02	-0.716	0.474	-0.026	0.012	0.578
	T_σ	-8.00E-03	1.30E-02	-0.633	0.527	-0.034	0.017	0.471

Table 2.5. Multi-model inference table using 12K section survey data.

Species	variable	Est	se	z value	p value	ci_{low}	ci_{high}	Import
EQLA	Q_{max}	-2.23E-04	2.95E-02	-0.008	0.994	-0.058	0.058	1.000
	B_{t-1}	1.46E-04	1.54E-04	0.949	0.343	0.000	0.000	1.000
	%water	7.02E-03	4.60E-03	1.525	0.127	-0.002	0.016	0.926
	T_σ	-9.36E-02	2.51E-01	-0.373	0.709	-0.586	0.399	0.558
	N_σ	-1.83E-01	4.15E-01	-0.441	0.659	-0.997	0.631	0.447
	ZFD	-5.46E-04	1.84E-02	-0.030	0.976	-0.037	0.035	0.416
	window	1.74E-04	1.77E-03	0.098	0.922	-0.003	0.004	0.295
	ZFD_{t-1}	6.22E-04	1.71E-03	0.363	0.716	-0.003	0.004	0.220
	NAA_{t-1}	-4.21E-04	1.05E-03	-0.400	0.689	-0.002	0.002	0.121
JUTO	B_{t-1}	-1.33E-03	5.20E-04	-2.560	0.010	-0.002	0.000	1.000
	window	1.64E-02	4.10E-03	3.999	0.000	0.008	0.024	1.000
	%water	4.19E-02	3.33E-02	1.260	0.208	-0.023	0.107	0.953
	T_σ	-2.60E-01	3.25E-01	-0.799	0.424	-0.897	0.377	0.539
	N_σ	1.21E-01	6.15E-01	0.197	0.843	-1.084	1.326	0.539
	Q_{max}	3.47E-02	4.60E-02	0.754	0.451	-0.055	0.125	0.406
	ZFD	1.02E-02	2.65E-02	0.383	0.702	-0.042	0.062	0.261
	ZFD_{t-1}	-6.37E-04	6.36E-03	-0.100	0.920	-0.013	0.012	0.158
	NAA_{t-1}	-1.09E-03	2.02E-03	-0.542	0.588	-0.005	0.003	0.100
PADI	Q_{max}	-3.12E-02	7.99E-02	-0.390	0.696	-0.188	0.125	1.000
	B_{t-1}	1.71E-04	1.36E-04	1.253	0.210	0.000	0.000	1.000
	%water	5.83E-03	3.00E-03	1.943	0.052	0.000	0.012	0.984
	T_σ	-5.79E-01	1.01E+00	-0.576	0.565	-2.551	1.393	0.551
	N_σ	-8.28E-01	1.16E+00	-0.716	0.474	-3.092	1.437	0.534
	ZFD	3.20E-02	8.18E-02	0.391	0.696	-0.128	0.192	0.416
	window	-3.36E-03	7.72E-03	-0.435	0.664	-0.018	0.012	0.351
	ZFD_{t-1}	4.65E-05	3.07E-03	0.015	0.988	-0.006	0.006	0.215
	NAA_{t-1}	-3.32E-04	2.62E-03	-0.126	0.899	-0.005	0.005	0.150
SCAM	Q_{max}	-2.60E-02	2.79E-02	-0.931	0.352	-0.081	0.029	1.000
	B_{t-1}	-2.93E-04	2.23E-04	-1.314	0.189	-0.001	0.000	1.000
	%water	5.82E-03	2.69E-03	2.158	0.031	0.001	0.011	1.000
	T_σ	-1.72E-01	3.34E-01	-0.515	0.606	-0.827	0.483	0.471
	N_σ	-2.45E-01	3.94E-01	-0.622	0.534	-1.018	0.527	0.460
	ZFD	1.09E-02	2.70E-02	0.405	0.685	-0.042	0.064	0.351
	window	-7.50E-04	2.03E-03	-0.370	0.711	-0.005	0.003	0.280
	ZFD_{t-1}	-3.49E-04	1.18E-03	-0.295	0.768	-0.003	0.002	0.222
	NAA_{t-1}	6.64E-05	8.07E-04	0.082	0.934	-0.002	0.002	0.143
TYDO	Q_{max}	-1.09E-02	4.56E-02	-0.240	0.810	-0.100	0.078	1.000
	B_{t-1}	-8.62E-05	4.67E-05	-1.846	0.065	0.000	0.000	1.000
	%water	5.26E-03	1.15E-03	4.573	0.000	0.003	0.008	1.000
	N_σ	-6.59E-01	5.76E-01	-1.144	0.253	-1.787	0.470	0.607
	T_σ	-4.63E-01	7.74E-01	-0.598	0.550	-1.979	1.053	0.538
	ZFD	3.42E-02	6.38E-02	0.537	0.591	-0.091	0.159	0.391
	window	5.98E-04	1.43E-03	0.420	0.675	-0.002	0.003	0.310
	ZFD_{t-1}	-1.05E-03	2.16E-03	-0.485	0.628	-0.005	0.003	0.258
	NAA_{t-1}	5.13E-04	1.59E-03	0.322	0.748	-0.003	0.004	0.147

Table 2.6. Best-fit model results for each species using maximum annual biomass at the reach-scale and combinations of max event peak (Q_{max}), time since sigma event (tσ), biomass in the previous year (B_{t-1}), cumulative dry days (ZFD), net annual anomalies in the previous year (NAA_{t-1}), and number of sigma events (Nσ) as explanatory variables.

Species	Model	ZFD		Nσ		Q max		Tσ		NAAt-1		Bt-1		P model	R2	Wt	AIC
		Est	P	Est	P	Est	P	Est	P	Est	P	Est	P				
TYDO	ZFD + Nσ + Q max + NAAt-1 + Bt-1	0.07	0.01	3.42	0.01	-0.13	0.08	-	-	-0.02	0.07	0.00	0.03	0.03	0.33	0.32	142.76
	ZFD + Nσ + Q max + Tσ + NAAt-1 + Bt-1	0.07	0.01	2.90	0.06	-0.11	0.20	-0.01	0.47	-0.01	0.22	0.00	0.06	0.05	0.31	0.17	143.99
	ZFD + Nσ + Q max + Tσ + Bt-1	0.06	0.01	1.44	0.10	-0.04	0.52	-0.02	0.12	-	-	0.00	0.08	0.05	0.29	0.16	144.14
SCAM	ZFD + Q max + Bt-1	0.02	0.15	-	-	-0.10	0.03	-	-	-	-	0.00	0.00	0.00	0.43	0.17	182.34
	Q max + Bt-1	-	-	-	-	-0.07	0.09	-	-	-	-	0.00	0.00	0.00	0.41	0.14	182.69
	Nσ + Q max + Bt-1	-	-	-0.53	0.28	-0.09	0.05	-	-	-	-	0.00	0.00	0.00	0.42	0.11	183.31
	Q max + Tσ + Bt-1	-	-	-	-	-0.08	0.06	0.01	0.39	-	-	0.00	0.00	0.00	0.04	0.08	183.82
	ZFD + Q max + NAAt-1 + Bt-1	0.02	0.13	-	-	-0.12	0.03	-	-	0.00	0.53	0.00	0.00	0.00	0.42	0.08	183.87
	ZFD + Nσ + Q max + Bt-1	0.01	0.32	-0.23	0.68	-0.10	0.03	-	-	-	-	0.00	0.00	0.00	0.42	0.07	184.14
	ZFD + Q max + Tσ + Bt-1	0.02	0.27	-	-	-0.10	0.03	0.00	0.94	-	-	0.00	0.00	0.00	0.41	0.06	184.34
EQLA	Q max + Bt-1	-	-	-	-	0.04	0.33	-	-	-	-	0.00	0.11	0.21	0.04	0.27	187.19
	Q max + NAAt-1 + Bt-1	-	-	-	-	0.03	0.50	-	-	0.00	0.73	0.00	0.11	0.36	0.01	0.11	189.05
	Q max + Tσ + Bt-1	-	-	-	-	0.04	0.43	0.00	0.82	-	-	0.00	0.12	0.37	0.01	0.10	189.13
	Nσ + Q max + Bt-1	-	-	-0.11	0.82	0.04	0.40	-	-	-	-	0.00	0.13	0.37	0.01	0.10	189.13
	ZFD + Q max + Bt-1	0.04	0.42	-	-	-	-	-	-	-	-	0.00	0.14	0.38	0.01	0.10	189.18
JUTO	Q max + Bt-1	-	-	-	-	0.06	0.64	-	-	-		0.00	0.65	0.71	-0.19	0.27	187.19
	Q max + NAAt-1 + Bt-1	-	-	-	-	-0.73	0.03	-	-	-0.11	0.02	0.00	0.68	0.07	0.56	0.11	189.05
	Q max + Tσ + Bt-1	-	-		-	0.05	0.71	-0.06	0.73	-	-	0.00	0.72	0.86	-0.39	0.10	189.13
	Nσ + Q max + Bt-1	-	-	-11.31	0.02	0.66	0.02	-	-	-	-	0.00	0.68	0.07	0.56	0.10	189.13
	ZFD + Q max + Bt-1	-0.12	0.00	-	-	-0.11	0.11	-	-	-	-	0.00	0.31	0.01	0.79	0.10	189.18

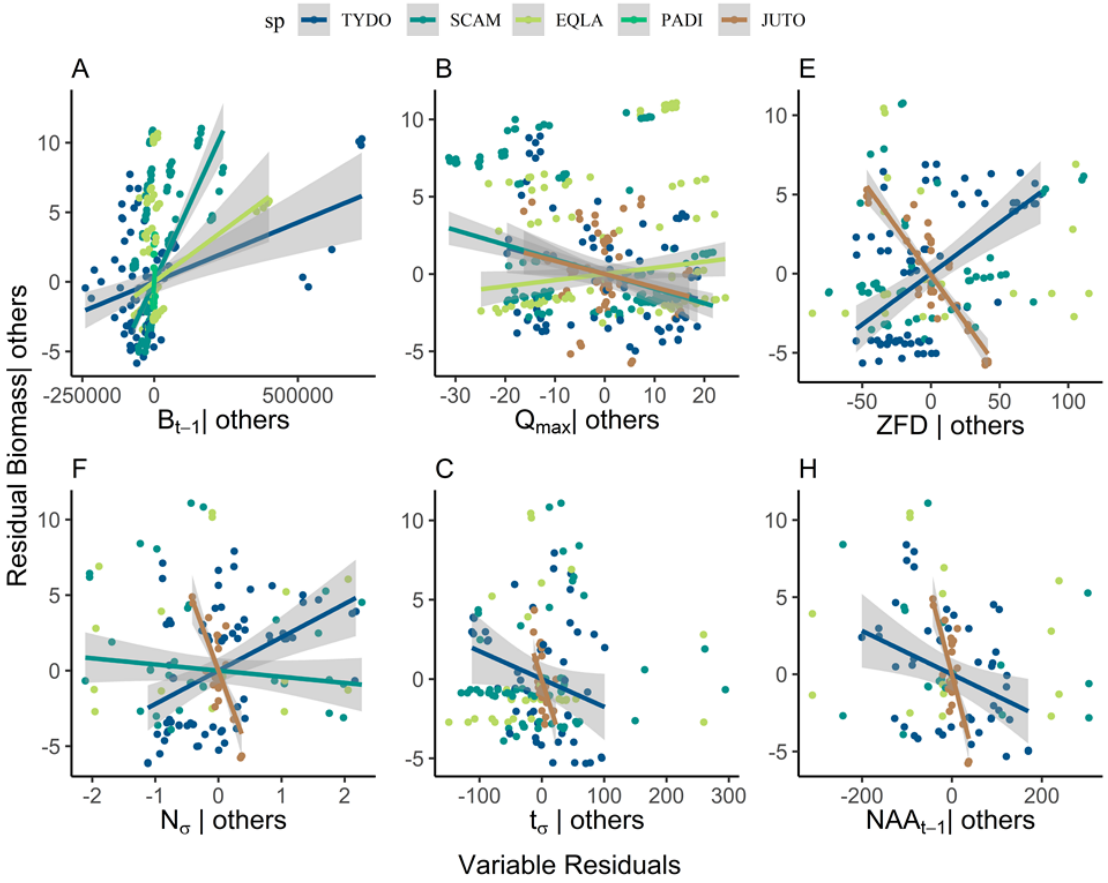

Figure 2.6. Partial regression plots combining the residuals from all of the best fit models (delta AIC < 2) of species-specific (sp) maximum annual biomass from reach data. Points depict the residuals for each modeled variable given while accounting for all other variables in a given model. Trendlines are depicted for all significant relationships, as determined by simple linear regression of the model residuals.

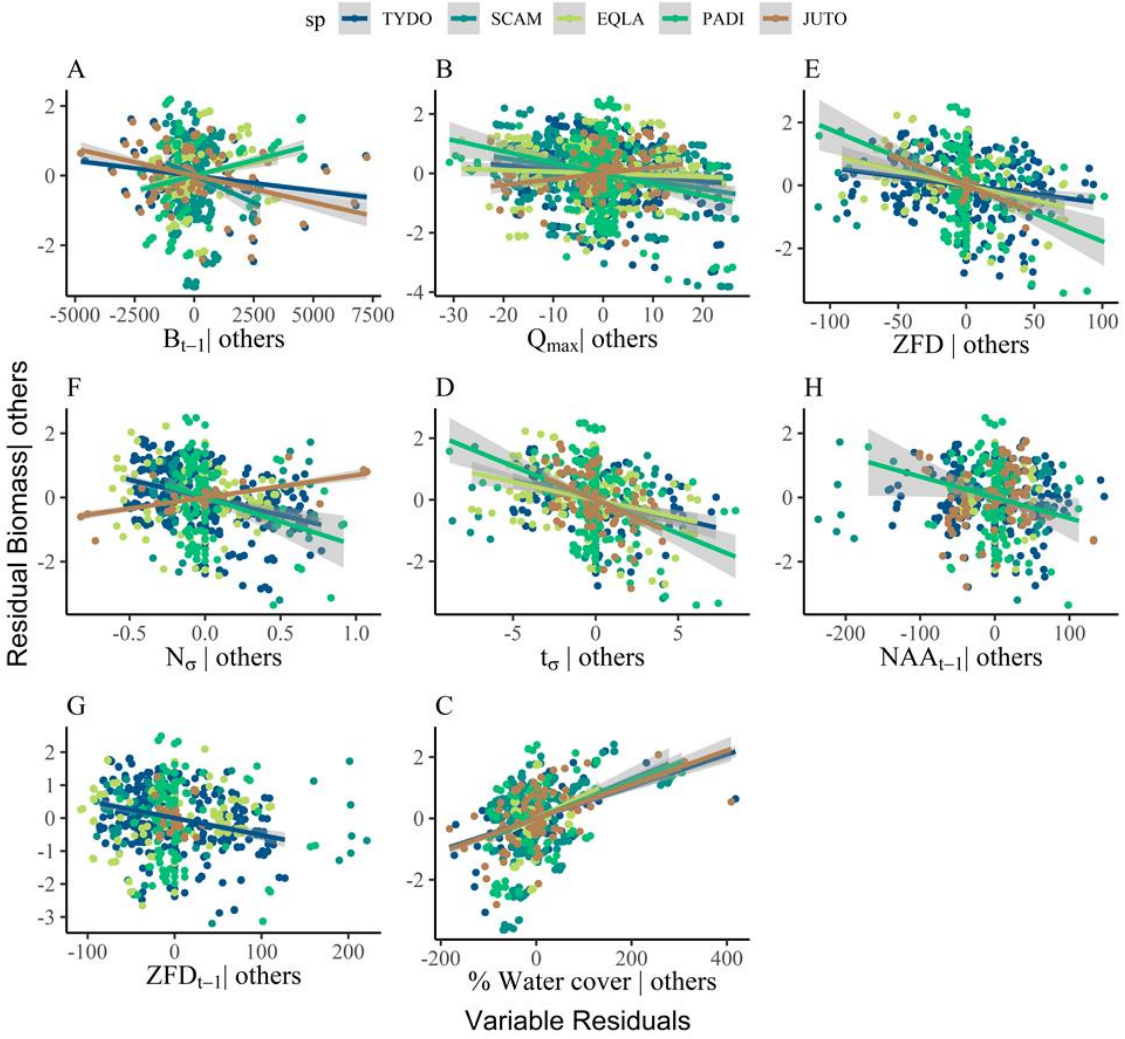

Figure 2.7. Partial regression plots combining the residuals from all of the best fit models (delta AIC < 2) of species-specific maximum annual biomass from the 12K data. Points depict the residuals for each modeled variable given while accounting for all other variables considered in a given model. Trendlines are depicted for all significant relationships, as determined by simple linear regression of the model residuals.

Table 2.7. Added-variable regression results using the 160-m reach scale data and the 12-km section survey data.

		B_{t-1}		NAA_{t-1}		tσ		ZFD		Q_{max}		Nσ		ZFD_{t-1}		wtr		wndw	
		R^2	p	R^2	p	R^2	p	R^2	p	R^2	p	R^2	p	R^2	p	R^2	p	R^2	p
Reach	TYDO	0.181	0	0.113	0.011	0.055	0.057	0	0.307	0.018	0.065	0.177	0						
	SCAM	0	0.342	-0.018	0.508	-0.008	0.49	0.024	0.112	0.128	0	0.006	0.242						
	EQLA	0.076	0	-0.027	0.721	-0.03	0.811	-0.032	0.936	0.017	0.05	-0.03	0.812						
	JUTO	0.078	0.059	0.454	0	0.267	0	0	0.725	0.036	0.04	0.454	0						
Section	ALL	0	0	0	0.64	0.04	0	0.03	0	0.01	0	0.03	0	0	0.01	0.2	0	0.3	0
	TYDO	0.03	0	0	0.52	0.03	0	0.01	0	0.01	0	0.06	0	0.1	0	0.2	0		
	SCAM	0.02	0.74	0.02	0.86	0.01	0.52	-0.14	0.54	0.08	0	0	0.4	0	0	0.1	0	0	0.6
	EQLA	0	0.45	0	0.87	0.05	0	0.05	0	0	0.22	0.01	0.05	0	0	0.1	0	0	0.9
	PADI	0	0.14	0.01	0.04	0.06	0	0.05	0	0.02	0	0.03	0	0.1	>0.001	0.2	0	0	0.8
	JUTO	0	0.21	0	0.7	0.21	0	0.49	0	0.04	0	0.29	0	0.1	0	0.2	0	0.9	0

CHAPTER 3

VEGETATION AFFECTS GREENHOUSE GASES AND ECOSYSTEM METABOLISM OF ARCTIC MIRE THAW PONDS

Introduction

Permafrost thaw is responsible for safeguarding a massive pool of labile carbon in peat (Schuur et al. 2013; Hugelius et al. 2014). Once thawed, permafrost carbon is highly labile, rapidly consumed by microbes, and the products of this microbial metabolism are released as greenhouse gases (Vonk et al. 2013). Ongoing warming at high latitudes has resulted in significant permafrost thaw, freeing the carbon-rich peat (Schuur et al. 2013). This trend has increased greenhouse gas (GHG) emissions and reduced the carbon sink capacity, with substantial implications for global carbon emissions (Schuur et al. 2015). Carbon emissions that result from melting permafrost create an amplifying feedback loop, promoting increased temperature that hastens permafrost thaw, resulting in further rises in carbon emissions and temperature (Zimov et al. 2006). Models of this feedback loop incorporate permafrost carbon dynamics, inhibition of respiration in frozen soil layers, and vertical mixing of soil carbon from the surface to permafrost layers. Combined with increased CH_4 emissions from flooded areas, these changes in carbon cycling in the Arctic portend a shift from a sink to a carbon source by the end of the 21st century (Koven et al. 2011).

In topographically irregular permafrost zones, water from melted permafrost can pool in low-lying areas termed thaw ponds. A recent study of carbon dynamics in thaw ponds in discontinuous permafrost mires of northern Sweden found that CO_2 and CH_4 emissions, which significantly offset the carbon sink capacity of the landscape, were significantly greater in open-water patches devoid of vegetation than vegetated patches (Kuhn et al. 2018). This result suggests vegetation may alter the retention of carbon in these ponds following permafrost thaw. Given the potential impact of permafrost regions on global carbon cycling and the likelihood of more permafrost thaw in the future due to climate change, understanding the changing carbon cycle in these ecosystems is a research priority.

Historical satellite data suggest thaw ponds undergo quasi-cyclic vegetation succession on a roughly decadal scale (Magnússon et al. 2020). Sedges colonize young, open water thaw ponds (termed initial stabilization), which are later dominated by sphagnum mosses (advanced stabilization) that provide infill and substrate for later colonization (and recovery) by woody shrubs. The balance between formation and recovery of thaw ponds may have consequences for the vegetation composition and GHG balance of arctic peatland ecosystems.

Plant communities in permafrost regions are shifting with rising temperature and water availability (Malmer et al. 2005; Johansson et al. 2006). Though, the projected landscape of permafrost zones confronting thaw is uncertain. Arctic functional plant groups have responded predictably to past changes in soil resources, including water and nutrients (Chapin et al. 1996b). Rising temperatures and increased permafrost thaw are also altering the landscape and arctic wetland plants communities. Malmer et al. (2005) demonstrated that permafrost thaw over the last 30 years resulted in an expansion of wet sites dominated by graminoids and contraction of hummock sites and hummock mosses. Other works confirm mosses are expected to react negatively to increasing temperature (Wijk et al. 2004; Walker et al. 2006).

Plant traits differentiating functional groups may help explain carbon patterns on the landscape and reduce or exacerbate projected carbon loss. For instance, root and aerenchyma structures of sedges provide a conduit for microbial CH_4 emissions to escape (Torn and Chapin 1993; Noyce 2011). Conversely, mosses in thaw ponds grow as floating mats and have been shown to provide a physical barrier to gas exchange in terrestrial landscapes (Strack et al. 2016). Mosses decompose more slowly than sedges due to recalcitrant tissue and phenols (Turetsky et al. 2008), whereas sedge root exudation and oxygen leakage may fuel benthic respiration. Incorporating functional group-specific traits can improve model estimates of GHG emissions and the carbon sink capacity of arctic wetlands.

Ecosystem metabolism, including gross primary production (GPP), ecosystem respiration (R), and net ecosystem production (NEP), are commonly used to describe aquatic ecosystem metabolism, which is related to food webs, ecosystem responses, and nutrient cycling. Primary

producers directly contribute to oxygen production and uptake of CO_2 via photosynthesis, whereas plants, microbes, and other biota contribute to oxygen consumption and release of CO_2. Net ecosystem production (NEP) reflects the difference between autotroph production (gross primary production, GPP) and heterotroph consumption (respiration, R) of organic energy. The difference between production and consumption informs whether a system is net auto- or, more likely in the case of arctic wetlands, heterotrophic. This metabolic balance also determines, in part, whether the ecosystem is a source or a sink for carbon with respect to the atmosphere. Net carbon emission from thaw pond systems is the result of net internal production of GHGs in the pond as well as GHG production from the terrestrial system. The relative contributions of internal versus terrestrial production of GHGs in aquatic systems and across biomes is still largely unknown.

This study examined the influence of functionally distinct primary producer groups, moss and sedge, on carbon dynamics and aquatic ecosystem metabolism in arctic mire thaw ponds. Using eight ponds varying along a gradient of relative abundance of moss, sedge, and open water, I related functional group biomass with variation in dissolved GHG (CO_2 and CH_4) in surface and pore water and ecosystem metabolism metrics (GPP, R, and NEP). My objectives were to use these data to explore how different plant functional groups across permafrost thaw ponds influence carbon dynamics and ecosystem energetics.

I expected vegetated ponds to be more metabolically active than open ponds, with functional group-specific traits influencing gas exchange and pond biogeochemical processes that affect the overall carbon balance. Because of slow growth and tough tissues, I expected moss-dominated ponds to exhibit lower GPP and R and less overall metabolic activity than sedge-dominated ponds. While slow growth of mosses makes them less efficient at capturing carbon, slow decomposition and a mat-like growth form that restricts gas exchange may mean that they store carbon more effectively. Conversely, sedges grow faster and decompose more readily, resulting in greater metabolic activity than open water or moss-dominated ponds. Further, I hypothesized that exudation of oxygen from water-logged sedge roots would promote benthic

respiration. Given the combination of faster decomposition, greater benthic respiration, and aerenchyma's capacity to transport gases from the rhizosphere to the atmosphere, I expected abundant sedges to elevate ecosystem respiration and carbon loss from thaw ponds.

Methods

Study site

I selected eight small (43-108 m^2), shallow (10-39 m) thaw ponds across Stordalen Mire (68◦220 N, 19◦030 E) in June 2019, representing a moss, sedge, and open water cover gradient (Table 3.1). Stordalen Mire is a discontinuous permafrost peatland in arctic Sweden. Warming has degraded permafrost in the region, increasing the depth of the active layer and reducing permafrost extent (Åkerman and Johansson 2008). The seasonal freeze and thaw regime causes frost-heaving and an uneven hummock landscape containing water-filled depressions known as thaw ponds. Concurrently, vegetation and carbon dynamics of the mire are changing – including expansion of graminoid-dominated wet sites, increased litter input, and accelerated carbon losses (Malmer et al. 2005).

Plant measurements

I surveyed three to five transects in each pond for macrophyte cover and depth at least one meter apart. Using a 1-m^2 quadrat with a 10x10 reference grid, I estimated the percent cover of sedge, moss, and open water and measured pond depth at each meter along the transect. The mean depth and cover values from each quadrat were aggregated by pond.

I collected plant biomass across a range of cover values. Moss and sedge were harvested at the peat line from 16 0.25-m^2 quadrats across seven different ponds, so as not to disturb other research groups' equipment in my monitored ponds. Depth was measured in each quadrat. Green biomass within the quadrat was collected in bags and laid out on newspaper in a drying room overnight before drying in an oven at 60 ^oC for 48-hours. Samples were weighed directly out of the oven to minimize moisture. The relationship between biomass per m^2 and the

relative cover of each vegetation type was calculated using regression (Appendix A). Pond-level relative cover derived from transects, or the average relative cover per quadrat, were fitted to the biomass-relative cover regression to estimate biomass per area for each pond.

$$B_{moss}=\beta_{\overline{moss,\ cover}}+\beta_{\bar{z}} \quad \text{(Eq. 2.1)}$$

$$B_{sedge}=\beta_{\overline{sedge,\ cover}} \quad \text{(Eq. 2.2)}$$

Carbon gases

Triplicate water samples were collected from sediment (pore) and surface water from each pond in a single day (July 9th, 2019) over a three-hour period (11:00 – 14:00 CET). A sipper and syringe sampled pore water at 20-cm peat depth. 30-mL water samples were collected in 60-mL syringes, filled with 30 mL of atmospheric air, and immediately shaken to equilibrate the water sample and headspace. The equilibrated headspace was transferred to a crimped and vacuumed 20-mL serum vial with rubber septa and sealed with silicone caulking to prevent leakage. Samples were transported via airplane from Stockholm, Sweden, to Phoenix, AZ, USA, and stored at room temperature and pressure for approximately 2 - 4 weeks before analyzing on a gas chromatograph (GC). Gas concentrations (CO_2 and CH_4) at the time of collection were calculated using Henry's law for ideal gases (Cole et al. 2010) modified to account for atmospheric air in the headspace. Headspace partial pressure in atm (~ L gas/L volume) was converted to µmoles gas/L for Ideal Gas Law calculations (PV = nRT), where V is 1 L, P is the measured partial pressure in atm, R is the constant 0.0821 L·atm $mole^{-1}$ K^{-1}, and T is the STP temperature in kelvins (273.15).

$$C_{gas}=n/V=(P/RT)\left(10^6 \mu moles/mole\right) \quad \text{(Eq. 2.3)}$$

The equilibrium concentration of each gas dissolved in the liquid phase (C_{liq}) was calculated by multiplying its partial pressure in the gas phase (P_{gas} in atm) by the Bunsen solubility coefficient (β):

$$C_{liq}=P_{gas}\times b_T\times P_{Barometric}\cdot\beta_T\cdot P_{Barometric} \quad \text{(Eq. 2.4)}$$

The original gas concentration, C^0_{liq} (µM), was calculated using a mass-balance equation

modified to account for the source headspace gas

$$C^0_{liq} = \frac{C_{liq}V_{liq} + C_{gas}V_{gas} - C_{source\ gas}V_{source\ gas}}{V^0_{liq}} \quad \text{(Eq. 2.5)}$$

Floating chambers, equipped with CO_2 sensors (ELG, SenseAir), measured the rate of CO_2 emission from each pond (Bastviken et al. 2015). Floating chambers were placed on the pond surface over patches representative of the pond's dominant cover, vegetation (moss, sedge) or open water, in each pond over for five minutes. The flux rate from water to air was calculated from the rate of change in CO_2 concentration over time. These values were then related to biomass and pond characteristics. Unfortunately, there were technical difficulties with the chamber on S1, data were lost, and I could not calculate the rate of CO_2 flux for that pond.

Metabolism

Oxygen loggers (miniDOT, Precision Measurement Engineering) were placed at a depth of 10 cm in each of the eight selected ponds for two weeks (July 4th – July 20th, 2019) to measure diel dissolved oxygen (DO mg L^{-1}) concentration and temperature. Photosynthetic radiation (PAR; umol m^{-2} s^{-1}) and wind speed (m s^{-1}) data for Stordalen Mire were obtained by the Integrated Carbon Observation System (ICOS). K_{600} was modeled from pond surface area and wind speed (Vachon and Prairie 2013). Pond metabolism was modeled using the maximum likelihood estimation (MLE) model in the LakeMetabolizer R package (Winslow et al. 2016). DO (α; mg O_2 L^{-1}) dynamics were calculated using incoming light (I; arbitrary light units; e.g., µmol m^{-2} s^{-1}), the average rate of respiration per natural log of water temperature (ρ), and the natural log of water temperature (log_e T; °C) at the DO observation depth. Net ecosystem production (NEP; mg O_2 m^{-2} d^{-1}) was calculated by summing gross primary production (GPP_t; mg O_2 m^{-2} d^{-1}), calculated as a function of incoming light and rates of production per incoming light (ı) over time, and ecosystem respiration (R_t; NEP mg O_2 m^{-2} d^{-1}), calculated as a function of temperature (log_e -T_t) and temperature-dependent rates of respiration (ρ) over time. Days in which metabolism estimates were outside the realistic range (GPP < 0 and R > 0) were discarded. The absolute

value of R, which is typically expressed as a negative quantity, was included in statistical analyses to avoid sign issues.

$$\alpha_t=\alpha_{t-1}\times I_{t-1}+\rho\times\log_e T_{t-1}+F^*_{t-1}+\varepsilon_t(2) \quad \text{(Eq. 2.6)}$$

$$F^*_t=\frac{k_t\times\Delta t}{z_t}\times\left(O_{s,t}-\alpha_t\right)(12) \quad \text{(Eq. 2.7)}$$

$$NEP_t\times\Delta t = \text{ı}\times I_t+\rho\times\left(\log_e-T_t\right)(13) \quad \text{(Eq. 2.8)}$$

$$GPP_t\times\Delta t = \text{ı}\times I_t(14) \quad \text{(Eq. 2.9)}$$

$$R_t\times\Delta t = \rho\times\left(\log_e-T_t\right)(15) \quad \text{(Eq. 2.10)}$$

Analyses

Pond surface area was estimated from pond width along transects and measured pond length. Depth was calculated as an average of depth measurements collected every meter along the transects. The percentage cover of moss, sedge, and open water for each pond was calculated as the average percent cover per quadrat.

Multi-model inference analyses and model selection of multiple linear regressions were used to evaluate the influence of dominant plant functional groups on dissolved CO_2 and CH_4 concentrations in pore and surface water (µmol CO_2 or CH_4 $m^{-2}d^{-1}$), and aquatic metabolism (mg O m^{-2} d^{-1}). I used the glmulti package in R (Calcagno and De Mazancourt 2010) to run model selection and multi-model inference statistics, including model-averaged importance of explanatory variables. Global models for each independent variable tested included moss biomass, sedge biomass (g/m^2), surface area (m^2), and depth (cm) as explanatory variables. GPP's global model also included dissolved CO_2 concentrations in pore and surface water aggregated to a mean value per pond, considering the potential for CO_2 limitation. Given my limited number of observations, gas evasion (µmol CO_2 $m^{-2}d^{-1}$) was modeled separately using only biomass and the proportion of pore to surface water dissolved gas concentrations.

Pearson correlation coefficients, r, were calculated for the full matrix of explanatory and response variables: mean moss biomass, mean sedge biomass, surface area, mean depth, $CO_{2,\,pore}$, $CO_{2,\,surface}$, $CH_{4,\,pore}$, and $CH_{4,\,surface}$. Pearson's r values were evaluated using conventional

correlation size categories: 0.1 - 0.3 small correlation, 0.3 - 0.5 medium correlation, 0.5 - 1.0 strong correlation). Thaw pond metabolism was evaluated similarly using model selection and Pearson r correlations.

Most ponds contained a mix of moss and sedge biomass, and model results included multiple significant explanatory variables. I used partial regression to evaluate the relationship of each dependent variable separately. For example, to assess the relationship between moss and GPP separate from sedge and other model variables, I analyzed the residuals of the best fit linear models ($\Delta AIC < 2$) for GPP as a function of other model variables sans moss ("| others"), and residuals of the best fit linear models of moss as a function all other model variables ("| others"). The result is the relative relationship between moss biomass and GPP incorporating all the best fit model results while collapsing variation due to other variables included in those models.

Results

Pond characterization

Ponds were shallow (mean z = 10 to 39 cm) and ranged in surface area from 53 m^2 to 304 m^2. Biomass represented a gradient of sedge and moss cover across the study ponds (Figure 3.1, Table 3.1). Very few ponds contained no sedge biomass, as sedges occurred just along the pond edges in moss and open water-dominated ponds. Sedge biomass negatively correlated with pond depth ($R^2 = 0.30$, $P << 0.001$, $r = -0.55$). Moss biomass was uninfluenced by pond depth or surface area.

Dissolved carbon gases

Dissolved gas concentrations were substantially higher in pore water (CO_2 166.9±100.7 mg/m^3, CH_4 220.7±60.7) than in surface water (CO_2 12.9±9.1 mg/m^3, CH_4 13±60.6), and highly variable (Table 3.1). Concentrations of CO_2 and CH_4 in pore water were weakly associated (R^2 =

0.14, P < 0.001, r = 0.39), but no relationship was observed between CO_2 and CH_4 concentration in surface water.

Sedge and moss biomass influenced CO_2 concentrations in pore and surface water differentially (Figure 3.2, Table 3.4). CO_2 concentration in pore-water (best fit model, P =0.01, R^2 = 0.28) was best explained by sedge biomass (P = 0.04, r = 0.45, Table 3.2 and 3.3) and surface area (P = 0.02, r = - 0.40). Surface-water CO_2 concentration was best explained (best fit model, P= 0.02, R^2 = 0.23, Table 3.3) by moss biomass (P = 0.03, r = 0.41) and pond depth (P = 0.02, r = 0.39, Figure 3.3A). CH_4 concentrations in both pore and surface water (best fit model P = 0.12, R^2 = 0.06 and P = 0.03, R^2 = 0.13, respectively) were weakly related with depth alone (best fit model P = 0.12, r = 0.32 and P = 0.03, r = 0.42, respectively).

Metabolism

Lake metabolism varied as a function of plant biomass (Figure 3.3**)**. GPP was lowest in ponds with little vegetation (O1, O2) and was highest and most variable in M2 and S2. R was elevated in ponds with sedge (S1, S2, and M2) than in open-water-(O1, O2,). NEP was strongly negative in three ponds (S1, S2, and O2) and trended near-zero to slightly positive in M1, M2, and O1. Ponds S1 and S2's greater R and more negative NEP values likely contribute to their higher CO_2 concentration.

The best fit model of GPP (P << 0.001, R^2 = 0.50) included moss biomass (P = 0.10, r = 0.42, Figure 3.4A), depth (P > 0.001, r = -0.47) and $CO_{2,\ pore}$ (P > 0.001, r = -0.47) as significant explanatory variables (Table 3.5 and 3.6). Other dissolved gases, $CO_{2,\ surface}$, $CH_{4,\ pore,}$ and $CH_{4,\ surface,}$ were moderately correlated with GPP (r = -0.34, -0.41, and -0.15, respectively). Surface area and depth exhibited medium-sized effects (r = 0.45 and -0.47, respectively) but were not included as significant variables in model analyses.

R was related to sedge biomass and dissolved gas concentrations. Multi-model inference analyses of R converged on two models. Both the best and second best fit models (both P << 0.001, R^2 = 0.65 and R^2 = 0.65, ΔAIC = 1.37, respectively) included sedge (P = 0.007, r =0.42),

surface area (P = 0.031, r =0.09), and depth (P << 0.001, r =-0.77) as significant explanatory variables. Moss biomass was marginally significant in the best fit model (P = 0.095) but did not correlate strongly with R (r = -0.09).

Model selection for NEP converged on a single best fit model (P << 0.001 , R^2 = 0.72, second best ΔAIC = 5.9). The best fit model included moss (P << 0.001 , r = 0.32) and sedge (P = 0.010, r = -0.60) biomass, surface area (P = 0.031, r = 0.36), and average depth (P << 0.001 , r = 0.59). Results from a separate, simple linear regression on the relationship between rates of NEP and evasion suggest NEP may be negatively related to CO_2 evasion (P = 0.10, R^2 =0.53); however, this relationship is driven by the single high CO_2 evasion rate and highly negative average NEP rate observed in Pond S2 and relatively few observations (n=5).

Gas evasion

CO_2 gas evasion ranged from 450 - 2116 mmol m^{-2} d^{-1} and was elevated in ponds with high sedge biomass. Open water dominated ponds exhibited the lowest rates of CO_2 evasion. The best-fit model of gas evasion (R^2= 0.73, P << 0.001) included sedge and moss biomass as significant explanatory variables (P << 0.001 for both variables, Figure 3.5A). A model with 2 Δ AIC included the concentration gradient of CO_2 in pore water and surface water (P << 0.001), as well as plant biomass. CO_2 evasion was also significantly, negatively correlated with NEP (P << 0.001, R^2 = 0.57) and R (P = 0.001, R^2 = 0.53), and exhibited a weak, marginally significant relationship with GPP (P = 0.055, R^2 = 0.14).

Discussion

Rising temperature and thawing permafrost are transforming arctic landscapes. While numerous studies predict large-scale shifts in arctic vegetation, the consequences of shifting vegetation on carbon and energy dynamics remain ambiguous. This study examined the influence of two dominant plant functional groups expected to expand or contract with thawing permafrost, mosses and sedges, on arctic thaw pond metabolism and carbon dynamics.

Thaw pond carbon dynamics and metabolism differed based on functional group biomass and pond morphological characteristics. Gas flux from ponds, CO_2 concentration in pore water, and R increased with sedge biomass, indicating an apparent positive influence on carbon loss. Sedge-dominated ponds had higher average rates of GPP compared to open-water-dominated ponds. Moss-dominated ponds presented greater GPP than sedge ponds. Still, daily NEP in moss ponds fluctuated between positive and negative. The increased surface-water CO_2 concentration observed in moss ponds may result from the trapping of gases below floating moss mats.

Sedges intensify carbon loss

I found CO_2 evasion was greater in sedge-dominated, relative to moss-dominated, ponds. Previous studies have demonstrated that sedges increase evasion because aerenchyma act as a conduit for gas release (Torn and Chapin 1993; Greenup et al. 2000; Noyce et al. 2014). Interestingly, Kuhn et al. (2016) found open-water ponds had significantly higher rates of CO_2 evasion than vegetated ponds, whereas, in my study, evasion correlated positively with sedge biomass. Ponds with little biomass experienced lower evasion. Two differences between the Kuhn et al. study and my study may explain these contrasting results. First, whereas Kuhn et al. monitored thaw ponds over 14 weeks, my study represents a snapshot of gas concentrations at a single point in time and metabolism over several days. My gas concentrations are intended to represent relative differences between ponds, and do not correspond directly to the metabolism estimates. Daily variation in temperature and wind would also affect gas concentrations over the period metabolism was measured. Second, the two years these studies were performed differed in temperature (high temperature in June 2015 was 20 ˚C whereas the high temperature in Jun 2019 was 27 ˚C). Higher temperature potentially resulted in greater plant growth and respiratory activity, intensifying the influence of vegetation.

Sedge roots were positively related to carbon gas in the rhizosphere. Hydrophilic plant roots have been shown to increase the oxygen concentration in their root zone via exudation or

transpiration of oxygen-depleted water (Sand-Jensen et al. 1982; Thursby 1984; Kemp and Murray 1986; Dodds et al. 2017). In addition to root respiration, increased oxygen in pore water can boost methane oxidation, further increasing CO_2 concentration. Sedges are also more labile and decompose faster than mosses, whose tissues have anti-microbial properties which slow their decomposition (Banerjee and Sen 1979; Verhoeven and Toth 1995; Basile et al. 1999; Turetsky et al. 2012). Hence, sedges' greater lability may also contribute to increased CO_2 in pore water. Disentangling the mechanism for increased CO_2 concentration in pore water will require additional mesocosm studies.

Mosses contribute to carbon retention

Moss's prostrate growth form was expected to provide a blanketing effect and reduce gas exchange, as observed in terrestrial systems (Turetsky et al. 2012). I found gas evasion was positively correlated with moss biomass, but the slope of the effect of moss on evasion was much shallower than that of sedge biomass. Moss biomass also was associated with increased surface-water CO_2 concentration. If I assume most decomposition occurs in the benthic zone, the effect of moss on surface-water CO_2 concentration and the relatively smaller gas evasion from moss ponds, compared to sedge ponds, may be attributable to moss providing a barrier for gas exchange. Further, while moss is slow-growing, it is to also slow to decompose. Moss tissue is generally more recalcitrant and contains anti-microbial phenols, the combination of which reduces decomposition rates. Slower decomposition rates of mosses indirectly influence gas evasion by retaining carbon in biomass longer. Additionally, I found a positive relationship between pond GPP and moss biomass.

Diverging effects on NEP

Metabolism estimates presented here are based on in-pond metabolism. Emergent plants, like sedges, can complicate estimates of GPP, as much of their production occurs outside of the water. Mosses here are mainly submerged, with only a few centimeters emerging over the

surface of the pond. Differences between submergent and emergent vegetation may explain why moss biomass has a more significant effect on GPP than sedge biomass. Even though emergent plants, like sedges, may not directly affect GPP, they can promote greater R through the input of organic matter and root actions (root respiration, O_2 leakage).

The relationship between functional group-specific biomass and NEP is complex. Simple linear regressions of NEP as a function of moss or sedge biomass yield divergent effects, wherein NEP increases with moss and decreases with sedge. Moreover, sedge-dominated ponds tended to have higher rates of R and lower NEP. However, when the effects of pond depth, surface area, and moss biomass are filtered out (via partial regression), sedge biomass exhibited a significant, positive relationship with NEP. Given the correlation between sedge distribution and pond depth (sedges prefer shallow ponds), further studies are needed to disentangle the interactions between sedge, pond morphology, and NEP.

My results suggest that sedges may boost R via two potential mechanisms: raising rhizosphere oxygen and increasing organic matter inputs. Increased oxygen from sedge roots in the otherwise anoxic rhizosphere has been shown to promote methane oxidation (Bhullar et al. 2013), and consequently, benthic respiration. This is consistent with the higher concentration of CO_2 observed in sedge-dominated ponds. The positive relationship between sedge biomass and pore-water CO_2 may also be attributable to the greater lability of sedges than mosses or the higher organic-matter content of sediments compared to sparsely vegetated ponds. Sedge-dominated ponds exhibited a great deal of variation in GPP. Yet, the promotion of increased R and more negative NEP supports the notion that a rising dominance of sedges would in significant carbon loss from thaw pond systems.

By comparison, mosses had only a moderate effect of increasing GPP and NEP, with little impact on R. The lack of relationship between R and moss biomass may be explained by prolonged decomposition rates in these ponds. While moss-dominated ponds contain more organic matter than open water-dominated ponds, moss biomass is fairly recalcitrant and decomposes slowly. Hence, microbial respiration in moss-dominated ponds should be lower than

sedge dominated ponds, whose tissue is relatively less recalcitrant. Moss ponds, while more productive, have similar NEP rates (near zero to slightly positive) to less metabolically active open-water ponds. Combining trapping CO_2 in the pond and increasing GPP and positive NEP, moss biomass provided primarily positive effects on the carbon sink of ponds relative to sedge biomass.

Vegetation can also act as a substrate for epiphytic algae, which can have opposing effects to that of the vegetation. On the one hand, promoting algae growth increases the rate of GPP. However, epiphytic algae can shade plants and reduce access to light, limiting production by submergent plants and benthic algae (Asaeda et al. 2004). It is unclear how much the relationships observed here between vegetation and metabolism are attributable to epiphytic algae.

Landscape implications

Sedge abundance is restricted by depth, and hence its future abundance will be moderated by topography and changes in water depth across the landscape. While sedges are flood-tolerant, they are not submergent. In contrast, mosses are not limited by depth and thrive on the moist pond edges and as thick floating mats in deeper ponds. However, mosses are expected to react negatively to increasing temperature (Wijk et al. 2004; Walker et al. 2006). Consequently, the landscape's topography and climate will likely control thaw-pond abundance, morphology, and plant communities. Permafrost thaw resulting in deeper ponds favors the proliferation of mosses provided temperatures remain moderate, while numerous shallow ponds and warming favor sedges over mosses.

The landscape of permafrost zones confronting thaw undergoing significant change. Malmer et al. (2005) demonstrated that permafrost thaw over the last 30 years resulted in an expansion of wet sites dominated by graminoids and contraction of hummock sites and hummock mosses. These changes in vegetation composition have big implications, including significant inputs to the litter pool, decreased soil stability, and increased erosion, thus fueling greater microbial

respiration. Thus, despite the increased productivity in thawing permafrost mires, which contributes to the atmospheric CO_2 sink function, these sites may ultimately become significant carbon sources to the atmosphere owing to increased CH_4 emissions (Johansson et al. 2006). Suppose thawing permafrost continues to drive wet-site sedge expansion. In that case, I expect greater rates of greenhouse gas evasion due to aerenchyma-driven gas exchange, and increased decomposition. However, considerable increases in precipitation in the Arctic are projected over the next century (Bintanja 2018). If the combination of permafrost thaw and increased precipitation results in increasingly deep thaw ponds, mosses would have a competitive advantage over depth-limited sedges. While moss-pond gas evasion and NEP may not be substantially different from non-vegetated ponds, they are significantly different from sedge-dominated ponds (lower evasion and higher NEP). They are ultimately more effective in retaining carbon than sedges.

Internal production of CO_2

While the contributions of inland waters to global carbon emissions are known to be substantial (Raymond et al.; Cole et al. 2007), the degree to which net C exchange of thaw ponds is the result of internal aquatic metabolism, relative to the input of GHG from soils, is less apparent. While this study was not designed to directly test the relative contributions of aquatic versus terrestrial CO_2 production, my data do provide some insights for this system.

Aquatic metabolism contributes to net CO_2 emissions when NEP is negative, as this is when ecosystem respiration is greater than gross primary production due to aquatic mineralization of terrestrial carbon. The relative proportion of CO_2 emissions due to internal production in aquatic systems can be estimated by dividing negative daily NEP rates (as positive NEP indicates net CO_2 storage) by the CO_2 flux (Hotchkiss et al. 2015). Using my negative daily NEP rates and single measurements of CO_2 flux, I calculated daily estimates of internal production of CO_2 within my study ponds using days with negative NEP values.

$$\% \text{ Internal production} = -NEP / CO_{2,\text{ emission}} \quad \text{(Eq. 2.11)}$$

Based on these estimations, internal production of CO_2 ranged from 0.3 – 23% (mean = 10.2%, sd = 7.3%) during the study period. Pond O1, which contained substantially less macrophyte biomass than my other study ponds, exhibited significantly greater internal production of CO_2. (Tukey HSD $p > 0.02$). Conversely, Pond M2, which contained the greatest overall and moss biomass, exhibited the lowest relative internal production of CO_2, though these rates were not significantly different from Ponds O2, M2, or S2.

I also related my estimates of internal production to moss and sedge biomass in each pond (Figure 3.6). These data suggest a negative relationship between internal production of CO_2 and biomass, though the relationship is driven by the high internal production and low biomass of Pond O2. When I examined the relationship between internal CO_2 production and moss and sedge biomass separately, moss biomass also demonstrated a significant, negative relationship with internal production ($p = 0.009$, $R^2 = 0.28$), while sedge biomass did not ($p = 0.17$, $R^2 = 0.05$). While these analyses are flawed (small N of gas samples), the negative trend suggests moss is associated with reduced production of CO_2 in the pond and is consistent with the positive relationship I observed between moss biomass and GPP. Moss biomass in associated with greater CO_2 consumption of via GPP and reduced production of CO_2 in the pond.

Conclusion

Primary producers have diverse impacts on carbon dynamics and ecosystem metabolism in arctic thaw pond ecosystems. These impacts are attributable to functional group-specific traits of dominant thaw pond primary producers: sphagnum moss and sedges. Broadly, sedges increase carbon evasion via aerenchyma, increase CO_2 concentration in pore-water via the promotion of methane oxidation and decomposition, promote greater ecosystem respiration, and positively influence carbon gas evasion (Figure 3.7). Moss ponds had higher GPP but exhibited NEP rates similar to non-vegetated, less metabolically active ponds; however, they may trap gases and effectively prevent evasion. Although this study highlights functional differences between mosses and sedges broadly, further examination of variation in effect traits, inter- and

intra- species, and over time, is needed to fully understand the impact of tundra-thermokarst regime shifts on carbon dynamics and metabolism in the arctic.

Tables and figures

Table 3.1. Pond characteristics, including percent cover (cover), surface area (SA), average depth (z), the average and standard deviations of CO_2 and CH_4 concentrations, and CO_2 flux. Ponds were named based roughly on dominant plant cover – M1 and M2 are dominated by moss; S1 and S2 are dominated by sedge; X1 and X2 are dominated by a mix of moss and sedge; O1 and O2 are largely open water.

Pond	Cover			SA (m_2)	z (cm)	CO_2 (mg/m^3)		CH_4 (mg/m^3)		Flux $_{CO2}$ (mg/m_3 min^{-1})
	Moss	Sedge	Open			Pore	Surface	Pore	Surface	
X1	61	32	1.2	180	26	69.3 ±93.4	26.4 ±0	78.7 ±80.3	3.2 ±0	4.38
M1	77	10	5	71	38	665.7 ±394	23.6 ±8.7	293.6 ±76.1	68.6 60.6	3.69
S1	0	58	37	115	18	328.2 ±219.5	0.5 ±0.4	657.0 ±25.9	2.3 ±2.8	-
S2	39	52	1	53	10	27.8 ±12.2	9.0 ±12.1	193.2 ±130.8	1.7 ±0.3	9.55
M2	67	15	9	304	18	20.4 ±1.5	2.1 ±0.1	4.3 ±0.5	8.3 ±8.6	3.78
X2	64	15	1	47	11	32.7 ±28.4	1.9 ±0.4	362.0 ±22.2	0.1 ±0	2.08
O1	0	2	97	114	38	68.1 ±37.4	29.4 ±40.3	113.8 ±66.9	2.7 ±1.8	2.02
O2	0	30	70	120	39	122.7 ±19.8	10.3 ±1.6	63.4 ±84.9	17.4 ±18.1	2.62

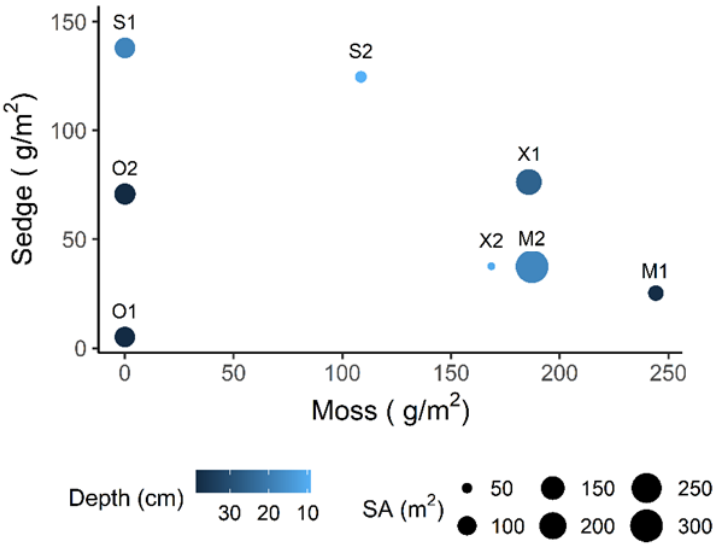

Figure 3.1. Gradient of dominant primary producer biomass and pond morphology across experimental thaw ponds. Moss and sedge biomass per pond calculated using percent cover data from surveys and biomass-cover relationships from biomass harvest data. Points labelled with pond ID indicating the dominate cover type based on preliminary categorization: Sedge (S), Moss (M), open (O), mixed moss and sedge (X). Point size denotes the surface area of the pond whereas point color denotes the average pond depth.

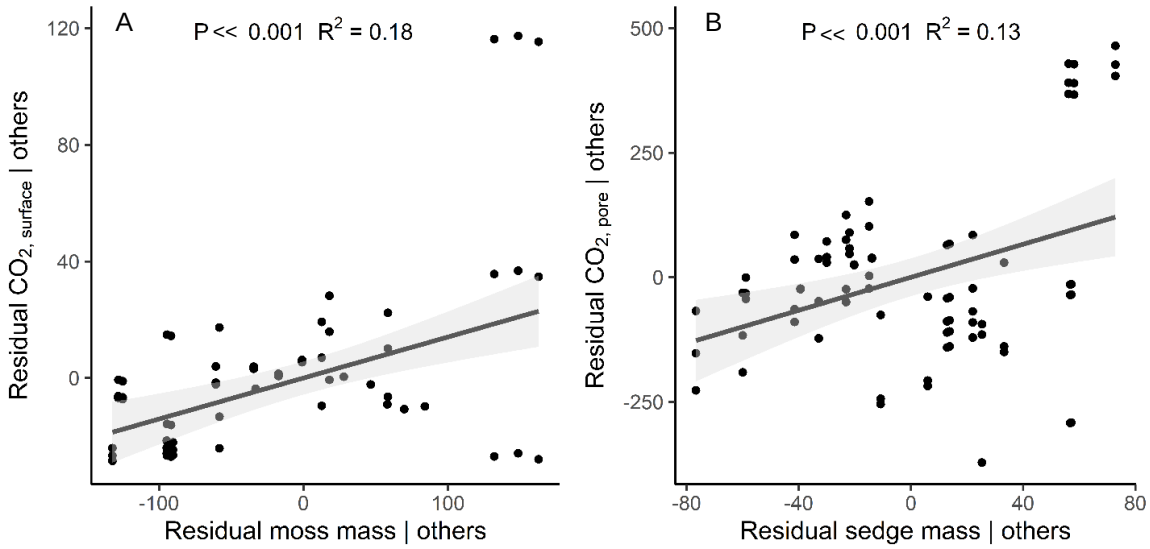

Figure 3.2. Partial regression plots of residuals from the best fit models of dissolved CO_2 in pore and surface water as a function of moss and sedge biomass. Best fit models of dissolved CO_2 concentrations in surface water (n=3) exhibited a significant, positive relationship with moss biomass. Best fit models of dissolved CO_2 concentrations in pore water (n=3) exhibited a significant, positive relationship with sedge biomass.

Table 3.2. Pearson r correlation coefficients for dissolved carbon gases in thaw ponds

	SA	z	Moss	Sedge	$CO_{2,\ pore}$	$CH_{4,\ pore}$	$CO_{2,\ surf}$	$CH_{4,\ surf}$
SA		0.06	0.00	-0.10	-0.40*	-0.18	-0.09	-0.05
z	0.06		-0.12	-0.55**	-0.33*	0.32*	0.39*	0.42*
Moss	0.00	-0.12		-0.35*	-0.12	0.22	0.41*	0.08
Sedge	-0.10	-0.55**	-0.35*		0.45*	-0.04	-0.28	-0.32*
$CO_{2,\ pore}$	-0.40*	-0.33*	-0.12	0.45*		0.39*	-0.03	-0.23
$CH_{4,\ pore}$	-0.18	0.32*	0.22	-0.04	0.39*		0.40*	0.10
$CO_{2,\ surf}$	-0.09	0.39*	0.41*	-0.28	-0.03	0.40*		0.18
$CH_{4,\ surf}$	-0.05	0.42*	0.08	-0.32*	-0.23	0.10	0.18	

* r > 0.3 ** r > 0.5

Table 3.3. Best fit model results for dissolved carbon gas measurements from multimodel comparison. Models less than 2 Δ AIC from the lowest model AIC were considered equally good fit. Stars indicate variables that were significant explanatory variables in the linear model – Moss mass (M), sedge mass (S), pond surface area (SA), and average pond depth (z). Linear model R^2, p value, AIC weight, and Δ AIC.

Model	M	S	SA	z	R2	p	wt	ΔAIC
$CO_{2,\ pore}$ ~ 1 + S + SA		*	*		0.28	*	0.30	
$CO_{2,\ pore}$ ~ 1 + S + SA + z			*		0.26	*	0.14	1.57
$CO_{2,\ pore}$ ~ 1 + M + S + SA		.	*		0.25	*	0.11	1.97
$CO_{2,\ surf}$ ~ 1 + M + z	*			*	0.23	*	0.31	
$CO_{2,\ surf}$ ~ 1 + M + SA + z	*			*	0.23	*	0.19	0.95
$CO_{2,\ surf}$ ~ 1 + M + S + z	*			*	0.20	*	0.14	1.63
$CH_{4,\ pore}$ ~ 1 + z					0.06		0.12	
$CH_{4,\ pore}$ ~ 1 + SA + z					0.07		0.10	0.46
$CH_{4,\ pore}$ ~ 1 + M + S + SA + z				*	0.13		0.09	0.57
$CH_{4,\ pore}$ ~ 1					-	*	0.09	0.63
$CH_{4,\ pore}$ ~ 1 + M + S + Z				*	0.09		0.09	0.72
$CH_{4,\ pore}$ ~ 1 + M + Z				.	0.06		0.08	0.78
$CH_{4,\ pore}$ ~ 1 + M + SA + Z				.	0.09		0.08	0.83
$CH_{4,\ pore}$ ~ 1 + S + Z					0.04		0.06	1.45
$CH_{4,\ pore}$ ~ 1 + SA					0.00		0.06	1.46
$CH_{4,\ pore}$ ~ 1 + M					-0.01		0.05	1.91
$CH_{4,\ pore}$ ~ 1 + S + SA + Z				.	0.05		0.05	1.95
$CH_{4,\ surf}$ ~ 1 + Z				*	0.13	*	0.26	
$CH_{4,\ surf}$ ~ 1 + M + Z				*	0.13	.	0.15	1.16
$CH_{4,\ surf}$ ~ 1 + S + Z				.	0.10		0.10	1.91
$CH_{4,\ surf}$ ~ 1 + SA + Z				*	0.10		0.10	1.99

*** P < 0.0001 ** P < 0.001 * P < 0.05 . P < 0.10

Table 3.4. Multi-model inference statistics for dissolved C gases. Each model statistic, including the estimate (Est), standard error (se), z value, p value, low and high confidence intervals (CI_{low}, CI_{high}), and importance (Import), is calculated via weighted averages across all models in which the variable appears.

	Variable	Est	se	z value	p value	ci_{low}	ci_{high}	Import
$CO_{2,\ pore}$	SA	-1.09	0.6	-1.81	0.07	-2.27	0.09	0.88
	Sedge	1.11	1.08	1.03	0.3	-1	3.21	0.67
	z	-1.61	2.78	-0.58	0.56	-7.05	3.83	0.42
	Moss	-0.07	0.19	-0.36	0.72	-0.43	0.3	0.31
$CO_{2,\ surf}$	z	1	0.64	1.57	0.12	-0.25	2.25	0.84
	Moss	0.11	0.08	1.43	0.15	-0.04	0.26	0.8
	SA	-0.02	0.04	-0.5	0.62	-0.11	0.06	0.36
	Sedge	0	0.06	0.07	0.94	-0.12	0.13	0.32
$CH_{4,\ pore}$	z	5.98	5.79	1.03	0.3	-5.37	17.32	0.68
	Moss	0.32	0.49	0.66	0.51	-0.64	1.28	0.46
	SA	-0.39	0.6	-0.65	0.52	-1.56	0.79	0.45
	Sedge	0.44	0.95	0.47	0.64	-1.42	2.31	0.38
$CH_{4,\ surf}$	z	0.5	0.38	1.33	0.18	-0.24	1.24	0.78
	Moss	0.01	0.02	0.46	0.64	-0.03	0.05	0.34
	Sedge	-0.01	0.04	-0.32	0.75	-0.1	0.07	0.32
	SA	0	0.01	-0.15	0.88	-0.03	0.02	0.27

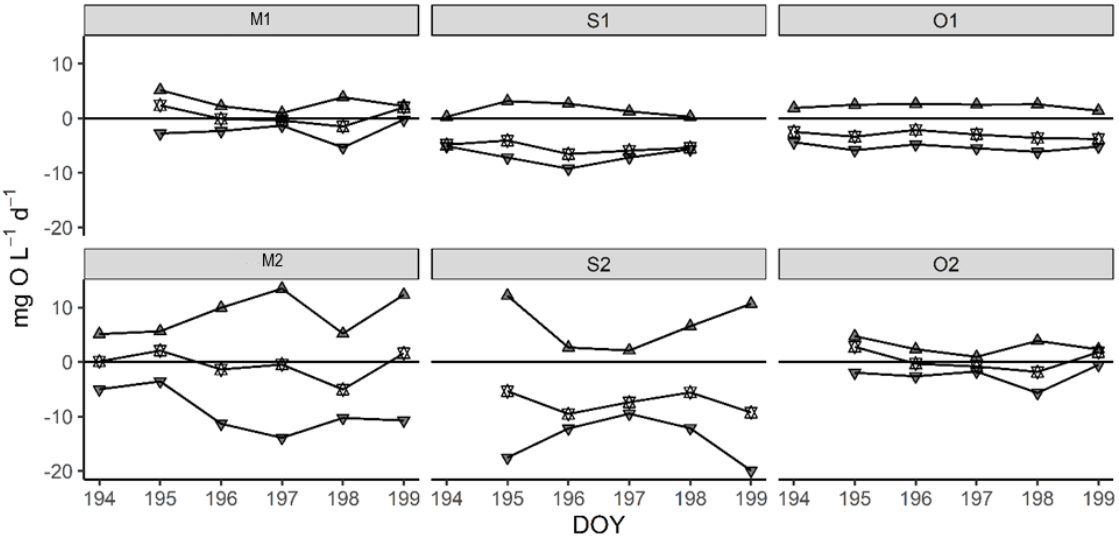

Figure 3.3. Pond metabolism between day of year (DOY) July 13^{th,S} (194) and July 18^{th,} (199) 2019, across six ponds representing moss- (M1, M2), sedge- (S1, S2), and open water (O1, O2)-dominated ponds. Values above zero (represented by upward arrows) refer to pond GPP; values below zero (represented by downward arrows) refer to pond R; stars-shaped points refer to pond NEP, the sum of GPP (+) and R (-), which may fluctuate between positive and negative.

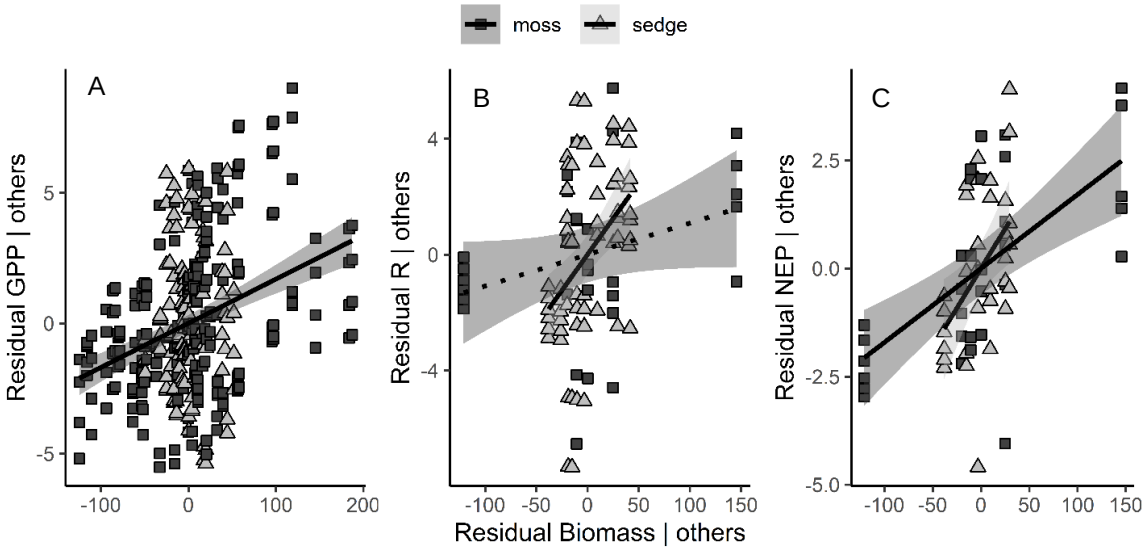

Figure 3.4. Partial regression of best fit models of GPP ($n_{best\text{-}fit}$=11), R ($n_{best\text{-}fit}$=2), and NEP ($n_{best\text{-}fit}$=1) as a function of moss and sedge biomass given other model variables. Each plots represents the residuals of the variable given all other variables in the model. For instance, NEP | others denotes the residuals of a single best fit linear model of NEP including all variables except either moss or sedge biomass, and biomass | others denotes the residuals of a linear model of moss or sedge biomass as a function of all other variables (moss or sedge biomass, surface area , and depth) in the model of NEP.

Table 3.5. Pearson r correlation coefficients for metabolism (GPP, R, and NEP) in thaw ponds.

	GPP	R	NEP
SA	0.45*	-0.09	0.36*
z	-0.47*	0.77**	0.59*
Moss	0.42*	-0.09	0.32*
Sedge	<0.01	-0.42*	-0.6*
$CO_{2,\ pore}$	-0.37*	0.48*	0.27
$CO_{2,\ surf}$	-0.34*	0.39*	0.18
$CH_{4,\ pore}$	-0.41*	0.04	-0.4*
$CH_{4,\ surf}$	-0.15	0.49*	0.53*
$CO_{2,\ pore:surf}$	-0.33*	<0.01	-0.35*

Table 3.6. Best fit model results for metabolism measurements.

model	M	S	SA	z	$CO_{2,\ surf}$	$CO_{2,\ pore}$	R^2	P	wt	ΔAIC
GPP ~ M + z + $CO_{2,\ pore}$	.			**		*	0.50	***	0.11	
GPP ~ z + $CO_{2,\ surf}$ + $CO_{2,\ pore}$				***		**	0.49	***	0.08	0.73
GPP ~ z + $CO_{2,\ pore}$				**		**	0.47	***	0.06	1.15
GPP ~ M + SA + z + $CO_{2,\ pore}$				*		*	0.49	**	0.05	1.45
GPP ~ M + $CO_{2,\ surf}$ + $CO_{2,\ pore}$	**				**		0.48	***	0.05	1.47
GPP ~ SA + z + $CO_{2,\ surf}$ + $CO_{2,\ pore}$				**		*	0.49	**	0.05	1.51
GPP ~ M + S + $CO_{2,\ surf}$ + $CO_{2,\ pore}$	**				*	.	0.49	**	0.05	1.63
GPP ~ M + z + $CO_{2,\ surf}$ + $CO_{2,\ pore}$						.	0.48	**	0.04	1.86
GPP ~ M + $CO_{2,\ surf}$	***				**		0.45	***	0.04	1.90
GPP ~ S + z + $CO_{2,\ pore}$				**		*	0.47	**	0.04	1.95
GPP ~ M + S + z + $CO_{2,\ pore}$				*		*	0.48	**	0.04	1.96
GPP ~ M + S + z + $CO_{2,\ surf}$	*	.		.	*		0.48	**	0.04	1.98
NEP ~ M + S + SA + z	**	*	***	***			0.72	***	0.95	
R ~ M + S + SA + z	.	*	*	***			0.65	***	0.44	
R ~ S + SA + z		*	.	***			0.63	***	0.22	1.37

*** P < 0.0001 ** P < 0.001 * P < 0.05 . P < 0.10

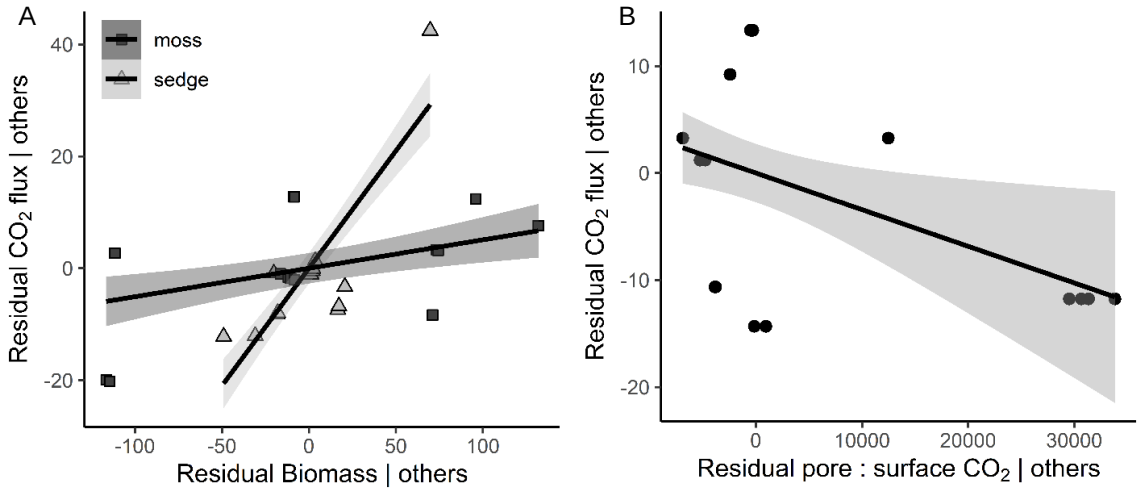

Figure 3.5. Partial regression plots of CO_2 flux from pond surface as a function of plant biomass and pore to surface water CO_2 concentration gradients.

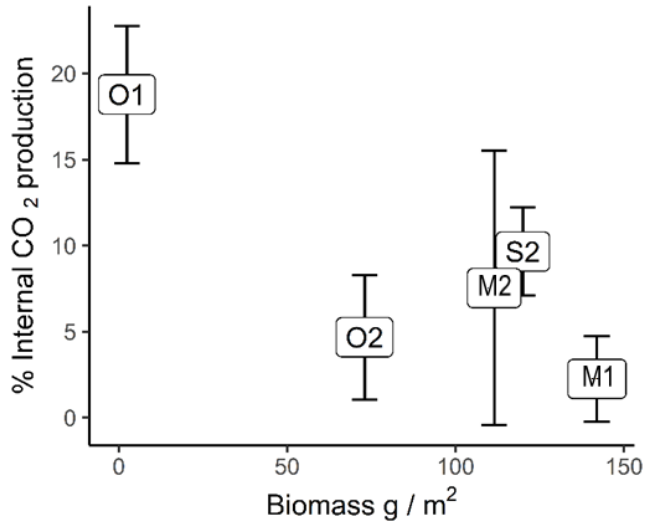

Figure 3.6. Internal CO_2 production in study ponds is estimated as a proportion of negative daily NEP values and CO_2 flux from the pond.

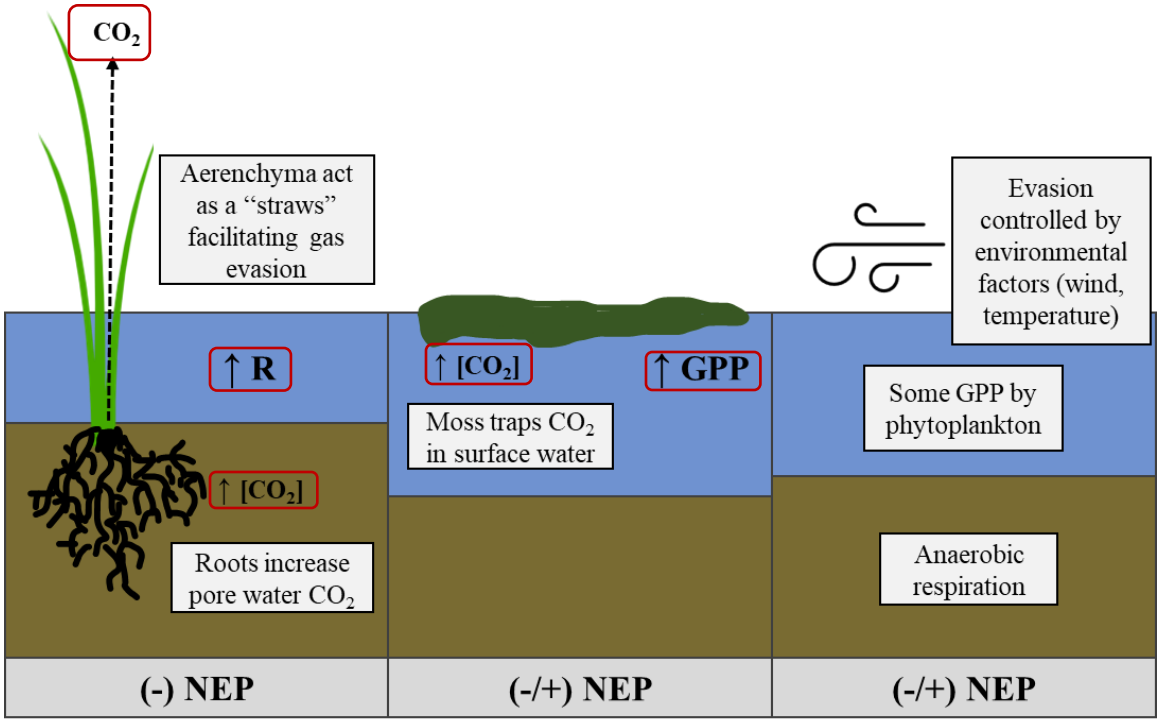

Figure 3.7. Effects of sedges and mosses on CO_2 concentrations, evasion, and ecosystem metabolism in arctic thaw ponds. Components of the conceptual model measured in this study are outlined in red. Sedges tended to be associated with increased evasion, R, and pore or sediment-water CO_2 concentrations, and mosses tended to be associated with increased surface water CO_2 concentrations and greater GPP. In open water-dominated ponds, evasion is controlled primarily by abiotic factors (e.g., wind, temperature), GPP is controlled by phytoplankton, and R is controlled by anaerobic respiration. Overall, NEP tended to be more negative in sedge-dominated ponds and fluctuated between positive and negative daily values in moss- and open water-dominated ponds.

CHAPTER 4

INTERACTIONS BETWEEN FUNCTIONAL RESPONSE AND EFFECT TRAITS IN WETLAND PLANT PATCHES IN AN ARID STREAM-RIPARIAN ECOSYSTEM

Introduction

Functional traits – morphological, biochemical, physiological, or behavioral characteristics that govern how a species interacts with its environment – provide a mechanistic link between communities and ecosystems (Lavorel and Garnier 2002). Functional traits include response traits, which characterize species' reactions to the environment (e.g., small, dense leaves confer drought tolerance), and effect traits, which dictate species' impacts on their environment (e.g., gas transfer structures, like aerenchyma, increase root-zone oxygen). As environmental conditions vary over time, populations of primary producer species will rise and fall due to their functional response traits and tolerances. For instance, as hydrological regimes in arid regions become more unpredictable with climate change and streams become more intermittent (Lawrence et al. 2021), the prevalence of in-stream primary producers, like algae and wetland plants, will likely contract with diminishing water availability. Likewise, the influence of primary producers is moderated by traits that influence ecosystem properties, processes, and functions—effect traits— which may vary between ecosystems. For example, in riparian ecosystems, plant root structures have been shown to indirectly reduce surface-subsurface water exchange (Heffernan et al. 2007) or increase it (Hendricks and White 1988) depending on the community composition and environmental conditions. Roots may also directly contribute to increased dissolved oxygen (DO) concentration via root uptake of deoxygenated water (Dodds et al. 2017**).** Additionally, traits that *respond* to environmental stimuli may also influence the *effect* of species on ecosystem processes. The relationship between response and effect traits remains a significant knowledge gap, yet answering this question is critical to understanding how shifts in species composition with global change will give rise to new combinations of functional traits that affect ecosystem functioning (Hooper et al. 2012).

Rising temperature, changes in seasonality, increased frequency and magnitude of extreme events, and acceleration of the hydrologic cycle are projected to shift ecosystem types and process rates (Grimm et al. 2013). Aridland streams already experience a high degree of seasonality, including seasonal drying and high-magnitude flash floods in the monsoon season, which are expected to intensify with further climate change (Lawrence et al. 2021). Aridland stream reaches fluctuate between algae- and wetland plant-dominated alternative stable states (Heffernan 2008), which may significantly affect ecosystem processes, like nutrient cycling (Dong et al. 2016).

Within wetland plants, species vary in functional traits that may influence both their response to environmental stimuli and their effects on ecosystem processes. Two wetland plant species that often co-occur but differ substantially in morphology and physiology are *Typha domingensis* (hereafter TYDO) or *Paspalum distichum* (hereafter PADI). TYDO is a cosmopolitan sedge associated with sites that are regularly inundated and is flexible, fast-growing, and highly competitive (Lorenzen et al. 2001). PADI is a low-lying rhizomatous knotgrass with a relatively low tolerance for dry conditions and a simultaneous low tolerance for submergence (Hsiao and Huang 1989). TYDO is much larger than PADI, often two to five in height, compared to PADI which rarely reaches a meter in height. While both are rhizomic, TYDO roots and rhizomes, on average, much wider in diameter than PADI roots and rhizomes, which may influence nutrient uptake.

In this study, I examined the interaction between plant trait *responses* and *effects* over environmental stress gradients in TYDO and PADI. Specifically, I monitored wetland plant traits that *respond* to changes in water flow and nutrient availability as the stream dried, including biomass production and tissue chemistry (i.e., carbon to nitrogen ratio, C:N). I then related those *response* traits to observed *effects* on concentrations of DO, carbon dioxide (CO_2), and dissolved organic carbon (DOC) (Figure 4.1). In arid systems, water is a vital resource that can be colimiting with N (Newman and Hart 2015). When water is more limiting than N, species are less likely to respond to N availability. Conversely, when a plant is not water stressed, assuming no

additional colimitation, increased N availability is likely to positively influence plant productivity and tissue N., Plant leaves not eaten by herbivores are ultimately deposited in stream., The nutritional content of leaves influences nutrient availability for microbes, and hence, microbial respiration, which consumes DO and produces CO_2. Additionally, according to the mass ratio hypothesis, the total effect of a species on ecosystem processes is proportional to its relative abundance in the community (Grime 1998). Hence, species *responses* resulting in greater biomass can amplify plant *effects*.

I expected plant response traits, like tissue N concentration, to respond positively to resource availability (e.g., bioavailable nitrogen), and that this relationship would be negatively affected by reduced water availability or flow. Additionally, I expected plant response traits, including tissue N, to affect ecosystem processes, such as oxygen and carbon, providing an illustration of the interaction between plant responses and effects. I expected DO to decline as a function of reduced flow and the presence of wetland plants. Conversely, I expected CO_2 in root-zone water and DOC in surface water to increase with macrophyte tissue carbon content and biomass due to organic matter inputs. These effects were expected to be relative to patch biomass, which was also anticipated to respond negatively to deduced water flow.

Emergent macrophyte oxygen production is not incorporated in estimates of metabolism derived from in-stream measures of diel oxygen, as gas exchange for photosynthesis is occurring out of the water. However, macrophytes do contribute to oxygen consumption via root respiration and organic matter inputs (Hoellein et al. 2013b). Additionally, in shallow, slow flowing streams, emergent macrophytes may persist in and along the stream channel in dense patches that shade in-stream primary producers (e.g., filamentous algae, diatoms, cyanobacteria). In-stream productivity in riparian systems is significantly constrained by light availability (Bernhardt et al. 2022), hence. To explore broad differences in species-specific *effects* on ecosystem metabolism, I measured and compared changes in ecosystem metabolism across a temporal water gradient in patches containing one of two wetland plant species, TYDO or PADI, or in gravel-dominated

patches (devoid of plants). I expected GPP to be reduced in macrophyte reaches compared to gravel reaches due to shading of in-stream producers and resource competition.

Methods

Sites

This project was conducted at riverine wetland sites along Sycamore Creek, an aridland stream northeast of the Phoenix metropolitan area in Tonto National Forest (Figure 4.2). Here, riverine wetlands occur along the stream from the bank into the active channel. I monitored several parameters every two weeks for two months (i.e. week 1 beginning May 11th) as the stream dried to determine how plants' responses to water and nutrients can influence their effects on ecosystem processes. I measured sediment dissolved gases, water and tissue chemistry, and biomass within species-specific patches.

Five patches for each species, TYDO and PADI, were monitored and sampled from May to June 2020 (Figure 4.2). During each sampling event, patch area was calculated by measuring one length dimension and three width dimensions, the latter of which were averaged. Plant stem density and height within patches were subsampled in three quadrats per patch per sampling event. Stems were counted at the sediment interface to measure density; quadrat size varied from 0.0625 m^2 to 0.25 m^2 depending on plant size. Stem height was averaged across five measurements per quadrat. Patch biomass was estimated using the stem-density and height data and species-specific stem height to biomass relationships developed from the Sycamore Creek long-term research in environmental biology (LTREB) project (Table 2.1).

Three cross-sectional transects were established within each patch to record wetted width and stream depth (five measurements per transect) and to calculate cross-sectional area (CSA) as a proxy for water availability. Flow velocity was estimated by measuring the speed of objects in the water over a three- to five-meter reach encompassing the patch. Discharge was calculated as the product of cross-sectional area and velocity.

Sample collection

Gas samples were collected every two weeks in pore water (root zone) and surface water in each species-specific patch (water permitting) to measure gases associated with respiration (CO_2 and DO). Samples were collected along a gradient of proximity to water with each patch: bank (no inundation, driest), edge (where inundated patch in wetted stream bed meets bank), center (roots inundated, within wetted stream bed), and open (beside patch in wetted stream; few or no roots). Pore water samples were siphoned from the root zone using a sipper apparatus attached to a battery-powered peristaltic pump. Pore water for DO sampling was collected into a container, ensuring an uninterrupted column of water without introducing air, and DO was measured in the container with an optical DO meter (Yellow Springs Instruments YSI PrODO). For dissolved carbon gas sampling, pore water was pumped into 60-mL syringes with stopcocks. Dissolved gases were extracted from pore water samples in the lab by mixing 30 mL sample with 30 mL N_2 gas, shaking for 3 minutes, and extracting the headspace into evacuated serum vials with septa. Gas samples were analyzed on an Agilent 7890 automated gas analyzer for CO_2 using a flame ionization detector.

Surface-water samples were collected within each patch in each sampling event where water was available. Samples were collected in 500-mL bottles between 6:00 and 11:00 AM, filtered in the lab, and frozen until analysis with a flow-injection analyzer (Lachat QC 8000) for soluble reaction phosphorus (SRP), chloride (Cl^-), nitrate (NO_3^-), ammonium (NH_4^+), and DOC. All chemical concentrations are expressed in units of elemental mass/volume.

Plant tissue samples were collected biweekly in each patch along the same water proximity gradient and were processed for carbon and nitrogen content. Tissue samples were dried at 60^{o}C for > 48 hours, ground in a ball mill, and analyzed for carbon, hydrogen, and nitrogen content with a Perkin-Elmer (PE 2400) CHN analyzer.

Six reaches between 25-45 m in length, representing TYDO-, PADI-, and gravel-dominated reaches, were selected along Sycamore Creek (Figure 4.2). Continuously recording DO meters (Yellow Springs Instruments YSI PrODO and MiniDot®) were installed at the bottom

of each reach. DO and temperature was recorded at 15-minute intervals continuously from July 4th to July 18th. Due to differences in the length of data captured by different probes, only the first week of data, the minimum captured by all probes, is reported here. Stream metabolism was modeled from the diel DO concentration and temperature data using the streamMetabolizer package in R statistical software (Appling et al. 2017).

Data Analysis

Important relationships between response traits and environmental variables, and response traits and ecosystem effects (dissolved gas concentrations (CO_2, CH_4, DO)) across species and time (in weeks) using multi-model inference via the glmulti package in R (Calcagno and De Mazancourt 2010). Each model was run with and without interaction terms using exhaustive screening. Variables and interaction terms with importance weights greater than 0.80 and weighted p-values less than 0.05 were examined further via linear regression and partial regression for interaction terms. The relationship between CO_2 and DO concentrations was evaluated using separate partial regressions for each species, including the effect of time in weeks. Species differences were clarified via Tukey's Honestly Significant Difference tests.

Results

Site changes

The stream contracted and velocity declined over the two-month study period (Figure 4.3A-D). CSA was reduced at the end of the study relative to the beginning, although a small precipitation event in early June (~ week 5) was observed in the USGS gauge (#09510200) located ~5 km below patch 5 resulted in a slight increase in CSA of downstream patches (P2 - P5). Streamflow velocity declined across all patch sites, but the decline was more prominent in the TYDO patch sites, which had higher mean velocity at the beginning of the study. Relative to PADI patches, TYDO patches were located upstream where the stream tended to be narrower. Hence, changes in CSA in TYDO sites were a function of decreasing stream depth.

Plant responses

Biomass in most patches peaked midway through the study (week 3, May 27th) and declined thereafter (Figure 4.3E-F), except for one of the TYDO patches, which was at its maximum observed biomass at the last time point (week 7, June 28th) and one PADI patch that had highest biomass during the first week. PADI patches covered more area but had total standing biomass (per patch) that was comparable to TYDO patches, which had greater biomass per area because of their greater height (Figure 4.3G-H). Factors affecting biomass production varied between the two species. TYDO biomass was not significantly related to any of the predictor variables. However, NO_3, CSA, and time (week) were significant predictors of PADI biomass (importance weight > 0.8, $P < 0.05$).

Overall, TYDO leaf tissue had higher nitrogen content and lower C:N than PADI tissue ($P << 0.001$), though both experienced an increase in C:N over time ($P << 0.001$) and with increased drying (Figure 4.4A, Table 4.1). However, the factors correlated with the increase in C:N varied between the two species. C:N in TYDO was negatively related to NO_3 in surface water ($p = 0.016$, $R^2 = 0.25$, Figure 4.4B), whereas there was no significant relationship between water NO_3 and tissue C:N in PADI. Rather, PADI C:N varied weakly as a function of CSA ($p = 0.047$, $R^2 = 0.21$, Figure 4.4C).

Response-effect interactions

Water chemistry variables did not vary significantly as a function of time in weeks, biomass, species patch, or CSA, except for DOC. DOC did not vary significantly as a function of species patch, species-specific biomass, or time independently (Figure 4.5A). DOC was more variable in TYDO patches, especially in later weeks, but not significantly different than DOC in PADI patches. However, there was a significant biomass-by-week interaction ($p = 0.02$). Specifically, there was a significant positive relationship between DOC and biomass, regardless of species, in week 7 ($p = 0.002$, $R^2 = 0.67$, Figure 4.5B).

DO concentration in pore water was slightly higher in PADI patches than in TYDO patches (ANOVA $p = 0.017$, Figure 4.6A). DO concentration in TYDO patches did not differ significantly across weeks but did appear to drop in week 7. No significant relationship was detected between DO concentration in patch pore water and patch biomass (overall, or between species), discharge, or cross-sectional area. While DO did not have a significant relationship with C:N or biomass alone, DO had a significant positive relationship with C:N assuming constant biomass in partial regression ($p = 0.04$, $R^2 = 0.11$, Figure 4.6B).

Overall, CO_2 concentration in pore water was significantly greater in TYDO patches compared to PADI patches ($P<<0.001$), but this was driven by differences in Week 1 (Figure 4.7A). By Week 3, CO_2 was dramatically reduced by an order of magnitude both in TYDO and PADI patches, eliminating the difference between species. The difference between weeks 1 and 3 was not significant in PADI patches.

CO_2 was significantly negatively related to tissue C:N given biomass when both species were considered together ($p = 0.014$, $R^2 = 0.27$), and in TYDO separately ($p = 0.044$, $R^2 = 0.43$, Figure 4.7B). However, while the trend was similar in PADI, the relationship was not significant when considering PADI separately ($p = 0.11$, $R^2 = 0.19$). No significant relationship was observed between CO_2 and DOC.

Metabolism

Metabolism varied across study reaches over 3 weeks. GPP and ER did not vary significantly as a function of reach (whether dominated by PADI, TYDO, or gravel). However, GPP in reaches with vegetation (both TYDO and PADI) diminished over the course of a week (Figure 4.8), whereas gravel-dominated reaches exhibited no significant pattern over time.

Discussion

In this study, I sought to identify interactions between response and effect traits of wetland plants along a water-stress gradient over time. I found species-specific differences in

responses to nutrient and water availability. PADI biomass declined with N and water availability, whereas TYDO biomass did not respond significantly to water or N. Tissue C:N of PADI *responded* more to CSA than to nitrogen availability, whereas TYDO tissue C:N *responded* to (or potentially drove) N availability, implying that species-specific differences in water tolerance influence plant tissue composition. PADI's ability to sequester N may be reduced if it relies on water to transport nutrients to the root zone. Likewise, reduced transpiration and photosynthesis in response to reduced water availability may also reduce N assimilation. Conversely, while TYDO C:N also increased over time as the stream dried, TYDO responded more to nitrogen availability than changes in water. Further, I found that plant tissue C:N ratios *affected* DO and CO_2 in the water. Specifically, DO increased and CO_2 decreased in pore water when the plants therein had higher C:N ratios. This may be due to the fact that plant tissue with high C:N ratios is of poor nutritional quality for aquatic heterotrophs: poor quality food in the ecosystem means there will be fewer heterotrophs consuming O_2 and producing CO_2, thereby reducing benthic respiration. This link between plants' C:N response to water availability and the subsequent effect that plant C:N has on DO and CO_2 serves as an example of response-effect traits interaction. Differences in responses to environmental conditions can influence the impact of plants on ecosystem properties.

Despite their similarities as hydrophilic graminoids, PADI and TYDO differed significantly in their response to hydrologic conditions**.** PADI exhibited a response to water availability and negligible response to nitrogen availability. PADI C:N was reduced when water flow was high, but remained unaffected at different levels of NO_3 availability, indicating that water is more limiting than N for PADI. This also suggests that PADI is experiencing water stress. Plants respond to water stress by reducing transpiration and photosynthesis via stomata closure (Hsiao 1973), and by reducing nitrogen metabolism (Xu and Zhou 2006). Plant uptake of nutrients like nitrogen is largely dependent on root mass, but it can also be augmented with mass flow when water is available (Matimati et al. 2014). If plants are acquiring nitrogen via water, as opposed to soils, access to nutrients relies on water availability. Reduced transpiration can result in reduced

nitrogen assimilation. PADI is a C4 grass, and C4 photosynthesis is highly sensitive to water stress (Ghannoum 2009). PADI in this system is correlated with locally low-lying elevations, which tend to be wetter for longer, and is more affected by water permanence than TYDO (Dong et al. 2016), which suggests that PADI is less tolerant to drying than TYDO. Conversely, TYDO responded more to nitrogen availability than water availability. There was no significant effect of CSA on TYDO C:N, but a relatively strong relationship between TYDO C:N and NO_3 in surface water, as would be expected if the plant is responding to N availability.

The relative differences in trait values between species may also differ as a function of resource stress. Previous studies in nearby arid riparian wetland systems have shown PADI to have significantly lower C:N and denitrification potential than TYDO (Suchy 2016); however, that study included a combination of perennial and intermittent sites. Conversely, in this study, PADI tended to have higher C:N than TYDO, and both PADI and TYDO patches experienced significant drying by the end of the monitoring period. PADI patches tended to occur downstream, and previous research at this site has demonstrated NO_3 availability declines downstream (Lewis et al. 2007; Dent et al. 2007). However, my data also show PADI did not respond to NO_3 availability, which suggests N availability did not drive differences in C:N between species. Rather, PADI's response to water stress drove the observed differences in C:N between the two species. Under higher water permanence conditions, PADI tends to have lower C:N than TYDO. But, under water stress, PADI C:N increases past TYDO, altering the relative relationship between the two species. As scientists, we often make assumptions based on aggregated and averaged data, such as the relative nutritional content of two plants. However, under changing contexts, these relationships may change.

Species-specific *response* traits, like C:N, may also have *effects* on stream chemistry, including CO_2 in the root zone. Previous studies in Sycamore Creek have demonstrated that wetland patches, as a whole, do not significantly affect surface water chemistry the way algae and cyanobacteria do (Dong et al. 2017). However, that study compared broad functional groups – wetland plants, algae, and cyanobacteria – and did not consider species-specific effects. Other

studies in Sycamore Creek have also shown that high herbaceous biomass is associated with low DO and NO_3 and high CO_2 and CH_4 in the hyporheic zone (Heffernan et al. 2008). However, in my study, patch biomass had a small but significant negative effect on CO_2 in the root zone, driven primarily by TYDO. Likewise, CO_2 increased with decreasing C:N given biomass. This could be due to nutritional differences between low and high C:N tissues for benthic microbes. If benthic microbes are also N limited, increased N (or lower C:N) would be expected to spur benthic activity and respiration. The relationship between biomass and CO_2 could also be influenced by CO_2 uptake by roots, which has been demonstrated in some emergent and submergent plants (Wium-Andersen 1971; Raven et al. 1988).

Species-specific *response* traits, like C:N, may also have *effects* on DO in the root zone. There was a significant overall effect of species on DO in pore water, wherein DO in TYDO patches was lower than in PADI patches. This may be due to the plants' growth forms and the effect this has on surface-air gas exchange. TYDO is substantially larger, and often grows in dense patches directly in the wetted stream channel, as well as the channel edges. TYDO's bulky emergent structure, standing meters over the water surface, has the potential to disrupt air and water flows, thus reducing surface-air gas exchange and surface water DO. Root zone DO and CO_2 also had a significant relationship with C:N given biomass. The increase in DO and decrease in CO_2 could also be interpreted as C:N promoting greater benthic productivity. This relationship was most substantial in TYDO but was true of biomass combined. Oxygen leakage from inundated plant roots has been demonstrated in anoxic wetland sediments to facilitate nitrification and NO_3 uptake (Brix and Sorrell 1996), but that is not expected in this lotic system.

Wetland plants tend to have a negative effect on aquatic ecosystem metabolism, as they tend to contribute to respiration but their production is often out of the water. In this study, I demonstrate that the relative impact of plants on ecosystem metabolism varied over time as the stream dried. GPP was on average greater in TYDO and PADI reaches compared to gravel reaches at the beginning of the metabolism sequence. However, GPP declined in TYDO and PADI reaches over time, while little change was observed in gravel patches. Given the

importance of light for ecosystem metabolism (Bernhardt et al 2022), this reduction in GPP could be a function of shading of in-stream primary producers (i.e., algae and cyanobacteria), as well as increased turbidity as a function of increased DOC later in the season. While we were not able to measure DOC with metabolism directly, the positive effect of biomass on DOC in the final sampling week suggests the contribution of these plants to DOC is primarily at the end of the season, as the stream dries, and plant patches contract, senesce, and decompose, . Despite a significant difference in tissue carbon content between the two species, there was no difference in DOC concentration between species patches. DOC is a primary food source in aquatic systems, but the late release of DOC into the system is out-of-step with in-stream consumers, who are reduced as the stream dries.

As the world warms and ecosystem dynamics change, I may have to re-evaluate my long-held paradigms explaining the relationships between communities and ecosystems. Changing environmental conditions are likely to alter relationships between organisms and the environment. While additional research examining a range of species and environmental conditions is necessary to fully elucidate response-effect trait interactions, this research contributes to my understanding of how species-specific plant responses to environmental change can alter their effect on important ecosystem processes, including carbon cycling. Understanding the interactions between plant responses to environmental change and their effects on ecosystem processes will help project future change**.**

Tables and figures

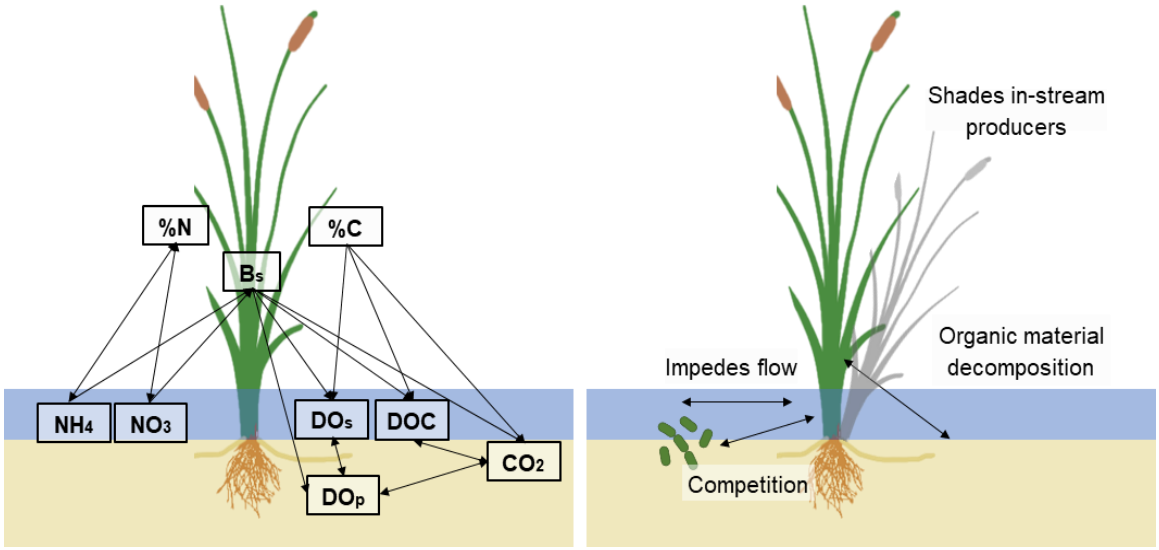

Figure 4.1. Hypothetical interactions between plant tissue content (effect and response trait), surface water chemistry, and pore water dissolved gases. (A) Chemical interactions: plant production and tissue nutrient content (%C, %N, C:N) are a function of the nutrients available (NH_4 and NO_3). (B) Physical interactions: traits such as root architecture, stem thickness, and plant height, that affect abiotic and biotic components of the system.

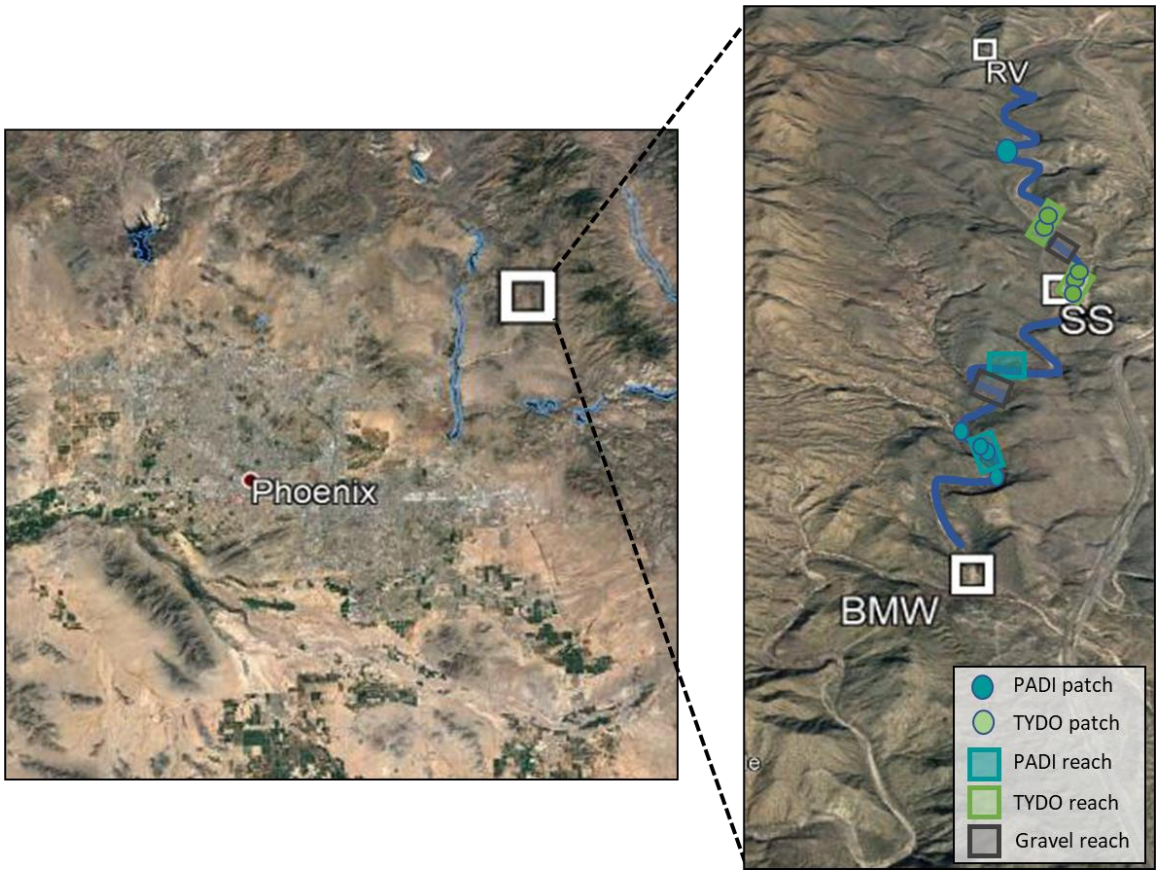

Figure 4.2. Study area along a ~4-km sections of Sycamore Creek, with pins denoting specific patches monitored approximately biweekly (green TYDO, blue, PADI) and rectangles denoting species-specific metabolism reaches (green-TYDO, blue-PADI, gray-GRAVEL).

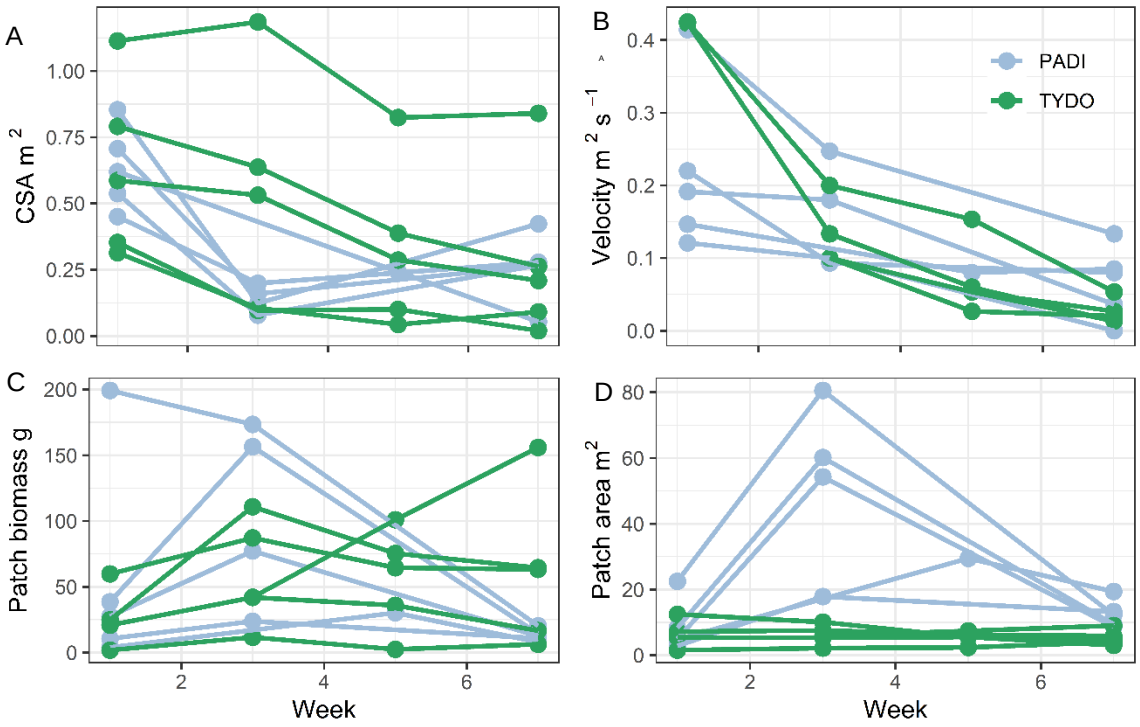

Figure 4.3. Changes in stream conditions and patch size over the experimental period (beginning week 1 May 11th). The cross-sectional area (CSA) and velocity demonstrate contraction and slowing of the stream over the study period. Patch size, measured in biomass and total patch area, peaked in most patches in week 3.

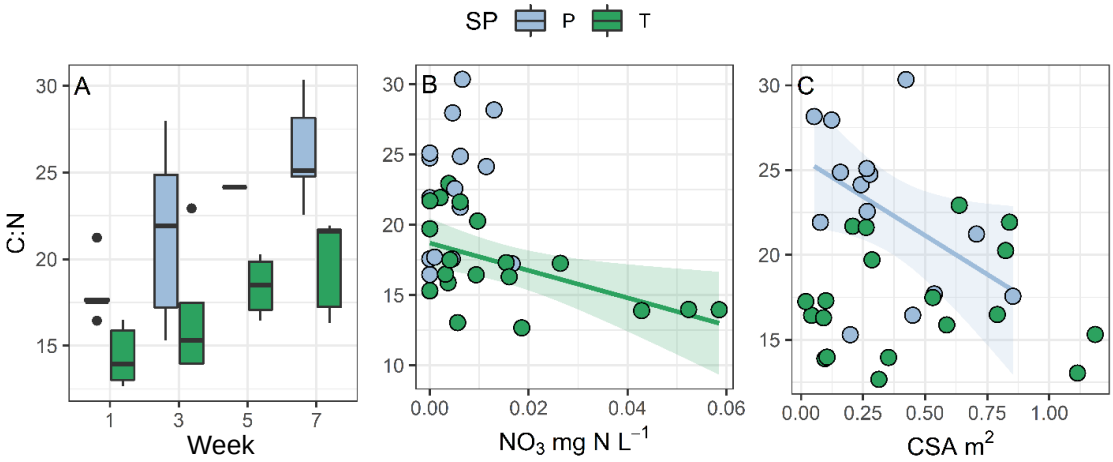

Figure 4.4. Tissue C:N concentrations tended to be higher (higher carbon content) in later weeks, where week 1 begins May 11th, ($p = 0.007$) and specifically in PADI patches (ANOVA $p = 0.001$) (A). Tissue C:N tended to decrease with increasing NO_3 in surface water in TYDO tissues ($p = 0.016$, $R^2 = 0.25$) but not PADI, which also tended to have lower levels of NO_3 (B). C:N ratio in PADI tissues was negatively correlated with greater CSA ($p = 0.047$, $R^2 = 0.21$) (C).

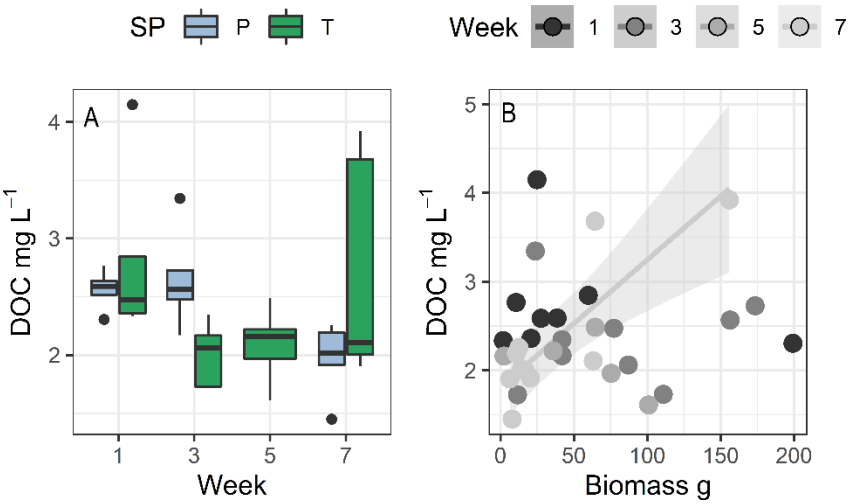

Figure 4.5. DOC did not vary significantly as a function of species or week (beginning week 1 May 11th). DOC in surface water varied as a function of biomass only in the last week (Week 7 p = 0.002, R^2 = 0.67) (B).

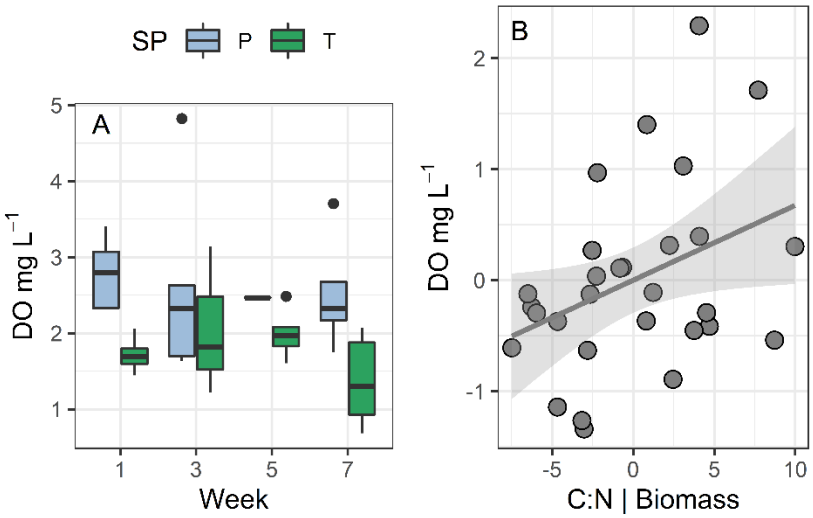

Figure 4.6. DO in root zone varied significantly by species (p = 0.001) but not over time (A), where week 1 begins May 11th. DO was positively correlated with C:N given biomass (p = 0.04, R^2 = 0.11), without consideration of species.

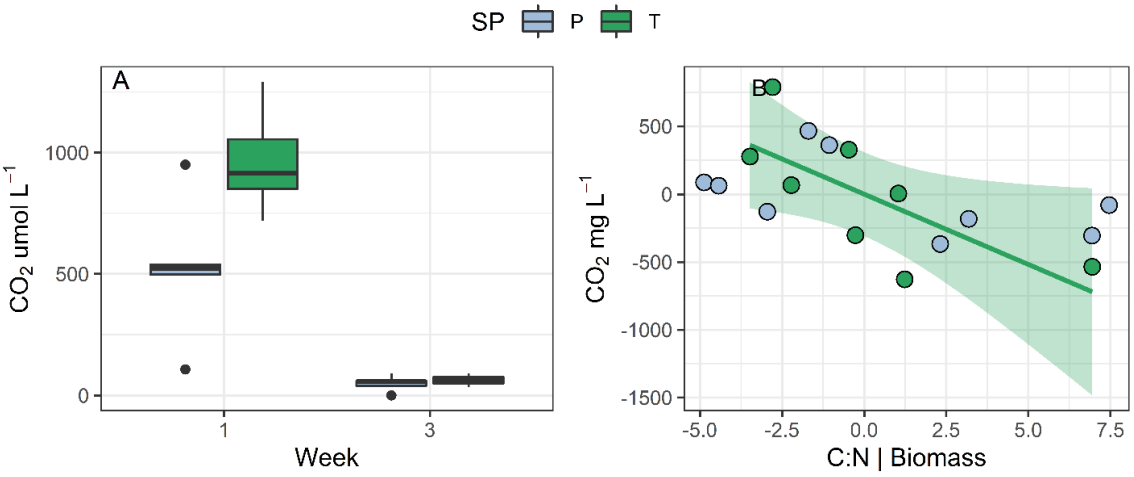

Figure 4.7. Root zone CO_2 as a function of species by week (beginning week 1 May 11th) and C:N. Root zone CO_2 was significantly correlated with C:N given biomass for all species combined ($p = 0.014$, $R^2 = 0.27$) and TYDO separately ($p = 0.044$, $R^2 = 0.43$), but not PADI.

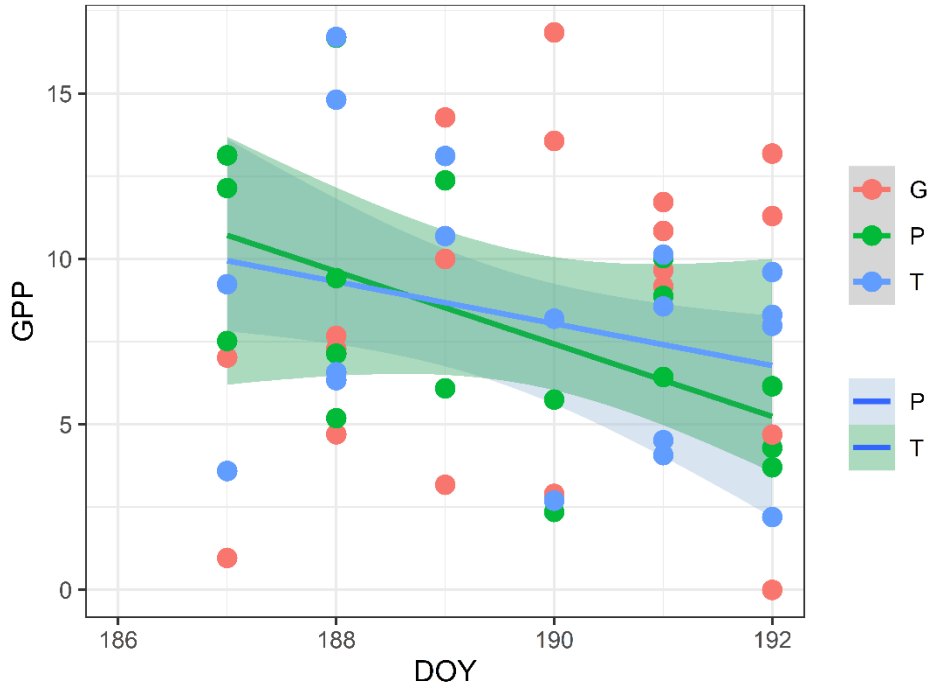

Figure 4.8. GPP values over time across reach types: gravel (G), PADI (P), and TYDO (T). GPP decreased significantly over the five days in reaches dominated by TYDO (P=0.003, R^2=0.75). GPP in PADI reaches also decreased over time, but was only marginally significant (P=0.090, R^2=0.30). No significant pattern was observed in gravel-dominated reaches.

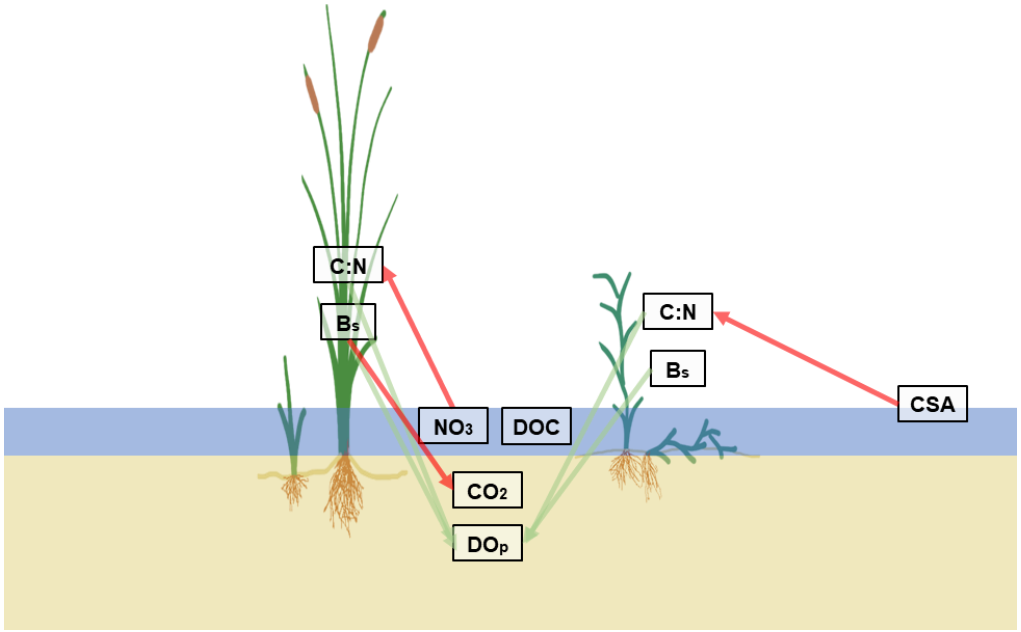

Figure 4.9. Interactions between response and effect traits in TYDO and PADI. Arrow colors indicate whether the relationship is positive (green) or negative (red) and are oriented from independent to dependent variables.

Table 4.1. Multi-model inference results, which summarizes the results of all the models for each variable.

	Variable	Est	se	z value	p value	Import
Biomass	Week	-0.1	0.09	-0.28	0.082	0.28
	C:N	0.06	0.06	-0.05	0.17	0.28
	SP	-0.48	0.44	-1.34	0.386	0.28
	Biomass	0	0	0	0	0.25
$Biomass_T$	Week	291.96	433.41	0.67	0.501	0.47
	NH4	16168.24	28722.07	0.56	0.573	0.4
	CSA	1074.46	2115.77	0.51	0.612	0.37
	NO3	17136.24	37732.74	0.45	0.65	0.35
$Biomass_P$	NO3	-705881.34	356850.33	-1.98	0.048	0.96
	CSA	-17741.03	7243.11	-2.45	0.014	0.95
	Week	-1546.10	671.97	-2.30	0.021	0.94
	NH4	59259.13	103783.21	0.57	0.568	0.49
C:N	Week	1.06	0.21	4.93	0	1
	SP	-5.23	1.09	-4.79	0	1
	Biomass	0	0	-1.66	0.097	1
	NO3	-22.02	32.8	-0.67	0.502	0.47
	NH4	-0.32	7.07	-0.05	0.964	0.27
DO	Biomass	0	0	1.1	0.271	0.81
	Week	-0.1	0.09	-1.08	0.281	0.7
	SP	-0.47	0.44	-1.06	0.29	0.68
	C:N	0.06	0.06	1.02	0.307	0.77
	NO3	-3.21	6.23	-0.51	0.607	0.37
	NH4	0.86	2.6	0.33	0.739	0.3
DOC	Biomass	0	0	1.15	0.249	0.82
	SP	-0.48	0.44	-1.08	0.279	0.69
	Week	-0.1	0.09	-1.08	0.28	0.7
	C:N	0.06	0.06	1.08	0.281	0.78
CO_2	C:N	-68.1	22.88	-2.98	0.003	0.98
	Biomass	-0.06	0.02	-2.47	0.013	1
	Carbon	-71.12	49.92	-1.42	0.154	0.84
	DOC	-216.81	199.34	-1.09	0.277	1
	DO	22.82	95.38	0.24	0.811	1
	Week	-0.31	17.3	-0.02	0.986	0.28
	SP	-0.79	65.94	-0.01	0.99	0.27

CHAPTER 5

PLANKTON TRAITS MEDIATE ECOSYSTEM FUNCTION IN THE COLORADO RIVER

Introduction

Phosphorus (P) concentration and availability are important factors controlling ecosystem metabolism in many freshwater ecosystems (Hoellein et al 2013). Phosphorus is an essential nutrient in photosynthesis, and when present in low supply it can limit the rate of gross primary production (GPP). The relationship between P and ecosystem metabolism in aquatic systems is complicated by additional environmental variables, such as erosion and hydrologic regime (Bernhardt et al. 2022) and co-limitation with light (Arteaga et al 2014) and other nutrients (Elser et al. 2007). For instance, in addition to P, nitrogen and silica are often limiting to phytoplankton growth (Tillman et al 1982, Elser et al. 2007). Stoichiometric demands for P and other nutrients vary among species and groups and influence nutrient cycling, process rates, and productivity. When whole communities are examined, as in metabolism, the relative abundances of these species are expected to influence community-level processes.

Ecosystem metabolism is a complex function conditional on multiple interacting climatic, hydrologic, and biogeomorphic factors, and is quantified as GPP and ecosystem respiration (ER). The balance between GPP and ER determines whether the system accumulates or loses carbon where import equals export. In streams and rivers, GPP varies largely as a function of light and hydrologic regimes (Bernhardt et al 2022) and usually exceeded by ER, resulting in lotic systems being mostly heterotrophic (i.e., GPP<ER; Mulholland et al 2001). However, in ecosystems where light is less limiting, like the desert Southwest, in-stream productivity is limited more by nutrients, hydrologic flow, and disturbance (Busch and Fisher 1981; Grimm and Fisher 1986; Grimm 1987). Contrary to more mesic systems, aridland streams cross the line between heterotrophic and autotrophic ecosystem metabolism, mainly in the early summers when slow but persistent flow from winter rains couples with high light to promote the growth of in-stream primary producers.

Phytoplankton are dominant primary producers in oceans, lakes, and large rivers, and thus are significant contributors to ecosystem metabolism. Phytoplankton are a widely diverse group of algal and microbial photosynthetic organisms that occupy the water column and vary in size, shape, color, type of metabolism, and life-history traits (Borics et al 2021). Phytoplankton traits also respond to changing environmental conditions, and those changes can have larger implications for ecosystem function. For instance, phytoplankton species can differ in individual cell volume by four orders of magnitude. Increasing temperature results in smaller phytoplankton cell size, at the species and community levels (Zohary et al 2021). Additionally, warming can alter food-web function and lead to selection for fast-growing phytoplankton species (Rasconi et al 2015), thus affecting rates of ecosystem metabolism. Cell size is a trait that, along with shape, influences the capacity of a cell to take up nutrients by affecting the surface area to volume ratio. A cell's access to spatially distributed nutrient pools is expected to be influenced by its ability to move (*motility*) and its attachment to other cells (*colonial*) or substrate (*attached*) reducing the surface area available for nutrient uptake.

Soluble reactive phosphorus (SRP) is the predominant form of biologically available phosphorus and thus is often a significant control on primary productivity in many freshwater systems (Heckly and Kilham 1988). However, the relationship between SRP and productivity is complicated by a number of factors, including colimitation with other nutrients (Elser et al. 1990; Lewis and Wurtsbaugh 2008), stoichiometric demands (Kerkhoff et al. 2005), among others. Assuming no colimitation exists, one would expect an increase in SRP to result in a greater abundance of phytoplankton (i.e., higher biovolume), and higher GPP.

The Colorado River is an integral water resource serving the southwestern US and Mexico, yet its ability to supply water has been under threat owing to climate change (Christensen et al. 2004). Multiple monitoring programs have documented fluctuations in water chemistry, primary productivity, and ecosystem metabolism in this waterway for decades (U.S. Geological Survey 2021). One long-term monitoring site is Lee's Ferry, situated below Glen Canyon Dam, which is the only site for hundreds of miles where the river is accessible on both sides. From

these long-term monitoring data, P is expected to be the limiting nutrient (when nutrients are limiting) because of its low concentration at Lee's Ferry (USGS 2017). The data demonstrate that metabolism fluctuates and is weakly related to phytoplankton biovolume but does not exhibit a clear relationship with P concentration.

I expected differential trait responses to available phosphorus (SRP), and effect traits influencing biovolume and GPP, to explain the lack of a direct relationship between SRP and metabolism. Instead, I expected to find that phytoplankton traits mediate this relationship, and obscure direct relationships between SRP, phytoplankton biovolume, and GPP. This study had three objectives. The first was to confirm patterns in GPP and SRP over time. Second, to examine patterns in phytoplankton traits and their importance to SRP, phytoplankton biovolume, and GPP via multimodal inference. Third, to examined the mediative relationships of phytoplankton biovolume and traits on SRP and GPP. To do this, I built a structural equation model to test the mediation effect of phytoplankton traits.

Methods

Phytoplankton data

Phytoplankton surveys have been conducted by the United States Geological Survey (USGS) at Lee's Ferry along the Colorado River since 1994, with sample frequency varying between 3-12 monthly observations per year. Phytoplankton were identified to the species level, where possible, and counted for abundance. Some of the specimen identified in these surveys are more commonly associated with benthic zones but have been transported in the water column while others are phytoplankton transported from reservoirs. Here, I define phytoplankton as algal and microbial photosynthetic organisms that occupy the water column. Average cell volume for each species was calculated from subsampled specimen each sampling event, which was used to calculate species-level biovolume. Water chemistry samples were collected along with phytoplankton samples. In this study, I focus specifically on SRP, which is the most bioavailable of the P forms, and therefore most relevant to productivity and phosphorus

uptake. A periodic time series of ecosystem metabolism (average length ~3 months, multiple times a year) for Lee's Ferry from data recorded since March 2008 was also acquired through USGS collaborator, Dr. Charles Yackulic.

Phytoplankton trait data were collected from online databases, mainly diatoms.org (Spaulding et al 2021) and freshwaterecology.info, for each identified species in the dataset, where available. Relevant species-specific trait information was coded into simplified categories for generalization and analysis. I focused on traits anticipated to mediate P uptake, either by influencing surface area to volume ratios and capacity for P uptake, or access to spatially distributed pools of SRP in the environment. Surface area to volume ratios in phytoplankton are a function of the size and shape of a cell. Cells vary in size, from 10 um^3 to 1,000,000 um^3, and in shape, commonly varying between rectangular, cylindrical, pyramidal, spherical, or some combination thereof. Cell biovolume calculations were based on the cell's geometric shape (Hillebrand et al 1999). Shape classifications used in modeling were further simplified into the most common shape categories: *rectangular, cylindrical, pyramidal,* or *spherical*. Motility, reported as a gradient from nonmotile to highly motile, was grouped into either *motile* (slightly motile to highly motile) or *nonmotile* (weakly motile to nonmotile). Four reported modes of colonialism were simplified into either *colonial* (classified as commonly occurs in colonies, occasionally occurs in colonies, forming zigzag colonies) or *solitary*. Four reported modes of attachment were simplified into either *attached* (tube-forming, vertical, prostrate) or *unattached*.

I calculated the proportion of the total observed biovolume belonging to each trait category by summing the total biovolume of each species in each category and dividing it by the total observed biovolume for each sampling event (Eq. 5.1). Trait biovolumes were calculated by summing the biovolumes of all species identified to have the given trait. The summed biovolume was converted into a proportion of the total biovolume.

$$\% \text{ Focal trait} = \sum B_{sp\,[trait],\,t} \,/\, \sum B_{phyt,\,t} \qquad \text{(Eq. 5.1)}$$

$B_{sp\,[trait]}$ is the biovolume of a species known to have the focal trait of interest and $B_{phyt,t}$ is the total plankton biovolume at a given time.

Multimodel inference

I performed multimodel inference analyses to quantify the relative importance of selected traits on each of the core model components (SRP, biovolume, and GPP) using the glmulti package in R Statistical Software (Calcagno 2020, R Core Team 2020). Exhaustive model screening was limited to first-order regressions (excluding interaction terms) for a total of 128 candidate models. Each global model for SRP, biovolume, and GPP included all of the selected trait variables (*colonial, motile, tolerant, attached, rectangular, spherical, cylindrical*) as proportions of the total biovolume. From these analyses, I selected those trait variables that surpassed the widely accepted model-averaged importance threshold weight of 0.8 or greater and occurred as significant explanatory terms in best fit models to include in the multiple mediation SEM model.

Structural equation modeling

I used structural equation modeling (SEM) to explore the complex relationship between SRP, phytoplankton biovolume, and GPP using the *lavaan* package in R Statistical Software (Ives 2012, R Core Team 2020). This model incorporates multiple mediating factors and levels (Figure 5.1). First, the model was centered on phytoplankton biovolume (B_{phyt}) mediating the relationship between SRP and GPP. Simply put, SRP is expected to increase biovolume (B_{phyt}), which in turn should raise overall GPP, though specific productivity (per unit biomass) decreases. Then, the mediating effect of significant traits (T_x, $T_{y,..}$, as identified in the multimodel inference analysis) was incorporated in the SRP–biovolume, biovolume–GPP, and SRP–GPP relationships. B_{phyt} was regressed as a function of SRP and the relative proportion of traits (T_x, T_y) in the community (Eq. 5.2), and GPP was regressed as a function of SRP, B_{phyt}, and T_x, or $T_{y\ ,..}$(Eq. 5.3). Each trait (T_x, T_y) was regressed as a function of SRP (Eq. 5.4).

$$B_{phyt} = a_1SRP + b_2T_x + b_3T_y \ldots \quad \text{(Eq. 5.2)}$$

$$GPP = b_1B_{phyto} + c_1SRP + c_2T_x + c_3T_x \ldots \quad \text{(Eq. 5.3)}$$

$$T_{x,y} = a_iSRP \quad \text{(Eq. 5.4)}$$

Regression coefficients were used to evaluate the indirect effects of the mediators, B_{phyt}, and $T_{x,y,..}$, and the total effects of the modeled variables (Eq. 5.5-8). Coefficients are denoted a - c and numbered by mediator (B_{phyt}, T_x, T_y, …) starting at 2 for trait mediators (e.g., a_2, a_3…), and marked *i* where equations are repeated for each trait.

Results

GPP varied over the 10-year period, ranging from 1 to 15 g O_2 m^{-3} d^{-1}, and averaged approximately 5 g O_2 m^{-3} d^{-1}. There was a strong seasonal signal, with GPP rising in the spring and falling in autumn each year (Figure 5.2A). Over the study period, SRP ranged from 0.001 to 0.018 ug L^{-1}, with a mean value of 0.006 ug L^{-1}; however, SRP varied between years, with the lowest values of SRP observed at the beginning (2008) and end (2018) of the study period. Likewise, total B_{phyt} was highest around 2012 and dropped considerably with declining P in later years. Contrastingly, the average volume of individual cells increased in later years, especially post-2014.

The phytoplankton dataset included 244 species identified to the species level (Appendix B). Approximately 30% of the species identified are considered benthic, and another 30% are classified as benthic or planktonic. Purely planktonic species made up about 24% of the total observed biovolume. The most abundant species over the study period was *Ellerbeckia arenaria,* accounting for over 30% of the total observed biovolume from 2008 to 2018, though its high rank is weighed heavily by a very high abundance in 2014. *Synedra ulna*, *Diatoma vulgaris*, and *Cocconeis placentula* made up an additional 32% of the total observed biovolume. Unlike *E. arenaria*, whose dominance varied widely from year to year, *S. ulna*, *D. vulgaris*, and *C. placentula* were among the top five most abundant species every year. *Puncticulata bodanica*, *Fragilaria crotonensis*, and *Melosira varians* biovolume were often in the top five to ten most abundance species each year, but their abundance varied over the study period.

Rectangular cells comprised about 36% of species identified, 52% of the total observed B_{phyt}, but varied from 2 to > 90 % of B_{phyt} per sampling event (Figure 5.3). Likewise, *cylindrical*

cells made up 36% of species identified, 41% of total B_{phyt} observed, and between 2 to 95% B_{phyt} per sampling event. Approximately 18% of species identified and 6% of the B_{phyt} were *spherical* cells, and atypical shapes were less common. *Colonial* species comprised 25% of identified species, ranging from >1 to <90 % observed B_{phyt}, were correlated with the proportion *rectangular* cells, especially from 2012 - 2014, coinciding with higher SRP concentrations during this period. *Motile* species comprised 32% of identified species, 6% of total biovolume on average, and ranged well below 1% to 28% of observed B_{phyt} per sampling event*. Attached* species comprised 25% of identified species, 52% of total biovolume on average, and ranged 1% to 98% of observed B_{phyt} per sampling event*. Tolerant* comprised 19% of identified species, 25% of total biovolume on average, and ranged >1% to 77% of observed B_{phyt} per sampling event. Patterns in the proportion *rectangular* and *colonial* species follow total phytoplankton biovolume over time, which start relatively high and drop considerably after 2013. On the contrary, *tolerant* and *attached* species mirror biovolume patterns, dipping between 2012 - 2016, with the greatest proportions in 2011 and 2017. *Spherical* cells roughly follow patterns in cell size over time, increasing notably after 2015. *Rectangular* and *cylindrical* proportions were correlated with colonial (r = 0.85 and -0.72, respectively), and *sensitive* was correlated with B_{cell} (r = 0.84, Table 5.1)

Multi-model inference analyses of SRP, B_{phyt}, and GPP yielded between 6 to 13 best-fit models accounting for 43 - 27% of model weights, while best-fit model weights ranged from 7% to 2% (Table 5.2 and 5.3). Best-fit models for SRP each included proportion *spherical* as a significant explanatory variable with a negatively weighted effect (B= -0.008, se= 0.0004, P = 0.09) and a model-averaged weighted importance of 0.86. Best-fit models of B_{phyt} each included the proportion *colonial* biovolume as a significant explanatory variable with a positive average effect ($B= 4x10^{-8}$, $se= 2x10^{-8}$, P = 0.12), and model-averaged weighted importance of 0.84. Trait importance varied between SRP, phytoplankton biovolume, and GPP (Figure 5.4). Proportion colonial was most important for phytoplankton biovolume and GPP, whereas proportion spherical

was most important for SRP. These variables identified as most important were incorporated in the mediation SEM.

The SEM explained approximately 37% of the observed variance in GPP and 25% of the variance in total B_{phyt} (Figure 5.5, Table 5.4). The baseline model contained 10 df ($t = 57.958$, $P < 0.001$), with a comparative fit index of 1, indicating good model fit. SRP had a marginally significant positive estimated effect on total B_{phyt} (10.7 mm^3, P=0.08), and a nonsignificant negative effect on GPP ($\beta = -14.24$, P=0.36). The relationship between SRP and the proportion *colonial* and *spherical* phytoplankton had contrasting effects. SRP was strongly positively associated with *colonial* biovolume ($\beta = 2.0$, $P = 0.10$), and negatively associated with *spherical* biovolume ($\beta = -1.7$, $P = 0.006$). In addition to SRP, B_{phyt} was significantly positively related to the proportion *colonial* biovolume ($\beta = 4.9$, $P < 0.001$), and negatively associated with *spherical* biovolume ($\beta = -1.4$, $P = 0.34$). GPP was also negatively influenced by proportion *spherical* biovolume ($\beta = -2.9$, $P = 0.25$), and positively associated with *colonial* biovolume ($\beta = -4.9$, $P < 0.001$). Direct effects of B_{phyt} and SRP on GPP were not significant (P=0.23 and 0.48, respectively).

Colonial biovolume had a positive mediation effect on the B_{phyt}–GPP relationship ($\beta = 1.98$, $P = 0.03$). The size of the estimated mediation effect of *colonial* phytoplankton on the relationship between SRP and GPP was large, but not significant ($\beta = 61.4$, $P = 0.12$). The total modeled effects were not significant ($P = 0.68$). While lower SRP is associated with a higher proportion *spherical* phytoplankton and a lower relative proportion *colonial* phytoplankton, the proportion *colonial* phytoplankton was generally higher than *spherical* at all observed levels of SRP. Combined with the greater effect size of *colonial* phytoplankton on total biovolume and GPP, the higher proportion *colonial* phytoplankton buffers the negative effects of spherical phytoplankton at lower concentrations of SRP, such that GPP is relatively unaffected.

Discussion

My results demonstrate the complexity and importance of phytoplankton traits in mediating ecosystem functions, namely primary productivity. The interactions of these traits with SRP, phytoplankton biovolume, and GPP appeared to dampen, or buffer, the mediation of biovolume on the SRP–GPP relationship.

My results illustrate that SRP exerts varying effects on phytoplankton traits, and likewise, phytoplankton traits exert varying effects on biovolume and GPP. For instance, *colonial* biovolume was not particularly influenced by SRP (AIC model weight < 0.5), but *colonial* biovolume was important for explaining total biovolume and GPP (AIC model weight > 0.8). Likewise, *spherical* biovolume was negatively influenced by SRP, and had weak negative effects on GPP and B_{phy}. I set conservative criteria for model variables, including only traits with a model-averaged importance weight > 0.8 and model-averaged significance of $P < 0.10$. Under less stringent conditions (i.e., importance weight > 0.5), *tolerance* and *cell size* traits are important factors regulating biovolume, whereas *attachment* traits are important for GPP.

I examined phytoplankton traits only in terms of their first-order interactions. However, many traits are not mutually exclusive, and co-occurring traits can exert diverging effects on focal variables or even cancel other trait effects. For instance, many *colonial* species are often rectangular or cylindrical in shape. While rectangular shapes have relatively high surface area to volume ratios, which would aid in nutrient diffusion, colonies of rectangular cells have thicker diffusion boundary layers and thus a reduced capacity for nutrient uptake (Beardall et al. 2008). Likewise, cell size can often mask the importance of cell shape. For example, while rectangularly shaped phytoplankton have a greater surface area to volume ratio relative to *spherical phytoplankton* of similar volume, a small *spherical* cell can have a greater surface area to volume ratio than a large rectangular cell. The total effect of the phytoplankton community is partly a function of the interaction of these related traits in individual species populations.

The total consequences of SRP and biovolume on GPP were buffered by the interaction of diverging trait effects. Given relatively low levels of SRP in this system (0.001 - 0.018 ug/L),

(Hoellein et al. 2013), one would expect fluctuations in SRP to be mirrored by changes in GPP and biovolume. Yet, while SRP and biovolume varied over the study period, annual mean GPP did not vary significantly. The proportion *spherical* biovolume had a negative relationship with SRP, biovolume, and GPP, while *colonial* biovolume was positively related to SRP, biovolume, and GPP. Decreased SRP resulted in a greater relative abundance of spherical cells in the community, which in isolation would theoretically reduce GPP, but the relative proportion *colonial* cells was still higher than *spherical* cells. Overall, *colonial* cells had a greater effect on the system than *spherical* cells due to their higher relative abundance: the positive effect of *colonial* on biovolume and GPP (+0.34, +0.46, respectively) was greater than the negative effect of *spherical* on biovolume and GPP (-0.10, -0.14, respectively). Thus, even though SRP had a stronger effect on *spherical* fraction than *colonial* faction (-0.28 vs +0.18), the greater abundance of *colonial* cells in the system dampened the negative effects of *spherical* cells on the system. In sum, the total effect of the phytoplankton community depended on the combination of the proportion of specific traits in the community, their relative response to SRP, and the strength of the effect of a given trait on observed biovolume and GPP.

As I have shown, phytoplankton community composition (i.e., abundance of *colonial* vs solitary cells, proportion *spherical* vs non-*spherical* species) affected community biovolume and GPP. However, other abiotic factors can also control phytoplankton community composition, and those factors should be included in future studies to further elucidate the complexity of the system. For example, temperature, light, and environmental stoichiometry can all affect phytoplankton growth rates, and this, in turn, affects food-web interactions and biogeochemical cycling (Finkel et al. 2010). Temperature can affect cell size, light availability can drive higher rates of GPP and thus increase P demand, and environmental stoichiometry can affect the energy and material requirements of phytoplankton cells to maintain their own internal stoichiometries (Sterner and Elser 2003). Thus, these abiotic factors can create conditions that favor the selection of certain phytoplankton species.

Environment-function relationships are often complicated, and difficult to measure given variable conditions and interactions over space and time. Studies focused on the diversity and abundance of species or functional groups miss the complexity and importance of specific traits in mediating ecosystem function. Incorporating functional traits is essential to clarify our ecosystem conceptual models. This work provides an example of how interactions between diverging trait responses to environmental conditions and differing effects on ecosystem functions can buffer total effects and explain counterintuitive interactions across ecosystems, or lack thereof in the case of SRP and GPP. Trait associations varied in direction and magnitude by trait and variable (SRP, biovolume, GPP), complicating the SRP – GPP relationship.

Tables and figures

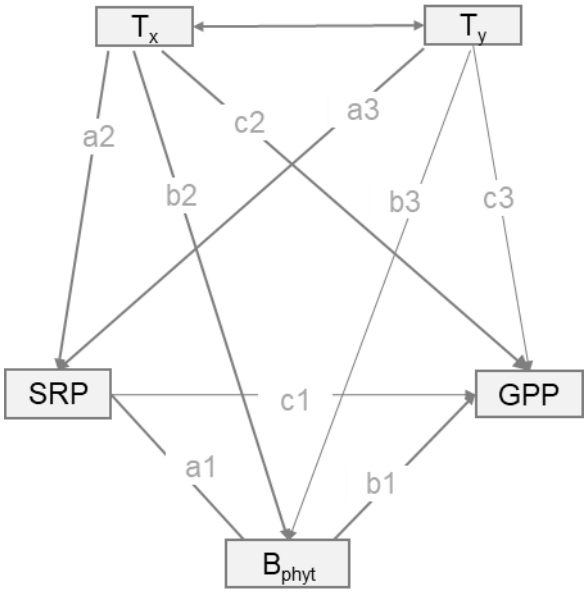

Figure 5.1. Structural equation model (SEM) format. Biovolume of phytoplankton (B_{phyt}) mediates the interaction between SRP and GPP, and traits influencing P uptake mediate the interaction between SRP (P) and phytoplankton biovolume (B_{phyt}). The proportion of the phytoplankton population that is trait x (T_x), and trait y (T_y) mediates the interactions of SRP with biovolume and biovolume with GPP. Coefficients are denoted with letters and numbered by the mediator (1 - biovolume, 2 - T_x, 3 - T_y).

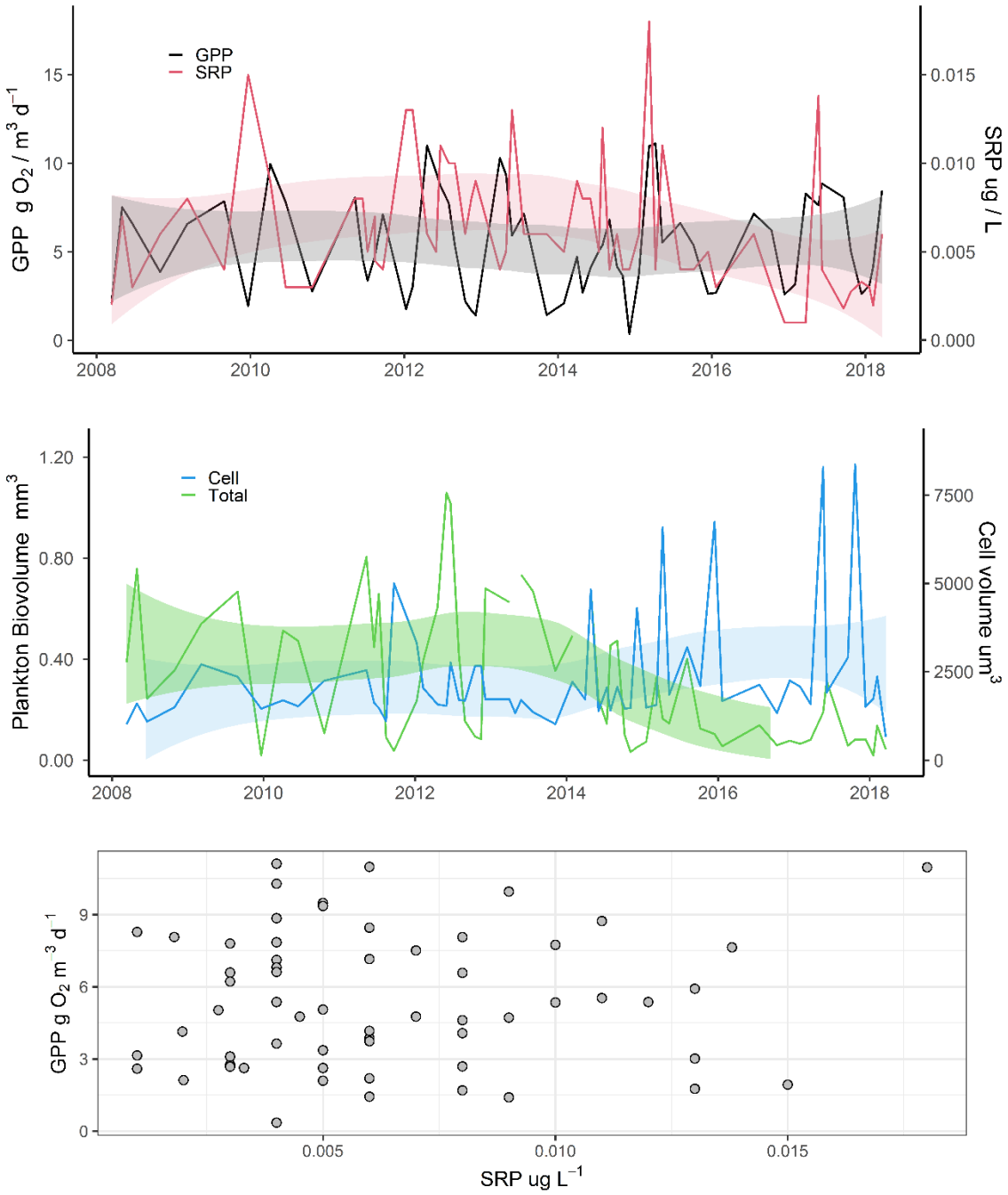

Figure 5.2. Patterns in gross primary production (GPP), soluble reactive phosphorus (SRP), and biovolume (total observed, average individual cell) were observed at Lee's Ferry from 2008 to 2018. Ribbons are centered on the running mean with a 12-month window and have height equal to one standard deviation of that window.

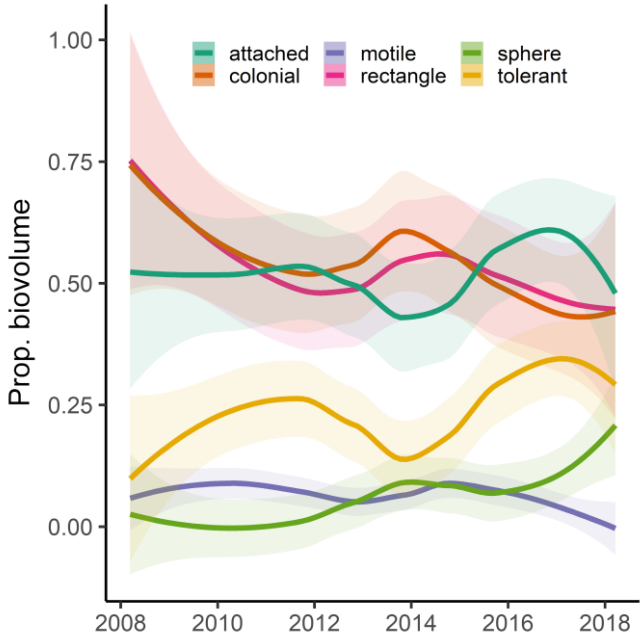

Figure 5.3. Variation through time in the proportion of total observed phytoplankton biovolume representing different trait characteristics associated with P uptake, including attachment, *colonialism*, *motility*, shape (*rectangular* or *spherical*), or tolerant to increasing levels of disturbance, as defined by the biological condition gradient conceptual model (Davies and Jackson 2006).

Table 5.1. Correlation matrix of model variables. Total phytoplankton biovolume (B_{phyt}) and soluble reactive phosphorus (SRP) values per sampling event. Gross primary production (GPP) and ecosystem respiration (ER) was averaged over seven days surrounding the sampling event. The proportion of the total phytoplankton biovolume that were identified traits influencing P access, including colonial (cln), motile (mot), and attached (att), tolerance (tol) to human disturbance, and or traits influencing shape and volume, including spherical (sph), cylindical (cyl), rectangular (rec), and the average individual cell volume (B_{cell}), were compared.

	B_{phyt}	*GPP*	*ER*	*SRP*	*cln*	*mot*	*att*	*tol*	*sph*	*cyl*	*rec*	B_{cell}
B_{phyt}	1.00	0.36	-0.04	0.24	0.40	-0.08	0.01	0.60	-0.28	-0.19	0.31	-0.17
GPP		1.00	-0.51	0.06	0.56	-0.10	0.35	0.23	-0.35	-0.42	0.55	0.01
ER			1.00	-0.10	-0.17	-0.05	-0.05	-0.09	0.13	0.05	-0.11	-0.12
SRP				1.00	0.18	-0.05	0.06	0.18	-0.28	0.04	0.11	0.01
cln					1.00	-0.02	0.25	0.00	-0.41	-0.72	0.85	0.06
mot						1.00	0.02	0.06	-0.18	0.03	0.06	0.10
att							1.00	0.12	-0.36	-0.23	0.38	0.18
tol								1.00	-0.28	0.34	-0.16	-0.13
sph									1.00	-0.06	-0.44	-0.11
cyl										1.00	-0.87	-0.01
rect											1.00	0.05
B_{cell}												1.00

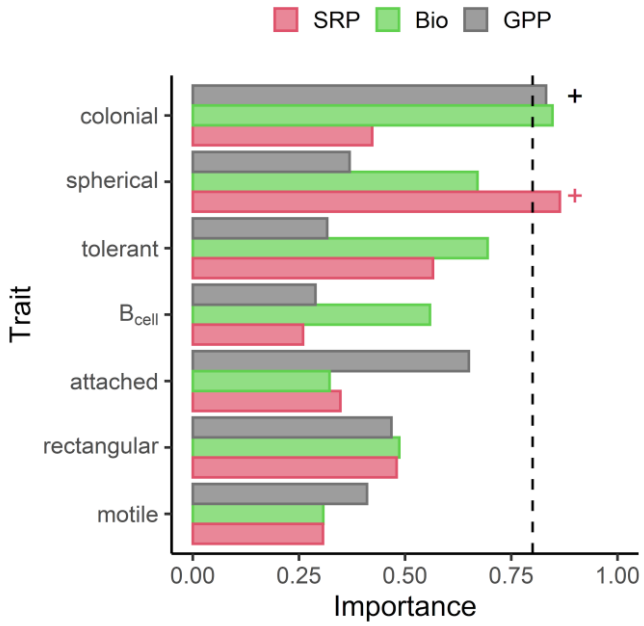

Figure 5.4. Model-averaged importance of trait variables explaining SRP, phytoplankton biovolume (Bio, or B_{phyt}), and GPP. Importance values are calculated via the sum of the weights of the models in which the variable appears and are interpreted as the overall support for each variable across all models in the candidate set. Dashed lined denotes the 0.80 importance threshold. Plus signs (+) denote variables significant in multi-model inference.

Table 5.2. Best fit model results for total phytoplankton biovolume (B_{phyt}), soluble reaction phosphorus (SRP) and gross primary production (GPP). Model fit was evaluated using Akaike information criterion (AIC) scores. Models with AIC scores less than 2 points from the lowest AIC model were considered equally best-fit. Phytoplankton traits are abbreviated as follows: average individual cell volume (B_{cell}), motility (mot), colonial (cln), rectangular (rec), spherical (sph), attached (att). Model weight (W) was calculated as Akaike weight.

	B_{cell}	mot	cln	rec	sph	att	tol	Δ AIC	W	R^2	p
B_{phyt}											
B_{cell} + cln + rec + sph + tol	0.14	-	0.02	0.09	0.40	-	0.03	0.00		0.23	0.00
cln + rec + sph + tol	0.00	-	0.02	0.07	0.05	-	0.02	0.36	0.07	0.21	0.00
B_{cell} + cln + rec + sph + att + tol	-	-	0.01	0.06	0.05	0.40	0.02	0.97	0.06	0.20	0.00
B_{cell} + cln + sph + tol	0.12	-	0.10	0.12	0.12	-	-	1.28	0.04	0.20	0.00
B_{cell} + cln	0.10	-	0.00	-	-	-	-	1.54	0.03	0.17	0.00
cln + rec + sph + att + tol	-	-	0.01	0.06	0.05	0.40	-	1.59	0.03	0.21	0.00
B_{cell} + mot + cln + rec + sph + tol	0.16	0.64	0.02	0.11	0.04	-	-	1.76	0.03	0.21	0.00
sln + sph + tol	-	-	0.13	-	0.14	-	-	1.87	0.03	0.18	0.00
B_{cell} + cln + sph + tol	0.80	-	0.01	-	0.22	-	-	1.89	0.03	0.18	0.00
B_{cell} + cln + tol	0.15	-	0.01	-	-	-	-	1.97	0.02	0.18	0.00
SRP											
sph	-	-	-	-	<0.001	-	-	0.00	0.06	0.07	0.03
cln + rec + sph + att + tol	-	-	0.08	0.02	0.02	0.13	-	0.02	0.06	0.12	0.03
sph + tol	-	-	-	-	0.02	-	-	0.34	0.05	0.07	0.04
cln + rec + sph + tol	-	-	-0.16	0.06	0.01	-	-	0.57	0.04	0.10	0.04
rec + sph + tol	-	-	-	0.20	0.01	-	-	0.64	0.04	0.08	0.04
mot + sph	-	0.40	-	-	0.02	-	-	1.27	0.03	0.06	0.06
rec + sph + att + tol	-	-	-	0.11	0.10	0.30	-	1.50	0.03	0.09	0.06
cln + sph	-	-	0.58	-	0.07	-	-	1.68	0.02	0.05	0.07
mot + sph + tol	-	0.45	-	-	0.02	-	-	1.75	0.02	0.07	0.07
sph + att	-	-	-	-	0.03	0.73	-	1.89	0.02	0.05	0.08
rec + sph	-	-	-	0.85	0.04	-	-	1.97	0.02	0.05	0.08
mot + cln + rec + sph + att + tol	-	0.85	0.10	0.02	0.01	0.15	-	1.98	0.02	0.10	0.06
B_{cell} + sph	0.88	-	-	-	0.03	-	-	1.99	0.02	0.05	0.08
GPP											
cln + att	-	-	<0.001	-	-	0.04	-	0.00	0.08	0.03	<0.001
mot + cln + att	-	0.35	<0.001	-	-	0.04	-	1.10	0.05	0.03	<0.001
cln + att + tol	-	-	<0.001	-	-	0.04	-	1.52	0.04	0.03	<0.001
cln + sph + att	-	-	<0.001	-	0.50	0.08	-	1.53	0.04	0.03	<0.001
cln + rec + att	-	-	0.50	0.52	-	0.09	-	1.57	0.04	0.03	<0.001
B_{cell} + cln + att	0.57	-	<0.001	-	-	0.04	-	1.67	0.03	0.03	<0.001

Table 5.3. Multimodel inference results relating total phytoplankton biovolume (B_{phyt}), gross primary production (GPP), and soluble reactive phosphorus (SRP), phytoplankton traits: colonial (cln), tolerant (tol), spherical (sph),rectangular (rec), average individual cell volume (B_{cell}), attached (att), and motile (mot). Results below include estimates of model coefficients (est), standard error (se), upper and lower confidence interval bounds (ci_{up}, ci_{down}), z-values, p-values, and model averaged importance values (Import).

Y	Trait	est	se	ci_{down}	c_{iup}	z	p	Import
	cln	4.407	2.882	-1.241	1.006	1.529	0.126	0.847
	tol	-3.662	3.424	-1.037	3.049	-1.069	0.285	0.694
	sph	-4.108	4.031	-1.201	3.794	-1.019	0.308	0.670
B_{phyt}	B_{cell}	-1.944	2.402	-6.652	2.764	-0.809	0.418	0.559
	rec	-1.985	3.214	-8.285	4.314	-0.618	0.537	0.486
	att	1.037	8.461	-1.555	1.762	0.123	0.902	0.322
	mot	-1.031	2.617	-6.161	4.099	-0.394	0.694	0.307
	cln	3.982	2.333	-0.591	8.556	1.707	0.088	0.832
	att	1.644	1.680	-1.649	4.936	0.978	0.328	0.650
	rec	1.587	2.385	-3.087	6.261	0.666	0.506	0.468
GPP	*mot*	-2.028	3.419	-8.730	4.673	-0.593	0.553	0.410
	sph	-0.918	1.742	-4.332	2.497	-0.527	0.598	0.369
	tol	-0.023	0.847	-1.684	1.637	-0.028	0.978	0.317
	B_{cell}	0.000	0.000	0.000	0.000	-0.302	0.763	0.289
	sph	-0.008	0.005	-0.018	0.001	-1.673	0.094	0.864
	tol	-0.003	0.004	-0.011	0.005	-0.822	0.411	0.566
	rec	-0.003	0.004	-0.011	0.005	-0.674	0.500	0.480
SRP	*cln*	0.001	0.003	-0.003	0.006	0.590	0.555	0.422
	att	0.001	0.002	-0.002	0.004	0.395	0.693	0.348
	mot	-0.001	0.003	-0.008	0.005	-0.410	0.681	0.306
	B_{cell}	0.000	0.000	0.000	0.000	0.007	0.995	0.260

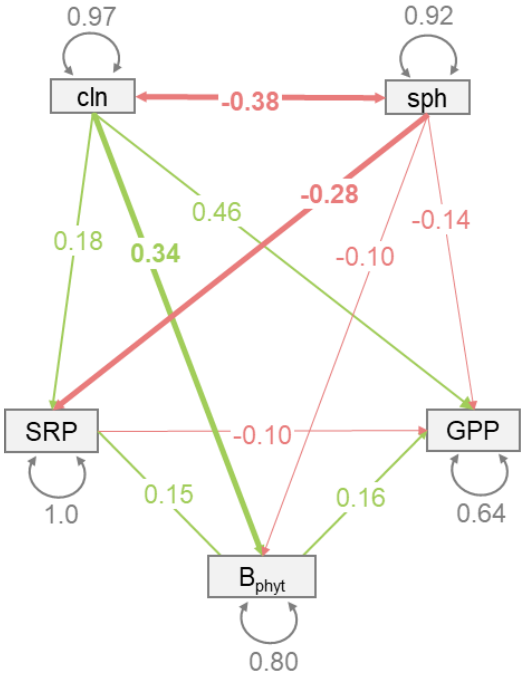

Figure 5.5. Multi-mediation model, wherein the effect of SRP) on GPP is mediated by phytoplankton biovolume, and the effect of P (SRP) on phytoplankton biovolume is mediated by the proportion of biovolume representing specific traits, *colonialism*, and *spherical* shape, which influence the surface area to volume ratio (*spherical* shapes have a relatively lower surface area to volume ratio) and access to P (*colonial*).

Table 5.4. SEM model results. Endogenous variable regressions for gross primary production (GPP) and phytoplankton biovolume (B_{phty}). Exogenous variable regression including proportion colonial (cln) and proportion spherical (sph) as a function of soluble reaction phosphorus (SRP). Mediation effects were estimated using the regression coefficients denoted in parentheses.

		est	se	z	p	R^2
Regressions						
GPP ~						0.36
	SRP (c1)	-14.3	15.8	-0.92	0.36	
	B_{phyt} (b1)	0.45	0.32	1.39	0.16	
	cln (c2)	4.93	1.37	3.6	>0.001	
	sph (c3)	-2.94	2.55	-1.15	0.25	
B_{phyt} ~						0.24
	SRP (a1)	10.7	6.18	1.73	0.08	
	cln (b2)	1.17	0.537	2.17	0.03	
	sph (b3)	-1.43	1.52	-0.94	0.34	
Trait responses						
cln ~						0.03
	SRP (a2)	-1.71	0.628	-2.73	0.006	
sph ~						0.09
	SRP (a3)	2.02	1.25	1.61	0.1	
cln ~~ sph		-0.11	0.005	-2.31	0.021	
Mediation effects						
	a1b1	4.91	4.85	1.01	0.321	
	a2b2	2.36	1.99	1.18	0.237	
	a3b3	2.45	2.62	0.93	0.349	
	b2c2	5.77	3.02	0.19	0.057	
	b3c3	4.22	12.75	0.33	0.74	
	a2c2	9.97	6.45	1.54	0.123	
	a3c3	5.04	3.91	1.29	0.197	
	total	13.79	17.48	0.78	0.43	

CHAPTER 6

CONCLUSION

This dissertation tested a conceptual framework linking environmental conditions, biotic communities, and ecosystem function via trait interactions. In aggregate, this work provides empirical support for the functional response–effect trait framework modeled after Lavorel and Garnier (2002). Additionally, this research provides explicit insights for specific ecosystems experiencing climate-driven regime shifts, especially riparian systems in the arid southwestern U.S. I conclude with a synthesis of key findings concerning functional trait theory, climate change, and implications for specific study systems undergoing change.

In Chapter 2, I examined species responses to environmental conditions. I used long-term data from a small, spatially intermittent, and highly seasonal aridland stream to examine differential responses of dominant wetland macrophytes to variable drying and flooding disturbances over time. Desert streams in the US Southwest, historically characterized by extreme hydrologic regimes, are experiencing more prolonged drying and more intense flash floods. These disturbances alter the geomorphology and biotic community of aridland streams, which are vital for promoting biodiversity (Sabo et al. 2005b), and biogeochemical processes, like nitrogen uptake and retention (Schade et al. 2005b). I demonstrate that interannual interactions between wetland plant biomass, disturbances, and species-specific tolerances to flood and drought stressors moderate patterns of riparian wetland productivity in arid stream ecosystems. I identified bio- and hydrologic factors explaining the distribution and abundance of specific wetland macrophytes over time. I found the most key factors across all species were biomass in the previous year and maximum flood peak, supporting the notion posed by Heffernan (2008) that an amplifying feedback loop promotes the wetland alternative stable state up to a threshold of disturbance. This work demonstrates not only the interannual feedbacks promoting greater biomass, but also provides an example of a species' drought tolerance

being exceeded (*Juncus torreyi*), resulting in its loss from the community following severe drought.

In Chapter 3, I explored effects of specific functional groups on ecosystem properties and function. Specifically, I examined the influence of functionally distinct primary producer groups, mosses and sedges, on carbon dynamics and aquatic ecosystem metabolism in arctic mire thaw ponds. Plant communities in permafrost regions are shifting with rising temperature and water availability (Malmer et al. 2005; Johansson et al. 2006), which may have significant implications for the carbon cycling and sink capacity of permafrost regions (Koven et al. 2011; Schuur et al. 2015; Kuhn et al. 2018). Ecosystem metabolism, quantified by gross primary production (GPP) and ecosystem respiration (ER), is expected to change as a function of temperature, hydrologic regime, and the biotic community. I found the two plant functional groups had different effects on dissolved carbon gases, CO_2 evasion, and pond metabolism. Sedges increase CO_2 concentration in pore-water, promote greater ecosystem respiration, and increase carbon gas evasion. Moss ponds had higher GPP but exhibited NEP rates similar to non-vegetated, less metabolically active ponds; however, they may trap gases and effectively prevent evasion. Taken together, sedges promoted benthic carbon gas production and loss from ponds, whereas moss was associated with greater GPP. This work contributes to my understanding of how effect traits vary between functional groups. My findings also inform how tundra-thermokarst regime shifts may impact carbon dynamics and metabolism in the arctic.

In Chapter 4, I tested the relationship between response and effect traits over environmental stress gradients in two functionally distinct wetland macrophyte species in a stream undergoing seasonal drying. Rising temperature, changes in seasonality, increased frequency and magnitude of extreme events, and acceleration of the hydrologic cycle are projected to shift ecosystem types and process rates (Grimm et al. 2013). The relationship between response and effect traits remains a significant

knowledge gap. Yet answering this question is critical to understanding how shifts in species composition will give rise to new combinations of functional traits that affect ecosystem functioning (Hooper et al. 2012). I found differences in leaf tissue chemistry (C:N), and root-zone gases (dissolved oxygen and CO_2) across species-specific patches. Differences in C:N indicate water stress in *Paspalum distichum* but not *Typha domingensis*, and hence differences in tolerance to drying conditions. Interestingly, the nitrogen content of these species differs substantially from tissue samples taken from the same species, in the same general region, under different water conditions (Suchy 2016). Specifically, *P. distichum* tissues are often reported to more nitrogen-rich than *T. domingensis* tissues. Yet, under drying conditions in my study, *T. domingensis* tissues had a significantly higher nitrogen content than *P. distichum.* This demonstrates the relationship between plant species (e.g., *P. distichum* having higher tissue nitrogen than *T. domingensis,* as seen in Suchy 2016) is conditional on the environment. Further, I found that plant tissue C:N, coupled with patch biomass, related to dissolved oxygen and CO_2 observed in the root zone. Thus, demonstrating the interplay between response and effect traits on ecosystem processes, such as oxygen and carbon fluxes

In Chapter 5, I tested the influence of response-effect trait interactions on ecosystem function. I examined the mediative relationships of phytoplankton biovolume and traits on soluble reactive phosphorus (SRP) and GPP. Using multimodel inference, I identified traits, specifically shape and colonization behaviors, to incorporate in a structural equation model that measured the mediation effect of these traits. SRP is the predominant form of biologically available phosphorus and thus is a significant control on primary productivity in many freshwater systems (Heckly and Kilham 1988). Reduced SRP often results in reduced abundance of primary producers (like phytoplankton), and lower GPP. However, in the Colorado River at Lee's Ferry, plankton, SRP, and GPP are decoupled. I found different phytoplankton traits were related to SRP and GPP. Specifically, the proportion of biovolume that was *colonial* had a positive

relationship with total biovolume and GPP but was not strongly influenced by SRP. in contrast, *spherical* biovolume proportion was negatively influenced by SRP, had negative effects on GPP and B_{phyt}. When SRP decreased, the proportion of spherical cells increased, but not enough to outweigh the influence of colonial cells, which were relatively more abundant. Hence, the total consequences of SRP and biovolume on GPP were buffered by the interaction of diverging trait effects. These results demonstrate the complexity and importance of traits in mediating ecosystem functions, especially those resulting in counterintuitive interactions in ecosystems undergoing change.

Altogether, this research demonstrates the importance of traits, varying across species and functional groups, in regulating biotic community structure and ecosystem function. Each data chapter (2-5) explores the response-effect trait framework, in part (Chapters 2 and 3) or as a whole (Chapters 4 and 5). I demonstrate variation in traits within and between functional groups, over time, and across environmental conditions. This research was conducted across a variety of aquatic systems, varying in size, climate, water permanence, and flow regimes. Chapter 2, which focused on primary producer responses to environmental factors, and Chapter 4, which tested the interaction of response and effect traits, were performed in Sycamore Creek, a small, spatially intermittent stream subject to seasonal drying and flooding regimes. Chapter 3 was conducted in arctic mire thaw ponds, which are small, lentic systems undergoing hydro- and geomorphological changes as a function of permafrost thaw. Chapter 5 used data from a larger river system also located in the arid Southwestern US. Together, they demonstrate the applicability of this framework across systems.

My research contributes to my understanding of the consequences of climate change in aridland systems. These systems already experience extreme variability in hydrology and temperature, are considered among the most vulnerable systems to climate change (Li et al. 2018), and have expanded across the globe over the last 60 years (Huang et al. 2015). In aridland systems, riparian areas are vital for harboring

different kinds of species, thereby increasing regional biodiversity (Sabo et al. 2005b), and according the diversity-function hypothesis (Tilman and Downing 1994), ecosystem function. Global studies have identified biotic exchange as an important driver of ecosystem change for aquatic systems under climate change (Sala et al. 2000). Plant functional traits can have consistent effects on biotic interactions, like competition, which traits generate trade-offs between performance with and without competition (Kunstler et al. 2015). Climate change is altering resources and species distribution, exacerbating existing stressors and introducing new ones. A trait-based approach allows us to better understand and explore these novel conditions.

The relationship between response and effect traits is complex. Unpacking this relationship requires a mass of data. While researchers have begun amassing these data, much of the research on functional response-effect trait interactions has focused on forestry systems (Zirbel et al. 2017; Refsland and Fraterrigo 2017). This research contributes to my understanding of, and provides empirical evidence for, response-effect trait interactions, and specifically provides insight on lesser studied wetland plant functional traits. In Chapter 4, I explicitly tested the response of plants to reduced water and nutrient availability, and the response between responding traits and the effect of the plant on ecosystem processes, like carbon flux, shading and competition with microbial producers, and oxygen dynamics. However, additional research is required to determine the consistency of these patterns across ecosystems and environmental conditions.

This work provides case studies in which the response-effect trait framework is applied. However, these investigations are necessary across functional groups, ecosystems, and environmental conditions. While growing interest in functional traits has resulted in a boom of databases providing trait data across organismal groups (see TRY-db.org, freshwaterecology.info, diatoms.org), significant gaps persist. Reducing these data gaps remains a challenge, especially given the importance of context for many traits in primary producers (Kattge et al. 2011)(and Chapter 4). Trait measurements explicitly

quantified across gradients of environmental conditions are necessary to fill these gaps. I focused on observing effects in the environment and comparing relative to identity and abundance of particular species or functional groups. Traits presumed to be causing observed effects should be measured in tandem with measurements of observed effects.

REFERENCES

Abnizova, A., J. Siemens, M. Langer, and J. Boike. 2012. Small ponds with major impact: The relevance of ponds and lakes in permafrost landscapes to carbon dioxide emissions. Global Biogeochem. Cycles **26**. doi:10.1029/2011GB004237

Ács, É., A. Földi, C. F. Vad, and others. 2019. Trait-based community assembly of epiphytic diatoms in saline astatic ponds: a test of the stress-dominance hypothesis. Sci. Rep. **9**: 1–11. doi:10.1038/s41598-019-52304-4

Adair, E. C., and D. Binkley. 2002. Co-limitation of first year fremont cottonwood seedlings by nitrogen and water. Wetlands **22**: 425–429.

Åkerman, H. J., and M. Johansson. 2008. Thawing permafrost and thicker active layers in sub-arctic Sweden. Permafr. Periglac. Process. **19**: 279–292. doi:10.1002/ppp.626

Appling, A., J. Rad, L. Winslow, and others. 2018. The metabolic regimes of 356 rivers in the United States. Sci. Data **5**.

Asaeda, T., M. Sultana, J. Manatunge, and T. Fujino. 2004. The effect of epiphytic algae on the growth and production of Potamogeton perfoliatus L. in two light conditions. Environ. Exp. Bot. **52**: 225–238. doi:10.1016/J.ENVEXPBOT.2004.02.001

Baker, V. 1977. Stream-channel response to floods, with examples from central Texas | GSA Bulletin | GeoScienceWorld. GSA Bull. **88**: 1057–1071.

Band, L. E., D. S. Mackay, I. F. Creed, R. Semkin, and D. Jeffries. 1996. Ecosystem processes at the watershed scale: Sensitivity to potential climate change. Limnol. Oceanogr. **41**: 928–938. doi:10.4319/LO.1996.41.5.0928

Banerjee, R. D., and S. P. Sen. 1979. Antibiotic Activity of Bryophytes. Bryologist **82**: 141. doi:10.2307/3242073

Basile, A., S. Giordano, A. Loâ Pez-Saâ Ez, and R. Castaldo Cobianchi. 1999. Antibacterial activity of pure ¯avonoids isolated from mosses. **52**: 1479–1482.

Bastviken, D., I. Sundgren, S. Natchimuthu, H. Reyier, and M. Gålfalk. 2015. Technical Note: Cost-efficient approaches to measure carbon dioxide (CO 2) fluxes and concentrations in terrestrial and aquatic environments using mini loggers. Biogeosciences **12**: 3849–3859. doi:10.5194/bg-12-3849-2015

Bateman, H. L., J. C. Stromberg, M. J. Banville, E. Makings, B. D. Scott, A. Suchy, and D. Wolkis. 2015. Novel water sources restore plant and animal communities along an urban river. Ecohydrology **8**: 792–811. doi:10.1002/eco.1560

Beauchamp, V. B., and J. C. Stromberg. 2008. Changes to herbaceous plant communities on a regulated desert river. River Res. Appl. **24**: 754–770. doi:10.1002/RRA.1078

Bernhardt, E. S., J. B. Heffernan, N. B. Grimm, and others. 2018. The metabolic regimes of flowing waters. Limnol. Oceanogr. **63**: S99–S118. doi:10.1002/LNO.10726

Bernhardt, E. S., P. Savoy, M. J. Vlah, and others. 2022. Light and flow regimes regulate the metabolism of rivers. Proc. Natl. Acad. Sci. U. S. A. **119**.

doi:10.1073/PNAS.2121976119/SUPPL_FILE/PNAS.2121976119.SAPP.PDF

Bhullar, G. S., M. Iravani, P. J. Edwards, and H. Olde Venterink. 2013. Methane transport and emissions from soil as affected by water table and vascular plants. BMC Ecol. **13**. doi:10.1186/1472-6785-13-32

Bintanja, R. 2018. The impact of Arctic warming on increased rainfall. Sci. Rep. **8**: 16001. doi:10.1038/s41598-018-34450-3

Brix, H., and B. K. Sorrell. 1996. Oxygen Stress in Wetland Plants: Comparison of De-Oxygenated and Reducing Root Environments. Funct. Ecol. **10**: 521. doi:10.2307/2389945

Busch, D. E., and S. G. Fisher. 1981. Metabolism of a desert stream. Freshw. Biol. **11**: 301–307.

Calcagno, V., and C. De Mazancourt. 2010. glmulti: an R package for easy automated model selection with (generalized) linear models. J. Stat. Softw. **34**: 12.

Chabbi, A., K. L. McKee, and I. A. Mendelssohn. 2000. Fate of oxygen losses from Typha domingensis (Typhaceae) and Cladium jamaicense (Cyperaceae) and consequences for root metabolism. Am. J. Bot. **87**: 1081–90.

Chapin, F. S., G. M. Woodwell, J. T. Randerson, and others. 2006. Reconciling Carbon-cycle Concepts, Terminology, and Methods. Ecosystems **9**: 1041–1050. doi:10.1007/s10021-005-0105-7

Chapin, S. F. I., S. M. Bret-Harte, and S. E. Hobbie. 1996a. Plant Functional Types as Predictors of Transient Responses of Arctic Vegetation to Global Change. J. Veg. Sci. **7**: 347–358.

Chapin, S. I., M. Bret-Harte, S. Hobbie, and H. Zhong. 1996b. Plant Functional Types as Predictors of Transient Responses of Arctic Vegetation to Global Change. J. Veg. Sci. **7**: 347–358.

Cheng, F. Y., and N. B. Basu. 2017. Biogeochemical hotspots: Role of small water bodies in landscape nutrient processing. Water Resour. Res. **53**: 5038–5056. doi:10.1002/2016WR020102

Christensen, N. S., A. W. Wood, N. Voisin, D. P. Lettenmaier, and R. N. Palmer. 2004. The Effects of Climate Change on the Hydrology and Water Resources of the Colorado River Basin. Clim. Chang. 2004 621 **62**: 337–363. doi:10.1023/B:CLIM.0000013684.13621.1F

Clarke, S. J. 2002. Vegetation growth in rivers: Influences upon sediment and nutrient dynamics. Prog. Phys. Geogr. **26**: 159–172. doi:10.1191/0309133302PP324RA

Cole, J. J., D. L. Bade, D. Bastviken, M. L. Pace, and M. Van de Bogert. 2010. Multiple approaches to estimating air-water gas exchange in small lakes. Limnol. Oceanogr. Methods **8**: 285–293. doi:10.4319/lom.2010.8.285

Cole, J. J., Y. T. Prairie, N. F. Caraco, and others. 2007. Plumbing the Global Carbon Cycle : Integrating Inland Waters into the Terrestrial Carbon Budget. 171–184. doi:10.1007/s10021-006-9013-8

da Cunha Cruz, Y., A. L. Martins Scarpa, M. P. Pereira, E. Mauro de Castro, and F. J. Pereira. 2020. Root anatomy and nutrient uptake of the cattail Typha domingensis Pers.

(Typhaceae) grown under drought condition. Rhizosphere **16**: 100253. doi:10.1016/J.RHISPH.2020.100253

Dent, C. L., N. B. Grimm, E. Martí, J. W. Edmonds, J. C. Henry, and J. R. Welter. 2007. Variability in surface-subsurface hydrologic interactions and implications for nutrient retention in an arid-land stream. J. Geophys. Res. Biogeosciences **112**: n/a-n/a. doi:10.1029/2007JG000467

DeWalle, D. R., B. R. Swistock, T. E. Johnson, and K. J. McGuire. 2000. Potential effects of climate change and urbanization on mean annual streamflow in the United States. Water Resour. Res. **36**: 2655–2664. doi:10.1029/2000WR900134

Dias, A. T. C., M. P. Berg, F. de Bello, A. R. Van Oosten, K. Bílá, and M. Moretti. 2013. An experimental framework to identify community functional components driving ecosystem processes and services delivery. J. Ecol. **101**: 29–37. doi:10.1111/1365-2745.12024

Díaz, S., and M. Cabido. 2001. Vive la différence: plant functional diversity matters to ecosystem processes.

Díaz, S., S. Lavorel, F. de Bello, F. Quetier, K. Grigulis, and T. M. Robson. 2007. Incorporating plant functional diversity effects in ecosystem service assessments. PNAS **104**.

Dodds, W. K., F. Tromboni, W. Aparecido Saltarelli, and D. G. Fernandes Cunha. 2017. The root of the problem: Direct influence of riparian vegetation on estimation of stream ecosystem metabolic rates. Limnol. Oceanogr. Lett. **2**: 9–17. doi:10.1002/lol2.10032

Dong, X., N. B. Grimm, J. B. Heffernan, and R. Muneepeerakul. 2020. Interactions Between Physical Template and Self-organization Shape Plant Dynamics in a Stream Ecosystem. Ecosystems **23**: 891–905. doi:10.1007/s10021-019-00444-z

Dong, X., N. B. Grimm, K. Ogle, and J. Franklin. 2016. Temporal variability in hydrology modifies the influence of geomorphology on wetland distribution along a desert stream. J. Ecol. **104**: 18–30. doi:10.1111/1365-2745.12450

Dong, X., A. Ruhí, and N. B. Grimm. 2017. Evidence for self-organization in determining spatial patterns of stream nutrients, despite primacy of the geomorphic template.doi:10.1073/pnas.1617571114

Elmqvist, T., C. Folke, M. Nyström, G. Peterson, J. Bengtsson, B. Walker, and J. Norberg. 2003. Response diversity, ecosystem change, and resilience. Front. Ecol. Environ. **1**: 488–494. doi:10.1890/1540-9295(2003)001[0488:RDECAR]2.0.CO;2

Elser, J. J., M. E. S. Bracken, E. E. Cleland, and others. 2007. Global analysis of nitrogen and phosphorus limitation of primary producers in freshwater, marine and terrestrial ecosystems. Ecol. Lett. **10**: 1135–1142. doi:10.1111/j.1461-0248.2007.01113.x

Elser, J. J., E. R. Marzolf, and C. R. Goldman. 1990. Phosphorus and Nitrogen Limitation of Phytoplankton Growth in the Freshwaters of North America: A Review and Critique of Experimental Enrichments. https://doi.org/10.1139/f90-165 **47**: 1468–1477. doi:10.1139/F90-165

Fisher, S. G., L. J. Gray, N. B. Grimm, and D. E. Busch. 1982. Temporal Succession in a Desert Stream Ecosystem Following Flash Flooding. Ecol. Monogr. **52**: 93–110.

doi:10.2307/2937346

Fisher, S. G., N. B. Grimm, E. Martí, R. M. Holmes, and J. B. Jones. 1998. Material Spiraling in Stream Corridors: A Telescoping Ecosystem Model. Ecosystems **1**: 19–34.

Garnier, E., M.-L. Navas, and K. Grigulis. 2016. Plant Functional Diversity. Organism traits, community structure, and ecosystem properties. Oxford Univ. Press.

Gattringer, J. P., T. W. Donath, R. L. Eckstein, K. Ludewig, A. Otte, and S. Harvolk-Schoning. 2017. Flooding tolerance of four floodplain meadow species depends on age. PLoS One **12**: e0176869. doi:10.1371/JOURNAL.PONE.0176869

Grace, J. B. 1989. Effects of water depth on Typha latifolia and Typha domingensis. Am. J. Bot. **76**: 762–768. doi:10.2307/2444423

Greenup, A. L., M. A. Bradford, N. P. Mcnamara, P. Ineson, and J. A. Lee. 2000. The role of Eriophorum vaginatum in CH4 flux from an ombrotrophic peatland. Plant Soil **227**: 265–272. doi:10.1023/A:1026573727311

Greet, J., J. Angus Webb, and R. D. Cousens. 2011. The importance of seasonal flow timing for riparian vegetation dynamics: a systematic review using causal criteria analysis. Freshw. Biol. **56**: 1231–1247. doi:10.1111/J.1365-2427.2011.02564.X

Gremer, J. R., J. B. Bradford, S. M. Munson, and M. C. Duniway. 2015. Desert grassland responses to climate and soil moisture suggest divergent vulnerabilities across the southwestern United States. Glob. Chang. Biol. **21**. doi:10.1111/gcb.13043

Grime, J. P. 1998. Benefits of plant diversity to ecosystems: immediate, filter and founder effects. J. Ecol. **86**: 902–910. doi:10.1046/J.1365-2745.1998.00306.X

Grimm, N. B. 1987. Nitrogen Dynamics During Succession in a Desert Stream. Ecology **68**: 1157–1170.

Grimm, N. B., F. S. Chapin, B. Bierwagen, and others. 2013. The impacts of climate change on ecosystem structure and function. Front. Ecol. Environ. **11**: 474–482. doi:10.1890/120282

Grimm, N. B., and S. G. Fisher. 1986. Nitrogen Limitation in a Sonoran Desert Stream Nancy B . Grimm and Stuart G . Fisher. J. North Am. Benthol. Soc. **5**: 2–15.

Grimm, N. B., and S. G. Fisher. 1989. Stability of Periphyton and Macroinvertebrates to Disturbance by Flash Floods in a Desert Stream. J. North Am. Benthol. Soc. **8**: 293–307.

Gustafsson, C., and A. Norkko. 2018. Quantifying the importance of functional traits for primary production in aquatic plant communities.doi:10.1111/1365-2745.13011

Harms, T. K., and N. B. Grimm. 2008. Hot spots and hot moments of carbon and nitrogen dynamics in a semiarid riparian zone. J. Geophys. Res. Biogeosciences **113**: n/a-n/a. doi:10.1029/2007JG000588

Heffernan, J. B. 2008. Wetlands as an alternative stable state in desert streams. Ecology **89**: 1261–1271. doi:10.1890/07-0915.1

Heffernan, J. B., R. A. Sponseller, and S. G. Fisher. 2007. Consequences of a biogeomorphic

regime shift for the hyporheic zone of a Sonoran Desert stream. Freshw. Biol. **53**: 1954–1968. doi:10.1111/j.1365-2427.2008.02019.x

Hillerislambers, J., P. B. Adler, W. S. Harpole, J. M. Levine, and M. M. Mayfield. 2012. Rethinking Community Assembly through the Lens of Coexistence Theory. Annu. Rev. Ecol. Evol. Syst **43**: 227–275. doi:10.1146/annurev-ecolsys-110411-160411

Hoellein, T. J., D. A. Bruesewitz, and D. C. Richardson. 2013a. Revisiting Odum (1956): A synthesis of aquatic ecosystem metabolism. Limnol. Oceanogr. **58**: 2089–2100. doi:10.4319/LO.2013.58.6.2089

Hoellein, T. J., D. A. Bruesewitz, and D. C. Richardson. 2013b. Revisiting Odum (1956): A synthesis of aquatic ecosystem metabolism. Limnol. Oceanogr. **58**: 2089–2100. doi:10.4319/lo.2013.58.6.2089

Hooper, D. U., E. C. Adair, B. J. Cardinale, and others. 2012. A global synthesis reveals biodiversity loss as a major driver of ecosystem change. Nature **486**: 105–108. doi:10.1038/nature11118

Hooper, D. U., F. S. Chapin, J. J. Ewel, and others. 2005. EFFECTS OF BIODIVERSITY ON ECOSYSTEM FUNCTIONING: A CONSENSUS OF CURRENT KNOWLEDGE. Ecol. Monogr. **75**: 3–35. doi:10.1890/04-0922

Hotchkiss, E. R., R. O. Hall, R. A. Sponseller, D. Butman, J. Klaminder, H. Laudon, M. Rosvall, and J. Karlsson. 2015. Sources of and processes controlling CO2emissions change with the size of streams and rivers. Nat. Geosci. **8**: 696–699. doi:10.1038/ngeo2507

Hsiao, A. I., and W. Z. Huang. 1989. Effects of flooding on rooting and sprouting of isolated stem segments and on plant growth of Paspalum distichum L. Weed Res. **29**: 335–344. doi:10.1111/J.1365-3180.1989.TB01303.X

Hsiao, T. C. 1973. Plant Responses to Water Stress. Annu. Rev. Plant Physiol. **24**: 519–570. doi:10.1146/ANNUREV.PP.24.060173.002511

Huang, J., M. Ji, Y. Xie, S. Wang, Y. He, and J. Ran. 2015. Global semi-arid climate change over last 60 years. Clim. Dyn. **46**: 1131–1150. doi:10.1007/s00382-015-2636-8

Hugelius, G., J. Strauss, S. Zubrzycki, and others. 2014. Estimated stocks of circumpolar permafrost carbon with quantified uncertainty ranges and identified data gaps. Biogeosciences **11**: 6573–6593. doi:10.5194/bg-11-6573-2014

Husby, C. 2013. Biology and Functional Ecology of Equisetum with Emphasis on the Giant Horsetails. **79**: 147–177. doi:10.1007/s12229-012-9113-4

Ikegami, M., D. F. Whigham, and M. J. A. Werger. 2009. Ramet phenology and clonal architectures of the clonal sedge Schoenoplectus americanus (Pers.) Volk. ex Schinz & R. Keller. Plant Ecol. **200**: 287–301. doi:10.1007/S11258-008-9453-7/FIGURES/6

Johansson, T., N. Malmer, P. M. Crill, T. Friborg, J. H. Åkerman, M. Mastepanov, and T. R. Christensen. 2006. Decadal vegetation changes in a northern peatland, greenhouse gas fluxes and net radiative forcing. Glob. Chang. Biol. **12**: 2352–2369. doi:10.1111/j.1365-2486.2006.01267.x

Jones, K. B., E. T. Slonecker, M. Nash, A. C. Neale, T. G. Wade, and S. Hamann. 2010. Riparian Habitat Changes Across the Continental United States (1972-2003) and Potential Implications for Sustaining Ecosystem Services Article . Landsc. Ecol. **25**: 1261–1275. doi:10.1007/s10980-010-9510-1

Kattge, J., S. Díaz, S. Lavorel, and others. 2011. TRY - a global database of plant traits. Glob. Chang. Biol. **17**: 2905–2935. doi:10.1111/j.1365-2486.2011.02451.x

Kelly, A. E., and M. L. Goulden. 2008. Rapid shifts in plant distribution with recent climate change. Proc. Natl. Acad. Sci. U. S. A. **105**: 11823–6. doi:10.1073/pnas.0802891105

Kemp, W. M., and L. Murray. 1986. Oxygen release from roots of the submersed macrophyte Potamogeton perfoliatus L.: Regulating factors and ecological implications. Aquat. Bot. **26**: 271–283. doi:10.1016/0304-3770(86)90027-6

Kerkhoff, A. J., B. J. Enquist, J. J. Elser, and W. F. Fagan. 2005. Plant allometry, stoichiometry and the temperature-dependence of primary productivity. Glob. Ecol. Biogeogr. **14**: 585–598. doi:10.1111/J.1466-822X.2005.00187.X

Knapp, A. K., P. Ciais, and M. D. Smith. 2017. Reconciling inconsistencies in precipitation–productivity relationships: implications for climate change. New Phytol. **214**: 41–47. doi:10.1111/NPH.14381

Kohler, J., O. Brandt, M. Johansson, and T. Callaghan. 2006. A long-term Arctic snow depth record from Abisko, northern Sweden, 1913–2004. Polar Res. **25**: 91–113. doi:10.3402/polar.v25i2.6240

Kominoski, J. S., J. Pachón, J. T. Brock, C. McVoy, and S. L. Malone. 2021. Understanding drivers of aquatic ecosystem metabolism in freshwater subtropical ridge and slough wetlands. Ecosphere **12**. doi:10.1002/ECS2.3849

Koven, C. D., B. Ringeval, P. Friedlingstein, P. Ciais, P. Cadule, D. Khvorostyanov, G. Krinner, and C. Tarnocai. 2011. Permafrost carbon-climate feedbacks accelerate global warming. Proc. Natl. Acad. Sci. U. S. A. **108**: 14769–74. doi:10.1073/pnas.1103910108

Kuhn, M., E. J. Lundin, R. Giesler, M. Johansson, and J. Karlsson. 2018. Emissions from thaw ponds largely offset the carbon sink of northern permafrost wetlands. Sci. Rep. **8**: 1–7. doi:10.1038/s41598-018-27770-x

Kunstler, G., D. Falster, D. A. Coomes, and others. 2015. Plant functional traits have globally consistent effects on competition. Nature **19**. doi:10.1038/nature16476

Lauck, M., and N. Grimm. Interactions between functional response and effect traits in wetland plant patches in an arid stream -riparian ecosystem. Prep. Wetl.

Lauck, M., N. Grimm, and D. Winkler. Lagged productivity responses mediated by seasonal flooding in an arid riparian system. Prep. Glob. Chang. Biol.

Lauck, M., R. Sponseller, J. Karlsson, and G. Nancy. Vegetation affects greenhouse gases and ecosystem metabolism of arctic mire thaw ponds. Prep. Freshw. Sci.

Lauck, M., C. B. Yackulic, and N. Grimm. Plankton traits buffer the mediation of biovolume on phosphorus-production relationships in the Colorado River. Prep. Freshw. Sci.

Lavorel, S., and E. Garnier. 2002. Predicting changes in community composition and ecosystem functioning from plant traits: revisiting the Holy Grail. Funct. Ecol. **16**: 545–556. doi:10.1046/j.1365-2435.2002.00664.x

Lavorel, S., S. McIntyre, J. Landsberg, and T. D. A. Forbes. 1997. Plant functional classifications: from general groups to specific groups based on response to disturbance. Trends Ecol. Evol. **12**: 474–478. doi:10.1016/S0169-5347(97)01219-6

Lawrence, J., B. Mackey, F. Chiew, and others. 2021. Weather and climate extreme events in a changing climate, *In* H.O. Pörtner, D.C. Roberts, M. Tignor, et al. [eds.], Climate Change 2022: Impacts, Adaptation, and Vulnerability. Cambridge University Press.

LeRoy Poff, N., J. David Allan, M. B. Bain, J. R. Karr, K. L. Prestegaard, B. D. Richter, R. E. Sparks, and J. C. Stromberg. 1997. The Natural Flow Regime. Bioscience **47**: 769–784.

Lewis, W. M., and W. A. Wurtsbaugh. 2008. Control of Lacustrine Phytoplankton by Nutrients: Erosion of the Phosphorus Paradigm. Int. Rev. Hydrobiol. **93**: 446–465. doi:10.1002/IROH.200811065

Li, D., S. Wu, L. Liu, Y. Zhang, and S. Li. 2018. Vulnerability of the global terrestrial ecosystems to climate change. Glob. Chang. Biol. **24**: 4095–4106. doi:10.1111/GCB.14327

Linstadter, A., and C. Zielhofer. 2010. Regional fire history shows abrupt responses of Mediterranean ecosystems to centennial-scale climate change. J. Arid Environ. **74**: 101–110. doi:10.1016/j.jaridenv.2009.07.006

Lipton, D., S. L. Carter, J. Peterson, and others. 2018. Ecosystems, Ecosystem Services, and Biodiversity. US Glob. Chang. Res. Progr. 268–321. doi:10.7930/NCA4.2018.CH7

Littel, J. S., D. McKenzie, D. L. Peterson, and A. L. Westerling. 2009. Climate and wildfire area burned in western US ecoprovinces, 1916–2003. Ecol. Appl. **19**: 1003–1021.

Lorenzen, B., H. Brix, I. A. Mendelssohn, K. L. McKee, and S. L. Miao. 2001. Growth, biomass allocation and nutrient use efficiency in Cladium jamaicense and Typha domingensis as affected by phosphorus and oxygen availability. Aquat. Bot. **70**: 117–133. doi:10.1016/S0304-3770(01)00155-3

Magnússon, R. Í., J. Limpens, J. Van Huissteden, D. Kleijn, T. C. Maximov, R. Rotbarth, U. Sass-Klaassen, and M. M. P. D. Heijmans. 2020. Rapid Vegetation Succession and Coupled Permafrost Dynamics in Arctic Thaw Ponds in the Siberian Lowland Tundra. JGR Biogeosciences **125**: 1–20. doi:10.1029/2019JG005618

Malmer, N., T. Johansson, M. Olsrud, and T. R. Christensen. 2005. Vegetation, climatic changes and net carbon sequestration in a North-Scandinavian subarctic mire over 30 years. Glob. Chang. Biol. **0**: 051006062331004-??? doi:10.1111/j.1365-2486.2005.01042.x

Martí, E., S. G. Fisher, J. D. Schade, J. R. Welter, and N. B. Grimm. 2000. Hydrological and chemical linkages between the active channel and the riparian zone in an arid land stream. SIL Proceedings, 1922-2010 **27**: 442–447. doi:10.1080/03680770.1998.11901270

Masson-Delmotte, V., P. Zhai, A. Pirani, and others. 2021. Climate Change 2021: The Physical Science Basis. Contribution of Working Group I to the Sixth Assessment Report of the Intergovernmental Panel on Climate Change.

Matimati, I., G. A. Verboom, and M. D. Cramer. 2014. Nitrogen regulation of transpiration controls mass-flow acquisition of nutrients. J. Exp. Bot. **65**: 159–168. doi:10.1093/JXB/ERT367

Mcclain, M. E., E. W. Boyer, C. L. Dent, and others. 2003. Biogeochemical Hot Spots and Hot Moments at the Interface of Terrestrial and Aquatic Ecosystems.doi:10.1007/s10021-003-0161-9

Mcgill, B. J., B. J. Enquist, E. Weiher, and M. Westoby. 2006. Rebuilding community ecology from functional traits. TRENDS Ecol. Evol. **21**. doi:10.1016/j.tree.2006.02.002

Messager, M. L., B. Lehner, C. Cockburn, and others. 2021. Global prevalence of non-perennial rivers and streams. Nat. 2021 5947863 **594**: 391–397. doi:10.1038/s41586-021-03565-5

Meyer, J. L., and G. E. Likens. 1979. Transport and Transformation of Phosphorus in a Forest Stream Ecosystem. Ecology **60**: 1255–1269. doi:10.2307/1936971

Milly, P. C. D., K. A. Dunne, and A. V Vecchia. 2005. US Geological Survey, 821 E. Interstate Ave. 58503–1199. doi:10.1038/nature04312

Montrone, A., L. Saito, P. J. Weisberg, M. Gosejohan, K. Merriam, and J. F. Mejia. 2019. Climate change impacts on vernal pool hydrology and vegetation in northern California. J. Hydrol. **574**: 1003–1013. doi:10.1016/J.JHYDROL.2019.04.076

Moor, H., H. Rydin, K. Hylander, M. B. Nilsson, R. Lindborg, and J. Norberg. 2017. Towards a trait-based ecology of wetland vegetation. J. Ecol. **105**: 1623–1635. doi:10.1111/1365-2745.12734

Mulholland, P. J., G. R. Best, C. C. Coutant, and others. 2005. Flow regime alterations under changing climate in two river basins: Implications for freshwater ecosystems. River Res. Appl. **21**: 849–864. doi:10.1002/RRA.855

Nagler, P. L., J. Cleverly, E. Glenn, D. Lampkin, A. Huete, and Z. Wan. 2005. Predicting riparian evapotranspiration from MODIS vegetation indices and meteorological data. Remote Sens. Environ. **94**: 17–30.

Naiman, R. J., and H. Decamps. 1997. THE ECOLOGY OF INTERFACES-Riparian Zones Send Proofs to. Annu. Rev. Ecol. Syst. **28**: 621–658.

Newman, G. S., and S. C. Hart. 2015. Shifting soil resource limitations and ecosystem retrogression across a three million year semi-arid substrate age gradient. Biogeochem. 2015 1241 **124**: 177–186. doi:10.1007/S10533-015-0090-7

Newman, S., J. Schuette, J. B. Grace, K. Rutchey, T. Fontaine, K. R. Reddy, and M. Pietrucha. 1998. Factors influencing cattail abundance in the northern Everglades. Aquat. Bot. **60**: 265–280.

Nilsson, C., and K. Berggren. 2000. Alterations of riparian ecosystems caused by river regulation: Dam operations have caused global-scale ecological changes in riparian ecosystems. How to protect. Bioscience **50**: 783–792.

Nilsson, C., M. Gardfjell, and G. Grelsson. 1991. Importance of hydrochory in structuring plant communities along rivers. Can. J. Bot. **69**: 2631–2633. doi:10.1139/B91-328

Noyce, G. L. 2011. Effect of Carex rostrata removal on methane emissions from a temperate peatland. University of New Hampshire.

Noyce, G. L., R. K. Varner, J. L. Bubier, and S. Frolking. 2014. Effect of *Carex rostrata* on seasonal and interannual variability in peatland methane emissions. J. Geophys. Res. Biogeosciences **119**: 24–34. doi:10.1002/2013JG002474

Odum, H. T. 1956. Primary Production in Flowing Waters. Limnol. Oceanogr. **1**: 102–117.

Pan, Y., E. Cieraad, B. R. Clarkson, T. D. Colmer, O. Pedersen, E. J. W. Visser, L. A. C. J. Voesenek, and P. M. van Bodegom. 2020. Drivers of plant traits that allow survival in wetlands. Funct. Ecol. **34**: 956–967. doi:10.1111/1365-2435.13541

Patten, D. T. 1998. Riparian ecosystems of semi-arid North America: Diversity and human impacts. Wetlands **18**: 498–512. doi:10.1007/BF03161668

Pérez-Ramos, I. M., L. Matías, L. Gómez-Aparicio, and Ó. Godoy. 2019. Functional traits and phenotypic plasticity modulate species coexistence across contrasting climatic conditions. Nat. Commun. 2019 101 **10**: 1–11. doi:10.1038/s41467-019-10453-0

Perry, L., D. Andersen, L. Reynolds, S. M. Nelson, and P. B. Shaforth. 2012. Vulnerability of riparian ecosystems to elevated CO2 and climate change in arid and semiarid western North America. Glob. Chang. Biol. **18**: 821–842. doi:10.1111/j.1365-2486.2011.02588.x

Petchey, O. L., and K. J. Gaston. 2006. Functional diversity: back to basics and looking forward. Ecol. Lett. **9**: 741–758. doi:10.1111/j.1461-0248.2006.00924.x

Pettit, N. E., and R. J. Naiman. 2007. Postfire response of flood-regenerating riparian vegetation in a semi-arid landscape. Ecology **88**: 2094–2104. doi:10.1890/06-1270.1

Prein, A. F., G. J. Holland, R. M. Rasmussen, M. P. Clark, and M. R. Tye. 2016. Running dry: The U.S. Southwest's drift into a drier climate state. Geophys. Res. Lett. **43**: 1272–1279. doi:10.1002/2015GL066727

Raven, J. A., L. L. Handley, J. J. Macfarlane, S. Mcinroy, L. Mckenzie, J. H. Richards, and G. Samuelsson. 1988. The role of CO2 uptake by roots and CAM in acquisition of inorganic C by plants of the isoetid life-form: a review, with new data on Eriocaulon decangulare L. New Phytol. **108**: 125–148. doi:10.1111/J.1469-8137.1988.TB03690.X

Raymond, P., J. Hartmann, R. Lauerwald, S. S.- Nature, and undefined 2013. Global carbon dioxide emissions from inland waters. nature.com. doi:10.1038/nature12760

Refsland, T. K., and J. M. Fraterrigo. 2017. Both canopy and understory traits act as response–effect traits in fire-managed forests. Ecosphere **8**: e02036. doi:10.1002/ECS2.2036

Reynolds, L. V, P. B. Shafroth, and N. L. Poff. 2015. Modeled intermittency risk for small streams in the Upper Colorado River Basin under climate change.doi:10.1016/j.jhydrol.2015.02.025

Richardson, D. M., P. M. Holmes, K. J. Esler, S. M. Galatowitsch, J. C. Stromberg, S. P. Kirkman, P. Pyšek, and R. J. Hobbs. 2007. Riparian vegetation: Degradation, alien plant invasions, and restoration prospects. Divers. Distrib. **13**: 126–139. doi:10.1111/J.1366-9516.2006.00314.X

Sabo, J., T. Harms, A. R.-A. F. M. Abstracts, and undefined 2019. 2019. Quantifying hydrologic regime shifts on ecological time scales using wavelets. AGU Meet. Abstr.

Sabo, J. L., R. Sponseller, M. Dixon, and others. 2005a. Riparian zones increase regional species richness by harboring different, not more, species. Ecology **86**: 56–62.

Sabo, J. L., R. Sponseller, M. Dixon, and others. 2005b. Riparian zones increase regional species richness by harboring different, not more, species. Ecology **86**: 56–62.

Sala, O. E., F. S. Chapin, J. J. Armesto, and others. 2000. Global Biodiversity Scenarios for the Year 2100 Science (80-.). **287**: 1770–1774. doi:10.1126/science.287.5459.1770

Sand-Jensen, K., C. Prahl, and H. Stokholm. 1982. Oxygen Release from Roots of Submerged Aquatic Macrophytes. Oikos **38**: 349–354.

Schade, J. D., S. G. Fisher, N. B. Grimm, and J. A. Seddon. 2001. The influence of a riparian shrub on nitrogen cycling in a Sonoran Desert stream. Ecology **82**: 3363–3376. doi:10.1890/0012-9658(2001)082[3363:TIOARS]2.0.CO;2

Schade, J. D., E. Marti, J. R. Welter, S. G. Fisher, and N. B. Grimm. 2002. Sources of nitrogen to the riparian zone of a desert stream: Implications for riparian vegetation and nitrogen retention. Ecosystems **5**: 68–79. doi:10.1007/s10021-001-0056-6

Schade, J. D., J. R. Welter, E. Martí, and N. B. Grimm. 2005a. Hydrologic exchange and N uptake by riparian vegetation in an arid-land stream. J. North Am. Benthol. Soc. **24**: 19–28. doi:10.1899/0887-3593(2005)024<0019:HEANUB>2.0.CO;2

Schade, J. D., J. R. Welter, E. Martí, and N. B. Grimm. 2005b. Hydrologic exchange and N uptake by riparian vegetation in an arid-land stream. J. North Am. Benthol. Soc. **24**: 19–28. doi:10.1899/0887-3593(2005)024<0019:HEANUB>2.0.CO;2

Schlesinger, C. A., and E. L. Westerhuis. 2021. Impacts of a single fire event on large, old trees in a grass-invaded arid river system. Fire Ecol. **17**. doi:10.1186/S42408-021-00121-4

Schuur, E. A. G., B. W. Abbott, W. B. Bowden, and others. 2013. Expert assessment of vulnerability of permafrost carbon to climate change. Clim. Change **119**: 359–374. doi:10.1007/s10584-013-0730-7

Schuur, E. A. G., A. D. McGuire, C. Schädel, and others. 2015. Climate change and the permafrost carbon feedback. Nature **520**: 171–179. doi:10.1038/nature14338

Scott, R. L., T. E. Huxman, and E. P. Barron-Gafford, G. A. Darrel Jenerette, G. Young, J. M. Hamerlynck. 2014. When vegetation change alters ecosystem water availability. Glob. Chang. Biol. **20**: 2198–2210.

Serrat-Capdevila, A., R. L. Scott, W. J. Shuttleworth, and J. B. Valdés. 2011. Estimating evapotranspiration under warmer climates: Insights from a semi-arid riparian system. J. Hydrol. **399**: 1–11. doi:10.1016/j.jhydrol.2010.12.021

Staudinger, M. D., S. L. Carter, M. S. Cross, and others. 2013. Biodiversity in a changing climate: a synthesis of current and projected trends in the US. Front Ecol Env. **11**: 465–473. doi:10.1890/120272

Steffan, W. L. 1996. A periodic-table for ecology: a chemist's view of plant functional types. J. Veg. Sci. **7**: 425–430.

Sterner, R. W., and J. J. Elser. 2003. Ecological Stoichiometry, Princeton University Press.

Strack, M., K. Mwakanyamale, G. Hassanpour Fard, M. Bird, V. Bérubé, and L. Rochefort. 2016. Effect of plant functional type on methane dynamics in a restored minerotrophic peatland. Plant Soil 2016 4101 **410**: 231–246. doi:10.1007/S11104-016-2999-6

Stromberg, J. C., K. J. Bagstad, J. M. Leenhouts, S. J. Lite, and E. Makings. 2005. Effects of stream flow intermittency on riparian vegetation of a semiarid region river (San Pedro River, Arizona). River Res. Appl. **21**: 925–938. doi:10.1002/rra.858

Stromberg, J. C., V. B. Beauchamp, M. D. Dixon, S. J. Lite, and C. Paradzick. 2007. Importance of low-flow and high-flow characteristics to restoration of riparian vegetation along rivers in arid south-western United States. Freshw. Biol. **52**: 651–679. doi:10.1111/j.1365-2427.2006.01713.x

Stromberg, J. C., S. J. Lite, and M. D. Dixon. 2010. Effects of stream flow patterns on riparian vegetation of a semiarid river: implications for a changing climate. River Res. Appl. **26**: 712–729.

Stromberg, J. C., R. Tiller, and B. Richter. 1996. Effects of ground water decline on riparian vegetation of semiarid regions: The San Pedro, Arizona. Ecol. Appl. **6**: 113–131. doi:10.2307/2269558

Suchy, A. K. 2016. Denitrification in Accidental Urban Wetlands : Exploring the Roles of Water Flows and Plant Patches by Amanda Klara Suchy A Dissertation Presented in Partial Fulfillment of the Requirements for the Degree Doctor of Philosophy Approved November 2016 by the. Arizona State University.

Tabacchi, E., H. Guilloy, A.-M. Planty-Tabacchi, E. Muller, and H. Decamps. 2000. Impacts of riparian vegetation on hydrological processes. Hydrol. Process. **14**: 29–59. doi:10.1002/1099-1085(200011/12)14:16/17<2959::AID

Team, R. C. 2015. R: A language and environment for statistical computing. R Found. Stat. Comput. Vienna, Austria.

Thursby, G. B. 1984. Root-exuded oxygen in the aquatic angiosperm Ruppia maritima *. **16**.

Tilman, D., and J. A. Downing. 1994. Biodiversity and stability in grasslands. Nature **367**: 363–365.

Tilman, D., J. Knops, D. Wedin, P. Reich, M. Ritchie, and E. Siemann. 1997a. The Influence of Functional Diversity and Composition on Ecosystem Processes. Science (80-.). **277**: 1300–1302. doi:10.1126/science.277.5330.1300

Tilman, D., C. L. Lehman, and K. T. Thomson. 1997b. Plant diversity and ecosystem productivity: Theoretical considerations. Proc. Natl. Acad. Sci. **94**: 1857–1861. doi:10.1073/pnas.94.5.1857

Torn, M. S., and F. S. Chapin. 1993. Environmental and biotic controls over methane flux from arctic tundra.

Turetsky, M. R., B. Bond-Lamberty, E. Euskirchen, J. Talbot, S. Frolking, A. D. Mcguire, and E.-S. Tuittila. 2012. The resilience and functional role of moss in boreal and arctic ecosystems. New Phytol. **196**: 49–67. doi:10.1111/j.1469-8137.2012.04254.x

Turetsky, M. R., S. E. Crow, R. J. Evans, D. H. Vitt, and R. Kelman Wieder. 2008. Trade-Offs in Resource Allocation among Moss Species Control Decomposition in Boreal. Source J. Ecol. **96**: 1297–1305. doi:10.1111/j

U.S. Geological Survey. 2021. National Water Information System data available on the World Wide Web (USGS Water Data for the Nation).

Udall, B., and J. Overpeck. 2017. The twenty-first century Colorado River hot drought and implications for the future. Water Resour. **53**: 2404–2418. doi:10.1002/2016WR019638

USGS. 2017. National Water Information System: Web Interface. Arizona Water Sci. Cent.

Vachon, D., and Y. T. Prairie. 2013. The ecosystem size and shape dependence of gas transfer velocity versus wind speed relationships in lakes. Artic. Can. J. Fish. Aquat. Sci. doi:10.1139/cjfas-2013-0241

Verhoeven, J. T. A., and E. Toth. 1995. Decomposition of Carex and Sphagnum litter in fens: Effect of litter quality and inhibition by living tissue homogenates. Soil Biol. Biochem. **27**: 271–275. doi:10.1016/0038-0717(94)00183-2

Violle, C., M.-L. Navas, D. Vile, E. Kazakou, C. Fortunel, I. Hummel, and E. Garnier. 2007. Let the concept of trait be functional! Oikos **116**: 882–892. doi:10.1111/j.0030-1299.2007.15559.x

Walker, M. D., C. Henrik Wahren, R. D. Hollister, and others. 2006. Plant community responses to experimental warming across the tundra biome. PNAS **103**: 1342–1346.

Webb, R., and S. Leake. 2006. Ground-water surface-water interactions and long-term change in riverine riparian vegetation in the southwestern United States. J. Hydrol. **320**: 302–323.

Wijk, M. T. Van, K. E. Clemmensen, G. R. Shaver, and others. 2004. Long-term ecosystem level experiments at Toolik Lake, Alaska, and at Abisko, Northern Sweden: generalizations and differences in ecosystem and plant type responses to global change. Glob. Chang. Biol. **10**: 105–123. doi:10.1111/J.1365-2486.2003.00719.X

Williams, D. G., R. L. Scott, T. E. Huxman, D. C. Goodrich, and G. Lin. 2006. Sensitivity of riparian ecosystems in arid and semiarid environments to moisture pulses. Hydrol. Process. **20**: 3191–3205. doi:10.1002/hyp.6327

Winkler, D. E., J. Belnap, D. Hoover, S. C. Reed, and M. C. Duniway. 2019. Shrub persistence and increased grass mortality in response to drought in dryland systems. Glob. Chang. Biol. **25**: 3121–3135. doi:10.1111/GCB.14667

Winslow, L. A., J. A. Zwart, R. D. Batt, H. A. Dugan, R. I. Woolway, J. R. Corman, P. C. Hanson, and J. S. Read. 2016. LakeMetabolizer: an R package for estimating lake metabolism from free-water oxygen using diverse statistical models. **6**: 622–636. doi:10.5268/IW-6.4.883

Wium-Andersen, S. 1971. Photosynthetic Uptake of Free CO2, by the Roots of Lobelia dortmanna. Physiol. Plant. **25**: 245–248. doi:10.1111/J.1399-3054.1971.TB01436.X

Woodward, K. B., C. S. Fellows, C. L. Conway, and H. M. Hunter. 2009. Nitrate removal, denitrification and nitrous oxide production in the riparian zone of an ephemeral stream. Soil Biol. Biochem. **41**: 671–680. doi:10.1016/j.soilbio.2009.01.002

Wright, I. J., M. Westoby, and P. B. Reich. 2002. Convergence towards higher leaf mass per area in dry and nutrient-poor habitats has different consequences for leaf life span. J. Ecol. **90**: 534–543.

Van Den Wyngaert, I. J. ., and R. Bobbink. 2009. Ecological dynamics. II. The influences of vertebrate herbivory on ecological dynamics in wetland ecosystems, p. 304. *In* The Wetlands Handbook.

Xu, Z. Z., and G. S. Zhou. 2006. Combined effects of water stress and high temperature on photosynthesis, nitrogen metabolism and lipid peroxidation of a perennial grass Leymus chinensis. Planta 2006 2245 **224**: 1080–1090. doi:10.1007/S00425-006-0281-5

Zirbel, C. R., T. Bassett, E. Grman, and L. A. Brudvig. 2017. Plant functional traits and environmental conditions shape community assembly and ecosystem functioning during restoration. J. Appl. Ecol. **54**: 1070–1079. doi:10.1111/1365-2664.12885

APPENDIX A

BIOMASS-COVER RELATIONSHIPS FOR MOSSES AND SEDGES

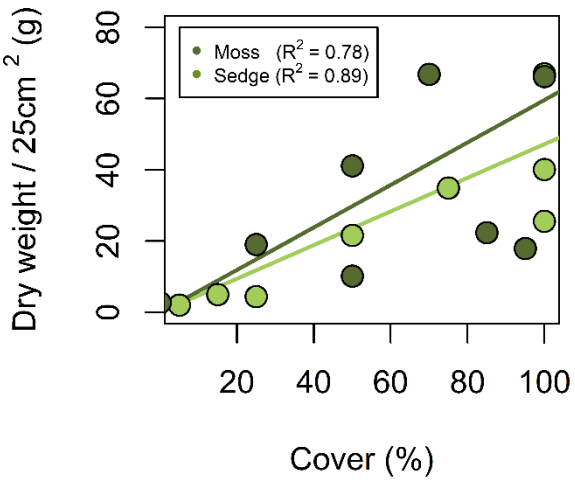

Appendix A. Biomass-cover relationships were used to estimate biomass in each pond.

APPENDIX B

PHYTOPLANKTON SPECIES AND THEIR TRAITS

Appendix B. Phytoplankton species observed at Lee's Ferry along the Colorado River and their associated traits. Trait data was compiled from diatoms.org. Colonial diatoms were reported as solitary (0), occasionally colonial (+), commonly colonial (++), or zigzag colonies (ZZ). Motility was reported on a scale including nonmotile (0), weakly motile (1), slightly motile (2), moderately motile (3), or highly motile (4). Attachment strategies were reported on a in categories including unattached (UN), prostrate (PR), vertical (VR), or tubeforming (TF). Biological condition gradient (BCG) was reported on a scale from BCG 1 (specialist) to BCG 5 (tolerant) based on their levels of tolerance to human disturbance.

Genus species	Division	Category	size um3	Colonial	Motility	Attach	BCG
Achnanthes ventralis	Bacillariophyta						
Asterionella formosa	Bacillariophyta	araphid	101-1000	++	0	UN	
Diatoma hiemale	Bacillariophyta	araphid	1001-10000		0	UN	
Diatoma mesodon	Bacillariophyta	araphid	101-10000	0	0	PR	
Diatoma moniliformis	Bacillariophyta	araphid	11-1000	ZZ	0	PR	
Diatoma tenuis	Bacillariophyta	araphid	101-1000	ZZ	0	UN	2
Diatoma vulgaris	Bacillariophyta	araphid	101-10000	ZZ	0	PR	3
Fragilaria capucina	Bacillariophyta	araphid	101-1000		0		3
Fragilaria capucina var. gracilis	Bacillariophyta	araphid	101-1000		0		3
Fragilaria construens	Bacillariophyta	araphid	11-100	++	0	VR	4
Fragilaria crotonensis	Bacillariophyta	araphid	101-1000	++	0	UN	3
Hannaea arcus	Bacillariophyta	araphid	101-1000	0	0	UN	2
Pseudostaurosira brevistriata	Bacillariophyta	araphid	11-100	++	0	VR	3
Pseudostaurosira pseudoconstruens	Bacillariophyta	araphid	11-100	+	0	UN	3
Staurosira brevistriata	Bacillariophyta	araphid	11-100		0	VR	3
Staurosira construens	Bacillariophyta	araphid	11-100	++	0	VR	4
Staurosira construens var. venter	Bacillariophyta	araphid	11-100	+	0		4
Staurosirella lapponica	Bacillariophyta	araphid					
Staurosirella leptostauron	Bacillariophyta	araphid	11-100	+	0		3
Staurosirella leptostauron var. dubia	Bacillariophyta	araphid	11-100	+	0	PR	
Staurosirella martyi	Bacillariophyta	araphid	11-100	0	0	VR	
Staurosirella pinnata	Bacillariophyta	araphid	11-100		0	VR	4
Synedra cyclopum	Bacillariophyta	araphid	101-1000	0	0	UN	3
Synedra delicatissima	Bacillariophyta	araphid	10001-100000	+	0	UN	
Synedra delicatissima var. angustissima	Bacillariophyta	araphid	10001-100000	+	0	UN	
Synedra fasciculata	Bacillariophyta	araphid					
Synedra mazamaensis	Bacillariophyta	araphid	1001-10000		0	PR	2
Synedra parasitica	Bacillariophyta	araphid	101-1000	+	0	VR	4
Synedra tenera	Bacillariophyta	araphid	101-1000		0	UN	3
Synedra ulna	Bacillariophyta	araphid	10001-100000	+	0	UN	
Tabellaria flocculosa	Bacillariophyta	araphid	11-1000	0	0	UN	2
Tabularia fasciculata	Bacillariophyta	araphid	101-1000		0		4
Amphora commutata	Bacillariophyta	asym. biraphid					
Amphora copulata	Bacillariophyta	asym. biraphid	1001-10000		2	PR	4
Amphora delicatissima	Bacillariophyta	asym. biraphid					
Amphora inariensis	Bacillariophyta	asym. biraphid					
Amphora libyca	Bacillariophyta	asym. biraphid					
Amphora ovalis	Bacillariophyta	asym. biraphid	1001-100000		2	PR	4
Amphora pediculus	Bacillariophyta	asym. biraphid	11-1000		2	PR	4
Amphora pediculus	Bacillariophyta	asym. biraphid	11-1000		2	PR	4
Cymbella affinis	Bacillariophyta	asym. biraphid	101-10000		2	VR	2
Cymbella amphicephala	Bacillariophyta	asym. biraphid	101-1000	0	2	UN	2
Cymbella caespitosa	Bacillariophyta	asym. biraphid					

Cymbella cistula	Bacillariophyta	asym.	biraphid		0	3	VR	
Cymbella delicatula	Bacillariophyta	asym.	biraphid		0	3	UN	2
Cymbella descripta	Bacillariophyta	asym.	biraphid		0	2	UN	
Cymbella helvetica	Bacillariophyta	asym.	biraphid	1001-10000	0	2	VR	
Cymbella leptoceros	Bacillariophyta	asym.	biraphid		0			
Cymbella mexicana	Bacillariophyta	asym.	biraphid	100001-1000000		4	VR	3
Cymbella minuta	Bacillariophyta	asym.	biraphid	1001-10000	+	3	TF	
Cymbella naviculiformis	Bacillariophyta	asym.	biraphid	101-1000	0	2	UN	3
Cymbella prostrata	Bacillariophyta	asym.	biraphid	100001-1000000	++	3	TF	
Cymbella proxima	Bacillariophyta	asym.	biraphid	10001-100000		3	VR	
Cymbella silesiaca	Bacillariophyta	asym.	biraphid	1001-10000	+	2	TF	
Cymbella tumida	Bacillariophyta	asym.	biraphid	10001-100000	+	2	VR	3
Cymbella turgidula	Bacillariophyta	asym.	biraphid	1001-10000		2	VR	2
Cymbopleura amphicephala	Bacillariophyta	asym.	biraphid	101-1000	0	2	UN	2
Cymbopleura naviculiformis	Bacillariophyta	asym.	biraphid	101-1000	0	2	UN	3
Didymosphenia geminata	Bacillariophyta	asym.	biraphid	100001-1000000		3	VR	2
Encyonema caespitosum	Bacillariophyta	asym.	biraphid	1001-10000		3	TF	3
Encyonema minutum	Bacillariophyta	asym.	biraphid	1001-10000	+	3	TF	
Encyonema prostratum	Bacillariophyta	asym.	biraphid	100001-1000000	++	3	TF	
Encyonema silesiacum	Bacillariophyta	asym.	biraphid	1001-10000	+	2	TF	
Encyonema temperei	Bacillariophyta	asym.	biraphid	10001-100000		3	TF	
Encyonopsis microcephala	Bacillariophyta	asym.	biraphid	11-100	0	3	PR	3
Gomphoneis eriense	Bacillariophyta	asym.	biraphid	1001-100000		3	VR	2
Gomphoneis eriense var. variabilis	Bacillariophyta	asym.	biraphid	1001-10000		3	VR	2
Gomphoneis olivacea	Bacillariophyta	asym.	biraphid	101-1000	++	3	VR	3
Gomphonema acuminatum	Bacillariophyta	asym.	biraphid	1001-10000		3	PR	3
Gomphonema angustum	Bacillariophyta	asym.	biraphid					
Gomphonema augur var. sphaerophorum	Bacillariophyta	asym.	biraphid	1001-10000			VR	3
Gomphonema clevei	Bacillariophyta	asym.	biraphid					
Gomphonema gracile	Bacillariophyta	asym.	biraphid					
Gomphonema hebridense	Bacillariophyta	asym.	biraphid					
Gomphonema johnsonii	Bacillariophyta	asym.	biraphid	101-10000		3	VR	
Gomphonema minutum	Bacillariophyta	asym.	biraphid					
Gomphonema olivaceoides	Bacillariophyta	asym.	biraphid	101-1000	++	3	VR	
Gomphonema olivaceum	Bacillariophyta	asym.	biraphid	101-1000	++	3	VR	3
Gomphonema parvulum	Bacillariophyta	asym.	biraphid	101-1000	++	3	VR	
Gomphonema pseudoaugur	Bacillariophyta	asym.	biraphid					
Gomphonema pseudotenellum	Bacillariophyta	asym.	biraphid					
Gomphonema sphaerophorum	Bacillariophyta	asym.	biraphid	1001-10000			VR	3
Gomphonema tenellum	Bacillariophyta	asym.	biraphid					
Reimeria sinuata	Bacillariophyta	asym.	biraphid	101-1000		1	PR	2
Rhoicosphenia abbreviata	Bacillariophyta	asym.	biraphid	101-10000	0	1	VR	3
Rhoicosphenia curvata	Bacillariophyta	asym.	biraphid	101-10000	0	1	VR	3
Aulacoseira ambigua	Bacillariophyta	centric		101-1000	++	0	UN	3
Aulacoseira granulata	Bacillariophyta	centric		101-1000	++	0	UN	5
Cyclostephanos dubius	Bacillariophyta	centric		11-1000	+	0	UN	4
Cyclotella bodanica	Bacillariophyta	centric		10001-100000	0	0	UN	
Cyclotella bodanica var. lemanica	Bacillariophyta	centric		10001-100000	0	0	UN	
Cyclotella meneghiniana	Bacillariophyta	centric		11-1000	+	0	UN	5
Cyclotella meneghiniana	Bacillariophyta	centric		11-1000	+	0	UN	5

Cyclotella ocellata	Bacillariophyta	centric	11-100	+	0	UN	
Cyclotella ocellata	Bacillariophyta	centric	11-100	+	0	UN	
Ellerbeckia arenaria	Bacillariophyta	centric	10001-100000		0	UN	2
Melosira varians	Bacillariophyta	centric	10001-100000	++	0	UN	4
Stephanodiscus alpinus	Bacillariophyta	centric	11-1000	0	0	UN	
Stephanodiscus hantzschii	Bacillariophyta	centric	101-1000	+	0	UN	5
Stephanodiscus medius	Bacillariophyta	centric					
Stephanodiscus niagarae	Bacillariophyta	centric	101-10000	0	0	UN	4
Stephanodiscus parvus	Bacillariophyta	centric	101-1000		0	UN	
Epithemia adnata	Bacillariophyta	epithemioid	1001-10000	0	3	PR	2
Rhopalodia gibba	Bacillariophyta	epithemioid	1001-10000	0	3	PR	2
Eunotia arcus	Bacillariophyta	eunotioid					
Eunotia circumborealis	Bacillariophyta	eunotioid	101-10000		2	UN	
Eunotia silvahercynia	Bacillariophyta	eunotioid					
Achnanthes felinophila	Bacillariophyta	monoraphid	1001-10000	0	2	UN	
Achnanthes hintzii	Bacillariophyta	monoraphid	11-100	0	2	UN	
Achnanthes joursacense	Bacillariophyta	monoraphid	101-1000	0	2	UN	
Achnanthes lanceolata	Bacillariophyta	monoraphid					4
Achnanthidium catenatum	Bacillariophyta	monoraphid					
Achnanthidium catenatum	Bacillariophyta	monoraphid					
Achnanthidium duthiei	Bacillariophyta	monoraphid			2	PR	
Achnanthidium exilis	Bacillariophyta	monoraphid					
Achnanthidium minutissimum	Bacillariophyta	monoraphid	11-100	+	2	PR	3
Cocconeis pediculus	Bacillariophyta	monoraphid	101-1000	0	2	PR	4
Cocconeis placentula	Bacillariophyta	monoraphid	101-100000	0	1	PR	4
Eucocconeis laevis	Bacillariophyta	monoraphid	101-1000		2	PR	2
Planothidium calcar	Bacillariophyta	monoraphid	11-1000	0	2	UN	
Planothidium delicatulum	Bacillariophyta	monoraphid	101-1000	0	2	UN	5
Planothidium dubium	Bacillariophyta	monoraphid	101-1000	0	2	UN	3
Planothidium frequentissimum	Bacillariophyta	monoraphid					4
Planothidium lanceolatum	Bacillariophyta	monoraphid					4
Planothidium rostratum	Bacillariophyta	monoraphid	101-1000	0	2	PR	3
Denticula tenuis	Bacillariophyta	nitzschioid	101-1000	0	3	PR	2
Nitzschia acicularis	Bacillariophyta	nitzschioid	11-1000		3	UN	4
Nitzschia amphibia	Bacillariophyta	nitzschioid	101-1000	0	3	PR	5
Nitzschia constricta	Bacillariophyta	nitzschioid	1001-10000	0	3	UN	5
Nitzschia dissipata	Bacillariophyta	nitzschioid	101-1000	0	4	UN	3
Nitzschia inconspicua	Bacillariophyta	nitzschioid					
Nitzschia intermedia	Bacillariophyta	nitzschioid	1001-10000	0	4	UN	
Nitzschia linearis	Bacillariophyta	nitzschioid	1001-10000	0	3	PR	3
Nitzschia palea	Bacillariophyta	nitzschioid	101-1000		3	PR	5
Nitzschia sinuata var. tabellaria	Bacillariophyta	nitzschioid	101-1000	0	3	UN	3
Amphipleura pellucida	Bacillariophyta	sym. biraphid	101-10000	+	0	TF	3
Brachysira microcephala	Bacillariophyta	sym. biraphid	101-1000		3		
Brachysira vitrea	Bacillariophyta	sym. biraphid	101-1000	0	3	UN	3
Craticula cuspidata	Bacillariophyta	sym. biraphid		0	4	UN	4
Diploneis elliptica	Bacillariophyta	sym. biraphid	10001-100000	0	3	UN	3
Gyrosigma acuminatum	Bacillariophyta	sym. biraphid	1001-100000	0	4	UN	4
Gyrosigma attenuatum	Bacillariophyta	sym. biraphid	10001-100000	0	4	UN	5
Hippodonta capitata	Bacillariophyta	sym. biraphid	101-1000	0	3	UN	4

Mastogloia elliptica	Bacillariophyta	sym. biraphid	1001-10000	0	3	UN	3
Mastogloia smithii	Bacillariophyta	sym. biraphid	11-100	0	3	UN	
Navicula angusta	Bacillariophyta	sym. biraphid	101-1000	0	3	UN	3
Navicula cari	Bacillariophyta	sym. biraphid	1001-10000	0	3	UN	4
Navicula cryptocephala	Bacillariophyta	sym. biraphid	101-1000	0	3	UN	4
Navicula cryptotenella	Bacillariophyta	sym. biraphid		0	3	UN	
Navicula elginensis	Bacillariophyta	sym. biraphid	11-100	0	3	UN	
Navicula exigua	Bacillariophyta	sym. biraphid					
Navicula gregaria	Bacillariophyta	sym. biraphid	101-1000	0	4	UN	4
Navicula lanceolata	Bacillariophyta	sym. biraphid	1001-10000	0	3	UN	4
Navicula margalithii	Bacillariophyta	sym. biraphid	1001-10000	0	3	UN	4
Navicula menisculus	Bacillariophyta	sym. biraphid	101-1000	0	3	UN	3
Navicula phyllepta	Bacillariophyta	sym. biraphid					
Navicula radiosa	Bacillariophyta	sym. biraphid	101-1000	0	3	UN	4
Navicula recens	Bacillariophyta	sym. biraphid	101-1000	0	3	UN	5
Navicula reinhardtii	Bacillariophyta	sym. biraphid	1001-10000	0	3	UN	3
Navicula tripunctata	Bacillariophyta	sym. biraphid	1001-10000	0	3	UN	4
Navicula trivialis	Bacillariophyta	sym. biraphid	101-1000	0	3	UN	4
Navicula veneta	Bacillariophyta	sym. biraphid	101-1000	0	3	UN	4
Navicula viridula	Bacillariophyta	sym. biraphid	1001-10000	0	3	UN	5
Navicula viridula var. rostellata	Bacillariophyta	sym. biraphid	1001-10000	0	3	UN	4
Placoneis clementioides	Bacillariophyta	sym. biraphid					
Placoneis elginensis	Bacillariophyta	sym. biraphid					
Sellaphora pupula	Bacillariophyta	sym. biraphid					
Stauroneis gracilis	Bacillariophyta	sym. biraphid	1001-10000	0	3	UN	3
Stauroneis smithii	Bacillariophyta	sym. biraphid	101-1000	0	3	UN	4
Characium ambiguum	Chlorophyta						
Chlamydomonas gloeopara	Chlorophyta						
Chlamydomonas reinhardtii	Chlorophyta						
Chlamydonephris pomiformis	Chlorophyta						
Closteriopsis acicularis	Chlorophyta						
Crucigenia tetrapedia	Chlorophyta		101-1000	++			
Elakatothrix gelatinosa	Chlorophyta		101-10000				
Golenkinia paucispina	Chlorophyta						
Oocystis lacustris	Chlorophyta		101-10000				
Oocystis parva	Chlorophyta		11-1000				
Pediastrum boryanum	Chlorophyta						
Quadrigula chodatii	Chlorophyta						
Quadrigula closteroides	Chlorophyta						
Quadrigula lacustris	Chlorophyta						
Scenedesmus balatonicus	Chlorophyta						
Scenedesmus bijuga	Chlorophyta						
Scenedesmus quadricauda	Chlorophyta						
Sphaerocystis planctonica	Chlorophyta		101-1000				
Stichococcus bacillaris	Chlorophyta						
Tetraedron minimum	Chlorophyta		101-10000				
Westella botryoides	Chlorophyta		101-1000				
Botryococcus braunii	Chlorophyta			++			3
Chlamydomonas globosa	Chlorophyta						
Chlorella minutissima	Chlorophyta						

Chlorella saccharophila var. ellipsoidea	Chlorophyta						
Chlorella vulgaris	Chlorophyta						
Dictyosphaerium pulchellum	Chlorophyta		11-1000	++			
Gonium pectorale	Chlorophyta		11-10000	++			
Sphaerocystis schroeteri	Chlorophyta		11-1000				
Mallomonas pseudocoronata	Chrysophyta						
Actinocyclus normanii	Chrysophyta	centric	1001-10000	0	0	UN	5
Discostella pseudostelligera	Chrysophyta	centric	11-100	0	0		4
Pleurosira laevis	Chrysophyta	centric	100001-1000000	++	0	PR	5
Puncticulata bodanica	Chrysophyta	centric	10001-100000	0	0	UN	
Stephanocyclus meneghiniana	Chrysophyta	centric					
Cryptomonas marssonii	Cryptophyta		1001-10000				
Cryptomonas platyuris	Cryptophyta		1001-10000				
Rhodomonas lacustris	Cryptophyta		101-1000				
Cryptomonas erosa	Cryptophyta		1001-10000				
Cryptomonas ovata	Cryptophyta		101-10000				
Plagioselmis nannoplanctica	Cryptophyta						
Rhodomonas minuta	Cryptophyta						
Aphanizomenon flosaquae	Cyanobacteria		1001-10000	++			
Aphanizomenon flos-aquae	Cyanobacteria		1001-10000	++			
Aphanocapsa delicatissima	Cyanobacteria		1-1000	++			
Aphanocapsa holsatica	Cyanobacteria						
Aphanocapsa planctonica	Cyanobacteria						
Aphanothece clathrata	Cyanobacteria		1-1000				
Chroococcus minutus	Cyanobacteria		11-1000				
Cylindrospermopsis raciborskii	Cyanobacteria			++			
Limnothrix redekei	Cyanobacteria		101-1000	++			
Merismopedia hyalina	Cyanobacteria						
Planktolyngbya limnetica	Cyanobacteria		11-1000	++			
Snowella lacustris	Cyanobacteria		11-1000	++			
Woronichinia naegeliana	Cyanobacteria		11-1000	++			
Chroococcus limneticus	Cyanobacteria		101-1000				
Chroococcus microscopicus	Cyanobacteria		1-100				
Chroococcus minimus	Cyanobacteria		1-11				
Gomphosphaeria aponina	Cyanobacteria		101-10000				
Microcystis aeruginosa	Cyanobacteria		11-1000	++			
Oscillatoria tenuis	Cyanobacteria						
Pseudanabaena limnetica	Cyanobacteria		11-1000	++			
Woronichinia karelica	Cyanobacteria		1-1000	++			
Trachelomonas pulchella	Euglenophyta						
Trachelomonas volvocina	Euglenophyta		101-10000				
Trachelomonas volvocina var. compressa	Euglenophyta		101-10000				
Glenodinium palustre	Pyrrophyrta						
Gymnodinium discoidale	Pyrrophyrta						
Gyrodinium fusiforme	Pyrrophyrta		10001-100000				
Peridinium umbonatum	Pyrrophyrta						
Ceratium hirundinella	Pyrrophyrta		10001-100000	0			
Audouinella hermanii	Rhodophyta						